5

Hydrothermal Growth of Some Selected Crystals

The hydrothermal technique has produced a wide variety of minerals and crystals, both in nature and in laboratory. In fact, it is the only technique to synthesize some of the inorganic compounds like quartz, berlinite, and so on. However, the method has some limitations as far as the size is concerned. Except quartz, the method has not yielded large single crystals. Although berlinite, gallium berlinite, and lithium tetraborate show many superior piezoelectric properties compared to α-quartz, it is not possible to obtain them as large as α-quartz crystals. Further, it is difficult to discuss here the growth of all the compounds of hydrothermal origin. Hence, the scope of this chapter has been restricted only to the growth of most important crystals.

5.1 QUARTZ

Quartz is one of the most abundant minerals and occurs both as an essential and accessory constituent of the rocks. References to quartz are known from 1505 onwards. It may have been derived from the Saxon word *querkluftertz,* or cross-vein-ore, which could easily have become condensed to *querertz* and then to *quartz*.[1]

Quartz, SiO_2, exists both in crystalline and amorphous forms in nature. The crystalline form of quartz has over 22 polymorphic modifications. The three principal crystalline forms of SiO_2 (quartz, tridymite, and cristobalite) possess a well-defined field of stability under equilibrium conditions for each one of them. The transformations from one to another are, however, somewhat sluggish, so that the higher temperature forms, cristobalite and tridymite, can exist metastably below their inversion temperatures. Each crystalline form of quartz, metastable tridymite and metastable cristobalite, has furthermore low- and high-temperature modifications designated as α- and β-, respectively.[2]-[4] Amongst them, α-quartz, which is stable below 573°C at atmospheric pressure, is the most popular and technologically very important. The structure of α-quartz is shown in Fig. 5.1.[5][6] The α-quartz has trigonal symmetry, belongs to the enantiomorphous crystal class 32, and its space group is $P3_121$ or $P3_221$ according to its right–or left–handedness. Its structure was among the first to be investigated by x-ray techniques as early as 1914 by Bragg.[6] The structure of quartz is made up of SiO_4 tetrahedra, which are linked by sharing each of their corners with another tetrahedron. In the 3-dimensional framework thus formed, every Si^{4+} has four oxygens and every oxygen has two silicons as nearest neighbors. There are several works on the hydrothermal synthesis of other varieties of silica—like coesite, β-quartz, stisshovite, cristobalite and tridymite.[7]–[10] However, the scope of this chapter has been restricted to the growth of large size single crystals of quartz by the hydrothermal technique. In this respect, it is only the α-quartz, which could be grown as large bulk single crystals, whereas the other varieties of silica have been obtained so far only as fine crystalline products, or tiny cristallites.

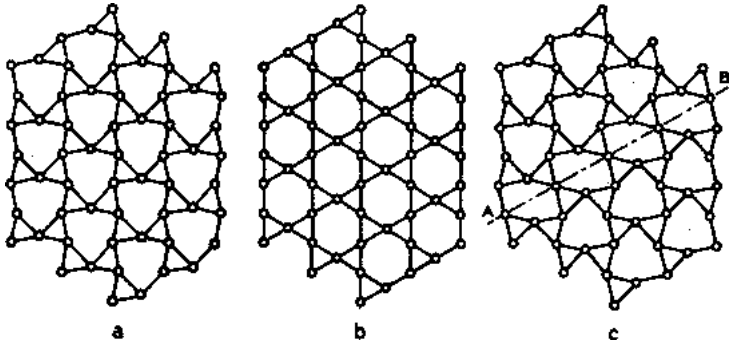

Figure 5.1. Structure of α-quartz.[5]

The α-quartz is one of the most extensively studied materials. It is the most popular, and technologically very important among all the hydrothermally grown crystals or materials. Quartz as a piezoelectric crystal has the ability to convert electric waves into mechanical waves and to reverse the process. Because of this property, quartz is widely used in filters, timing and frequency control applications, optical fibers, dielectric applications, and so on. In the recent years, quartz "tuning forks" have become essential for timing functions in electronic watches and in timing circuits for computers and telecommunications. Quartz crystal is one of the most transparent materials over a wide range of optical frequencies from UV (ultraviolet) to IR (infrared) regions, and it has double refraction (birefringence) and optical rotation power. Because of these properties, the quartz crystal is utilized as optical device on a large scale. Typical applications are in optical low pass filters (OLPF) for video cameras and waveplates for optical pick up. Table 5.1 gives a wide range of applications for α-quartz.

Table 5.1. Applications for α-quartz

Industrial equipment	Precision oscillators, optical fibers, dielectric materials, radiocommunications, cable communications, electronic applications, measurement equipment, pagers, security systems (alarms)…
Consumer equipment	Electronic hand calculators, watches, clocks, timers, cable TVs, color TVs, video recorders, RF converters, transceivers, radio equipment, microphones, electronic appliances, microphones, microcomputer and computer terminals, TV-game machines, telephones, copy machines…

The principal source of electronic grade natural quartz is Brazil. Today, the electronic industries are largely inclined to use synthetic quartz, because natural quartz crystals are generally irregular in shape, automatic cutting is cumbersome and the yield is low. Over 3000 tons of quartz are produced annually for a variety of applications. These applications range from optical components (due to its high transparency) to precise time and frequency oscillators based on its piezoelectric properties. The important

countries contributing to the world production are USA, Japan, China, Korea, Taiwan, Poland, Belgium, France, Germany, Russia, and so on. Japan alone produces more than 50% of the worldwide production, followed by USA.[11] Figure 2.11 shows a photograph of synthetic quartz crystals pulled out from the world's largest autoclave located at the Toyo Electric Co., Japan.[12] The inner diameter of the autoclave is 65 cm. To quote an example, the combined production quantity of quartz crystal units, filters, and oscillators in 1980 was 390 million pieces in Japan and it was remarkably increased to 2.13 billion pieces in 1990. The hydrothermal growth of quartz has been described and reviewed in several earlier works.[12]–[17] Hence, we will only consider the conventional method of the growth of α-quartz and its kinetics data in brief. Instead, we discuss the more recent developments in the growth of high purity and low dislocation quartz.

The α - β transition in quartz takes place at about 573°C, and the crystal growth of quartz insists upon a growth technique suitable to the low-temperature crystal growth process. This led to the development of hydrothermal process. In fact, much of our knowledge of the hydrothermal technique has resulted from the success in the growth of quartz crystals. The first publication in hydrothermal research is again pertaining to the synthesis of quartz by Schafhaul during 1845.[18] The best known source of natural quartz, even today, is Brazil, which has large occurrences of high quality electronic grade quartz. As a matter of fact, Brazil was the only supplier of large crystals of high quality natural quartz for electronic applications until World War II. Shortages in U.S.A and Europe caused by German submarine activity prompted efforts to synthesize large crystals of quartz, in the laboratory, using seeds. Spezia (1900–1909) was the first to attempt the seeded growth of quartz crystals and to carry out a systematic study of the solubility. However, the growth rate was poor. It was only during World War II that Nacken could achieve higher growth rates for quartz by the hydrothermal technique. The pilot scale production of quartz began during mid 1950s in U.S.A. and erstwhile USSR. Several countries attempted the artificial growth of large size single crystals of quartz. Especially, after the publication of the works of Nacken in 1950[19] and the captured German reports,[20][21] several laboratories began studying quartz crystal growth almost simultaneously and the hydrothermal technique became a very popular tool for developing many complex inorganic compounds. Industrial scale production occurred essentially during 1960s and 1970s, with a peak development between 1968 and 1976, especially in USA, Japan, and Europe.

In the growth of α-quartz by the conventional method, the autoclaves used by most of the workers were modified Bridgman type autoclaves. The design and construction of the modified Bridgman autoclave is described in Ch. 3. The typical laboratory size autoclave is 1" diameter × 1' length. The pressure autoclave used in Europe and USA is 13 inches diameter and > 10' length with 350 liters internal volume, which gives some 150 kg of quartz per cycle. But an evolution concerning vessel's dimensions has to be noted, especially in Japan, where autoclaves with 1000 liters to 5000 liters of internal volume are in operation producing 500 to 2000 kg quartz per cycle. The evolution of the autoclaves, the sealing involved, and the volume are discussed in Ch. 3. These larger internal volume autoclaves are provided with Grey-Loc type of sealing. Parallel to the increase in output, electronic components manufacturers have been looking, for the past 2½ decades, for a material with steadily increasing performances for professional applications in the telecommunications field, civilian as well as military.

In the growth of α-quartz, available nutrient material such as small particle size α-quartz, silica glass, high quality silica sand, or silica gel is placed in a liner made up of iron or silver with a suitable baffle and a frame to hold the seed plates. A mineralizer solution with a definite molarity is poured into the liner to make the required percent fill. The increased solubility in the presence of mineralizer increases the supersaturation without spontaneous nucleation and consequently allows more rapid growth rates on the seeds. Figure 3.3 shows the cross section of the modified Bridgman autoclave used in the growth of quartz crystals. The commercial autoclaves used have 10 inch inner diameter, and are10 feet long unlined. These autoclaves can work at conditions up to 30,000 psi and 400°C. Most of these experiments are carried out for 25 to 90 days to obtain full size crystals, 4 cm in the *Z*-direction and 12.5 to 15 cm in *Y*-direction. Temperature gradient is varied according to the nutrient used. About 1N NaOH or Na_2CO_3 is the most commonly used mineralizer. The solubility change with temperature is smaller in NaOH and slightly larger in Na_2CO_3. The temperature of the autoclave at the nutrient zone is usually kept at 355-369°C and, in the growth zone, it is kept at 350°C. The addition of lithium improves the growth rate and small amounts of Li salts are routinely added to the solution.[22] The solubility is also, to some extent, a function of increasing pressure. The pressure is controlled by the percent fill in the autoclave, and it is usually about 80% for hydroxyl mineralizer (20,000 psi internal pressure). In most of the experiments, the

percent opening of the baffle is 20%; even lower percents are used by several workers. However, the actual percent opening of baffle area and its geometry are not disclosed, especially by commercial growers.

The optimum growth conditions for synthesis of quartz based on the work in Bell Laboratories are:[23][24]

Dissolution temperature	-	425°C
Growth temperature	-	375°C
Pressure	-	15,000–25,000 psi.
Mineralizer concentration	-	0.5–1.0 M NaOH
Temperature gradient (ΔT)	-	50°C
% fill	-	78-85%
Growth rate in (0001)	-	1.0–1.25 mm/day

The quality of the grown crystals is also a function of the seed orientation and its quality. Strained seeds generally produce a strained growth region.[25] The seeds are polished to a very fine finish before use. Most high quality crystals are grown using seeds with surfaces perpendicular to *Z*-direction since the *Z*-growth region is the lowest in aluminum concentration. Though the main part of quartz production consists in of *Y-bar* crystals, that is, small crystals (*Z* = 20 to 25 mm, 64 mm seed) capable of several Y-bars per crystal, the pure *Z-bars* are also produced, representing 10 to 20% of this production. In medium and high quality grades, we notice a rise in demand for crystals of very large dimensions and upper medium quality, especially in USA, for manufacturing wafers used in surface wave applications.[11] Earlier, most of the seeds used were natural quartz cut into a definite orientation, but in recent years this practice is only used when a high quality crystal is desired.

The growth of quartz crystals has been understood precisely with reference to the growth temperature, temperature gradient, percent of fill, solubility, percent of baffle open, orientation and nature of seed, and type of nutrient. Also, many kinetic studies have been carried out.[13][14] Figures 5.2 and 5.3 show the solubility of quartz with temperature, growth rate as a function of seed orientation, and growth rate as a function of percent of fill. Figure 5.4 shows hydrothermally grown quartz crystals.

The type of crystal to be grown depends on the application, as different properties are required in each case. For optical use, high uniformity, low strain and low inclusion counts are needed since all of these can affect the transparency. For surface acoustic wave devices, large pieces

are needed which can take a very high quality surface finish. The quality of the material required for resonators used in time and frequency devices varies with the application. The more precise the need, the more stringent are the requirements. For most applications, a truly high quality material is not needed. For high precision uses, such as in navigational devices and satellites, a very high quality material must be used. Most of the recent research on quartz growth is for improved resonator performance, which requires the growth of high quality, and low dislocation quartz, which is discussed in Sec. 5.2.6. Figure 5.5 shows the fabrication of resonators from a single crystal.

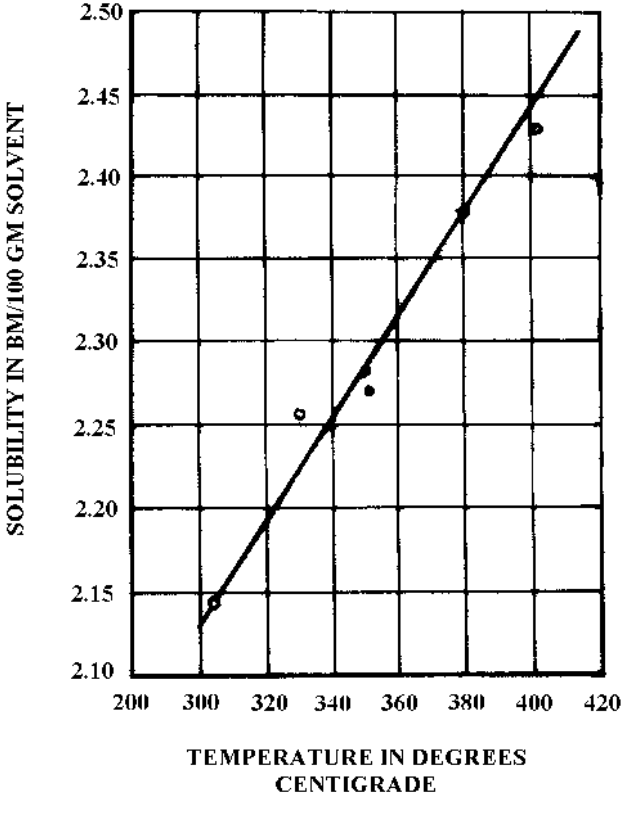

Figure 5.2. Solubility of quartz with temperature.[14]

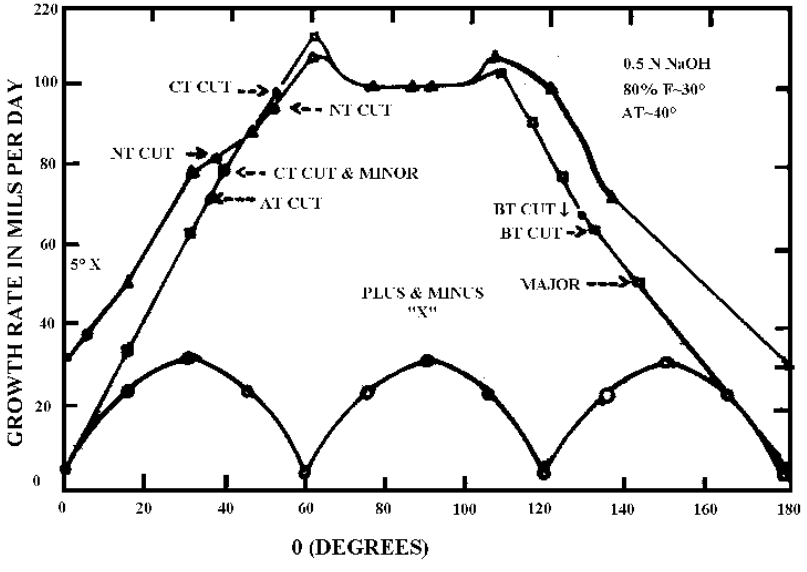

(a)

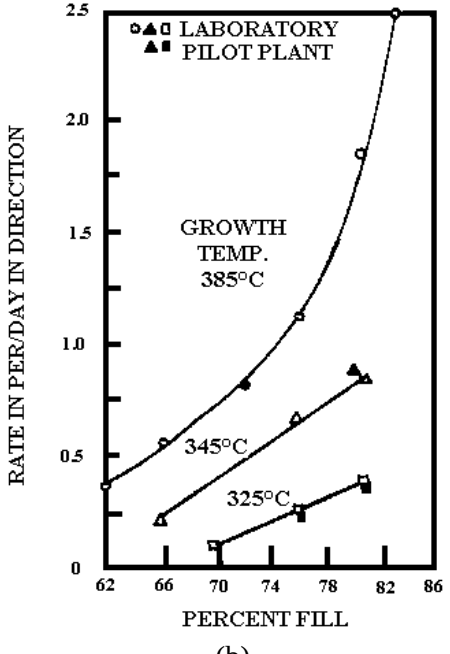

(b)

Figure 5.3. Growth rate of quartz as *(a)* a function of seed orientation, and, *(b)* a function of percent of fill.[14]

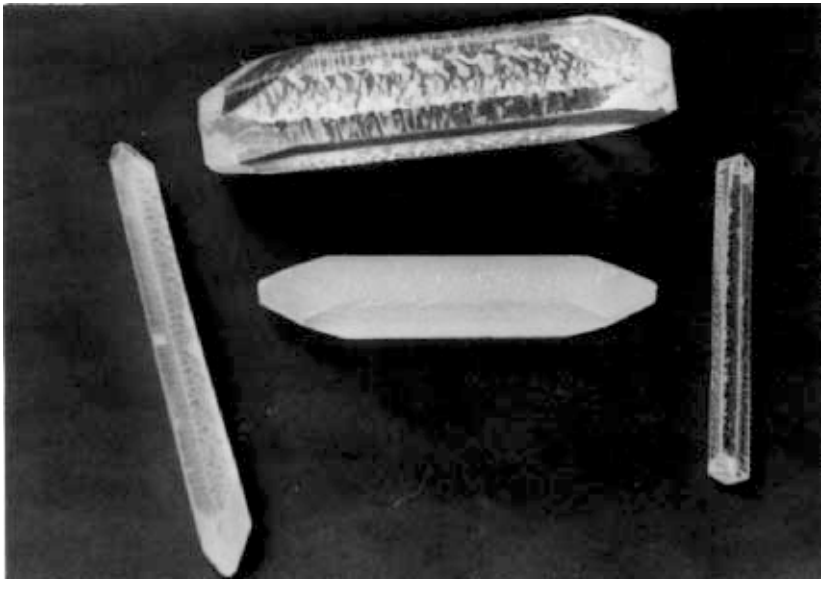

Figure 5.4. Hydrothermally grown quartz crystals.[17]

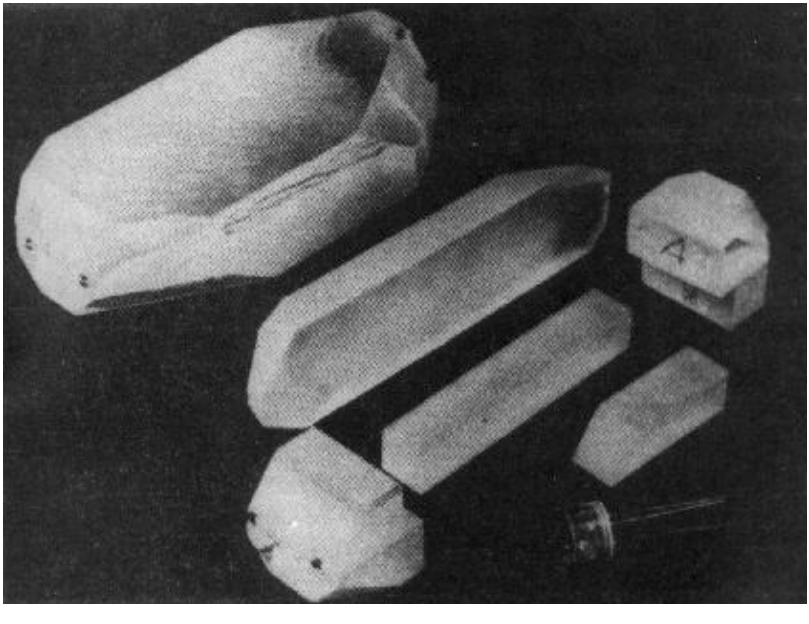

Figure 5.5. Fabrication of resonators from a single crystal.[16]

5.2 GROWTH OF HIGH-QUALITY (AND DISLOCATION FREE) QUARTZ CRYSTALS

It is well known that the hydrothermal growth of quartz in the industrial sector is at least 45 years old. Though many improvements have been brought about, it is still more an art than a truly reproducible industrial and scientific process. We discussed in Ch. 1 the shortcomings in the hydrothermal growth of crystals, especially with reference to the theoretical knowledge. This applies even to quartz growth under hydrothermal conditions. The growth of high quality quartz crystals insists on so many parameters like phase relationships, nutrient's solubility, thermodynamics (state equations, kinetics of reaction, impurities repartition), crystal defects characterization, and so on. The other aspect is that the needs for cheaper material in a wide range of applications like clocks, microprocessors, etc., result in content with a medium quality product, and the low profitability precludes financing long and expensive studies. Though much of the recent publications on quartz is on the possibility of obtaining/growing high quality quartz crystals for stringent electronic applications, this group is still in minority. Except for quartz, no other material coming from hydrothermal synthesis has sizable industrial use; even though $AlPO_4$, $GaPO_4$, $Li_2B_4O_7$, and microcrystallites show interesting promise, industry does not seem ready to make an important R & D effort concerning these products. Thus, it is difficult to get financial support to acquire a better knowledge of hydrothermal growth, which is highly intricate and necessitates an important effort for a long duration of time. Private industry cannot deal alone with the costs of such a program; even in the USA, research programs are government sponsored, especially in defense field.[11]

Several criteria are used to evaluate the quality of quartz crystals. The most commonly used criterion is the Q value or quality factor, which is a measure of the acoustic loss of the material. It is important for a resonator to have high electrical Q value and superior frequency-temperature characteristics. In a piezoelectric resonator, electrical energy and mechanical energy are interconvertible. In such a case, Q is expressed as:

$$Q = \frac{[X]}{R}$$

where X is the inductive or capacitive reactance at resonance and R is the resistance.

The quality factor, Q, can be considered as the inverse of the fraction of the energy lost per cycle. The highest values of Q are required in order to prevent loss of energy into coherent phonons. The acoustic Q for natural α-quartz crystal varies in the range of 1 to 3×10^6 while for synthetic quartz crystals, the value drops down to 2.105 to 1.106. Thus, in the last two decades, the main objective among quartz crystal growers has been to improve Q, which in turn leads to the production of a low concentration of physico-chemical and structural defects. We shall discuss the growth of such quartz crystals of high quality through the study of growth rate, mineralizers, solubility liner material autoclave, seed effect, nutrient effect, and finally the recent advances in the processing of defect-free quartz for stringent electronic applications.

5.2.1 Growth Rate

Growth rate is determined by the ratio of increase in thickness of seed and duration of the run. The growth rate along the main crystallographic axes, R_c, is determined by dividing the thickness of the layer grown on the seed, $(h_1 - h_0)/2$, by the run duration t, and is expressed in mm per day. A much more precise procedure is to determine R_c as a function of weight increment provided the surface area does not change during the run, $R_c = (P_t - P_o)/2S_t\,\delta$, where $\delta = 2.65 \text{g/cm}^3$ is the density of quartz. The growth rate increases with the run duration, the increment being relatively faster during the early hours and days.[26] The growth rate depends upon various factors like growth temperature, experimental pressure (% fill), impurities concentration, presence of defects, seed orientation, solvent/mineralizer, % of baffle opening, and so on. It has also been known for sometime that, qualitatively, acoustic Q is inversely proportional to the growth rate and directly related with to chemical impurities which will be discussed separately. The internal friction (inverse of mechanical Q) is dependent on growth rate of synthetic quartz crystals. This was first demonstrated by Brown.[27] Chakraborty (1977) has studied the dependence of mechanical Q on the growth rate of quartz crystals using different mineralizers, and concludes that the inverse relationship (exponential) between mechanical Q and growth rate is independent of the nature of the solvent in which the crystals have been grown.[28] Thus, the mechanical Q is not dependent on growth rate only, but also upon various other operational variables. For example, for growth on surface normal to (0001) (basal plane growth) or on samples 5° from (0001) (+5° X cut surface), high Q quartz ($Q > 10^6$) can be grown at rates below 20 mil/day

(0.5 mm/day) while even in the presence of Li^+, *Q*'s above 10^6 have ordinarily not been obtained at growth rates much above 60 mil/day (1.5 mm/day). Techniques for obtaining high *Q* at high rates have obvious economic importance. In particular, rates above 100 mil/day (2.5 mm/day) with *Q*'s > 10^6 would provide significant savings in both capital and operating expenses in commercial quartz growth.[29]

5.2.2 Seed Effect

The seed plays a predominant role in the quality of the resulting crystal. For higher frequency applications, a smaller *X*-axis dimension is needed. Material with growth along the *Z*-axis (*Z*-growth material) is desired for resonators as it has been shown that this material is about an order of magnitude lower in aluminum concentration.[30] The thickness of the seed is usually between 1 to 2 mm. Until recently, it was necessary to use natural seeds for the preparation of low dislocation crystals. This is an extremely tedious process since only a small portion of natural crystal is of sufficient quality for seed use, resulting in a complicated selection process. The seeds must also be of sufficient size for useful crystal growth. Christie et al. (1983) have reported that small seeds can be fastened together to make longer seeds, but this has not always been successful.[31] Most seeds used today are fabricated from synthetic quartz crystals. This is a much simpler process since the seeds can be cut parallel from the original seed. Most crystals grown from synthetic seeds, however, contain a large number of dislocations of the order of several hundred per square centimeters. This results in the formation of etch channels in the resonator, which weaken it mechanically and cause problem when electronic devices are deposited on the surface.[32] The studies of Armington and Larkin (1985) have shown that, when a seed perpendicular to the *Z*-axis (but from the *X*-growth region) is used, the dislocation density can be reduced to below ten, and sometimes to zero dislocations per square centimeter (Table 5.2, Figs. 5.6, and 5.7).[33] Although the reasons for this are not entirely understood, it may be related to the fact that, unlike dislocations in the *Z*-region where they form at the seed and grow close to the *Z*-axis, most dislocations in the *X*-region grow at an angle of at least 45°, and are usually close to 90° from the *Z*-axis. Studies have shown that aluminum in the seed does not migrate into the growth regions. Thus, the purity of the crystals produced using seeds cut from the *X*-region is as good as crystals produced from the usual *Z*-seed.

Table 5.2. Dislocation Density in Different Seeds

Seed	Mineralizer	Etch Channel Density
Z	Hydroxide	253
Z	Carbonate	247
X+	Hydroxide	1
X+(reused)	Hydroxide	14

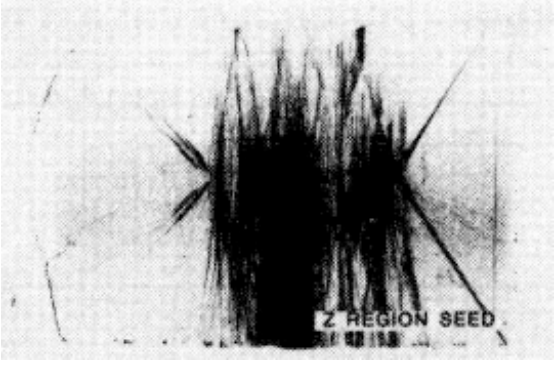

Figure 5.6. Dislocation density in quartz.[33] *(Courtesy of A. F. Armington.)*

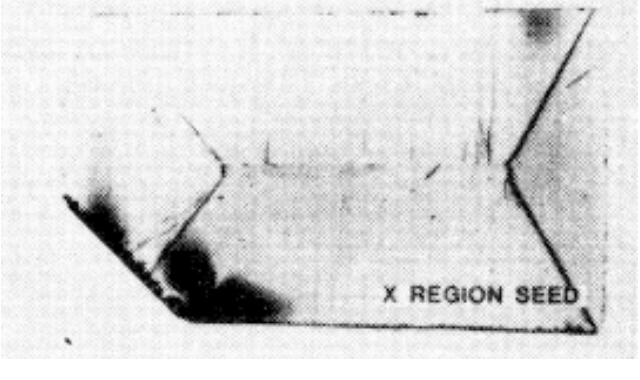

Figure 5.7. Dislocation density in quartz.[33] *(Courtesy of A. F. Armington.)*

5.2.3 Nutrient Effect

The quality of the nutrient has a profound effect on the purity of the grown crystal. It appears that most of the impurities incorporated into the crystal come from the nutrient and not from the autoclave walls. The search for new sources of nutrient is not a new field of research. In the 19th century, earlier workers tried several varieties of nutrient materials to obtain α-quartz under hydrothermal conditions. However, the results were not satisfactory owing to the lack of knowledge on the solubility data for quartz, which resulted in a very low growth rate. In this respect, some serious efforts were initiated by Kolb et al. during 1976. They examined new sources of nutrient to replace Brazilian α-quartz for hydrothermal crystallization.[34] It was found that the acoustic *Q* strain depends upon the source of the nutrient and also its geographic region/location. Both vein and appropriately chosen pegmatite quartz can be used as nutrient. High purity sand can be used as nutrient provided process conditions are altered so as to compensate for its effective lower surface area. Non α-quartz nutrients such as silica glass and silica gel produce initially higher supersaturation and fast growth rates leading to poor quality of crystal growth. However, alterations in process conditions can be made to reduce initial growth rates and prepare reasonable quality crystals. Therefore, in the growth of high quality quartz crystals, *Z*-growth material and recrystallized glass is used as the nutrient material. If future requirements become more stringent, particularly for radiation damage, it will be necessary to reduce the aluminum content even further. In this case, recrystallized glass will be the leading candidate, as higher purity glass is available. This generally requires two runs, since the glass must first be converted to α-quartz.

There are several laboratories throughout the world working to find a suitable nutrient for high quality quartz growth. Hosaka and Miyata (1991) have obtained high quality α-quartz crystals using cristobalite as the nutrient.[35] The authors have used high-purity α-cristobalite powder compacted into grains of 0.5–1.00 mm or into lumps of approximately 1 cm in diameter for the hydrothermal synthesis of α-quartz.

Alpha-cristobalite is a polymorphic form of silica as are quartz and tridymite and has a higher solubility than quartz.[36] Alpha-cristobalite powder[37] has the following advantages: it can be obtained in a high-purity state with low contents of Al and alkaline metallic ions, and can be prepared with relative ease as particles of uniform size. As compared with

the conventional growth of synthetic quartz crystals using Brazilian lascas, the use of α-cristobalite powder may be expected to allow:

(i) Synthesis of high-purity large quartz crystals.

(ii) Synthesis of micro quartz crystals having uniform grain size.

Hosaka (1991) had attempted to crystallize micro quartz crystals by hydrothermal hot pressing method using α-cristobalite powder as a source material.[38] Figure 5.8 shows α-quartz crystals grown at high (left) and low (right) fillings using α-cristobalite as the nutrient. The % fills or pressure greatly influences the growth rate. However, a considerable amount of work has to be carried out for the industrial production of α-quartz using cristobalite as the nutrient.

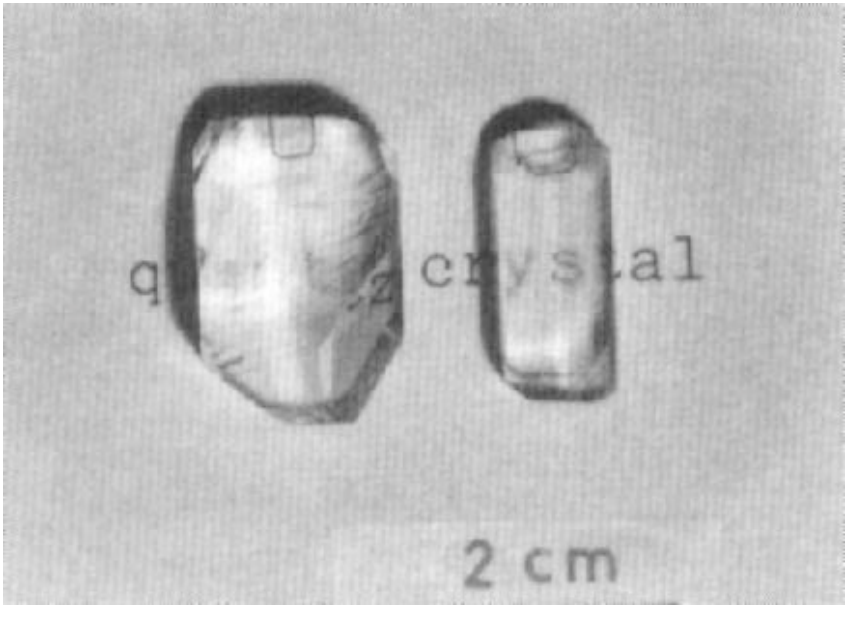

Figure 5.8. *Alpha*-quartz crystals.[38]

5.2.4 Solubility

Solubility is one of the most important aspects in hydrothermal crystal growth. The early literature survey clearly shows that the very slow growth rate achieved until the works of Nacken (Germany 1950) and Wooster and Wooster (1946) were published was mainly attributed to the lack of knowledge of the solubility of quartz.[19][39] The same applies to other compounds also. The first systematic study of the solubility of quartz was carried out by Spezia (1905).[40] Since then, a lot of progress has been achieved in the understanding of the solubility in general for various inorganic compounds. During 1960s, new methods of investigating the solubility and the new experimental set up for the determination of solubility under hydrothermal conditions were proposed.[41][42]

The solubility of quartz in pure water was found to be too low for crystal growth (0.1–0.3 wt %), but the solubility could be markedly increased by the addition of OH^-, Cl^-, F^-, Br^-, I^-, and acid media which act as mineralizers. For example, the reactions

$$SiO_2 + 2OH^- \rightarrow SiO_3^{2-} + H_2O$$

$$2OH^- + 3SiO_2 \rightarrow Si_3O_7^{2-} + H_2O$$

show the formation of various complexes or species during the hydrothermal crystallization of quartz. Hosaka and Taki have used Raman spectra to identify and quantify such species.[43]

In pure aqueous solutions (even at 400°C and 25000 psi), the solubility of quartz is too low to allow growth to take place in any reasonable time. Alkaline additions, such as NaOH, Na_2CO_3, KOH and K_2CO_3 are all effective as mineralizers in this pressure and temperature range. A small increase in molarity results in only a slight increase in the growth rate, whereas large increase begins to produce an additional phase along with quartz. The minimum molarity for good growth rate is about 0.25 M for NaOH. Concentrations of about 4.0 M for NaOH and 2.0 M for KOH form sodium or potassium silicates along with α-quartz. Laudise and Ballman (1961) have measured the solubility of quartz in 0.5 M NaOH as a function of % fill and temperature. The quartz solubility dependence on % fill is shown in Fig. 5.9.[44]

An important result of solubility determinations is the delineation of the pressure, temperature, and composition regions where the temperature coefficient of solubility is negative. These regions are to be avoided in the growth of quartz, since they require a different setup; otherwise, they result in the loss of seed crystals.

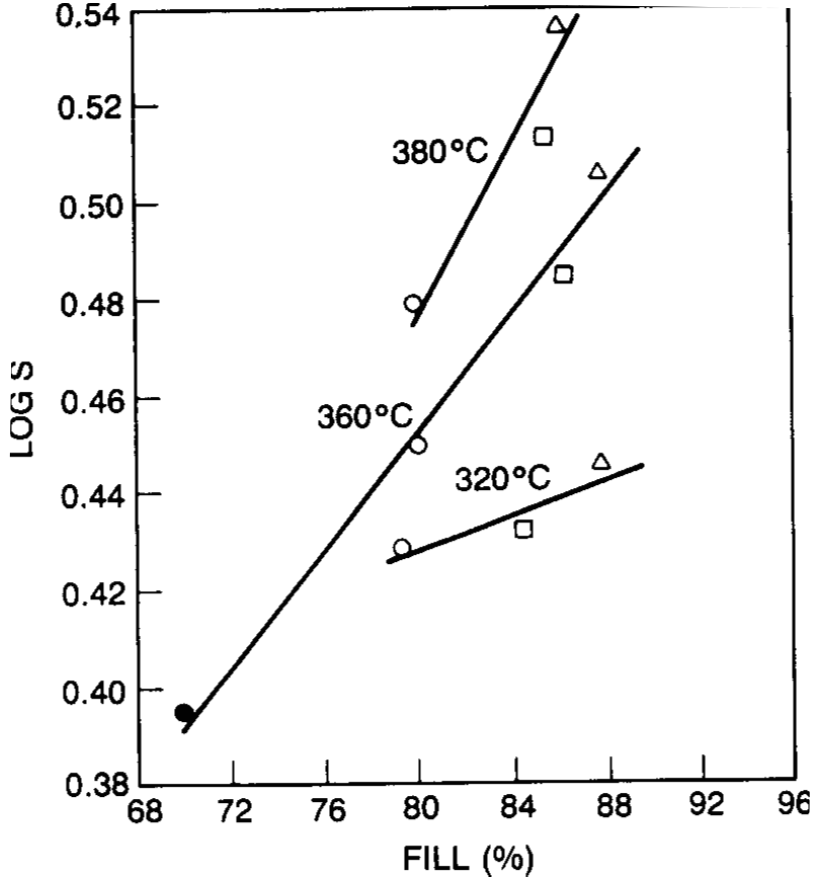

Figure 5.9. Quartz solubility dependence on % fill.[44]

In recent years, mixed solvents are being used even in the growth of quartz. High-quality large quartz crystals have been obtained in NaCl and KCl solutions, NaOH and Na_2CO_3 solutions, (10%).[45][46] Most of the literature data available on the solubility of α-quartz deals with the data in various solutions at elevated temperatures and pressures. It was recently observed that, in the growth of quartz crystals under hydrothermal conditions, the evaluation of pressure generation and its effect on the dissolution in different aqueous solutions are the important steps. Hence the authors have studied the solubility of α-quartz in NaOH (1M) + Na_2CO_3 (1M) using high-pressure conditions from 200 MPa to 350 MPa at temperatures of 400°C.[46] The impetus for this work was provided by the fact that high frequency applications of α-quartz require sheets with small thickness of the same order of size as the defects (such as inclusions, etch pits and dislocations). Thus, the pressure can make new solvents viable for hydrothermal growth, especially by reducing their concentrations. Figures 5.10 and 5.11 show the solubility limit comparison between NaOH (1M) and Na_2CO_3 (1M) vs. pressure at 400°C; and log solubility (S_1) in NaOH (1M) and in Na_2CO_3 (1M) vs. 1/*P*. These experimental results show that Na_2CO_3 appears to be a better solvent than sodium hydroxide in high-pressure domain for a temperature close to 400°C. From Fig. 5.11, the enthalpy values have been calculated and the values are as follows:

$\Delta H_T = 2395 \pm 5$ cal/mole for NaOH (1M); $200 \leq P \leq 350$ MPa

$\Delta H_T = 4001 \pm 2$ cal/mole for Na_2CO_3 (1M); $150 \leq P \leq 350$ MPa

5.2.5 Defects Observed in Synthetic α-quartz Single Crystals

The defects present in the synthetic α-quartz crystals play an important role in determining its quality and in turn applications. Much of the recent works on quartz is essentially focussed on the defect studies. All the defects present in quartz can be classified into two types:

- The physico-chemical defects
- The structural defects

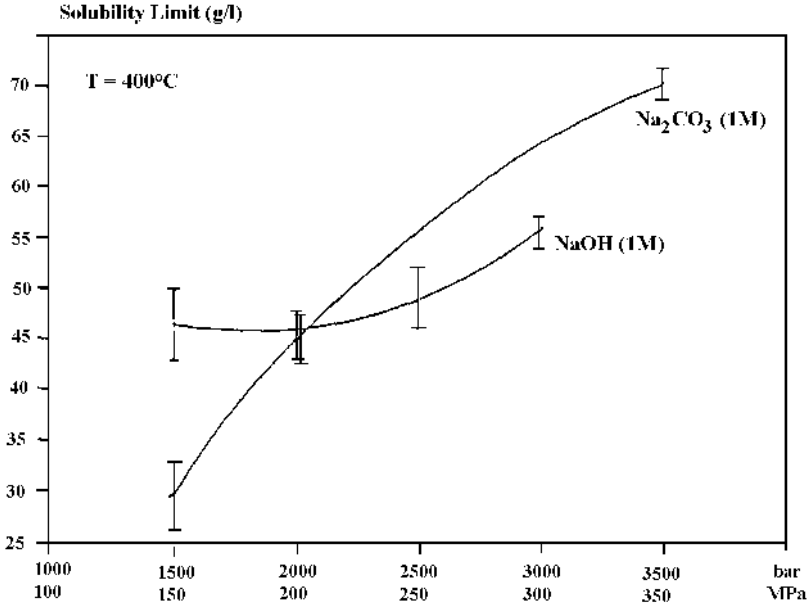

Figure 5.10. Solubility limit comparison between NaOH (1M) and Na_2CO_3 (1M) vs. pressure at 400°C.[46]

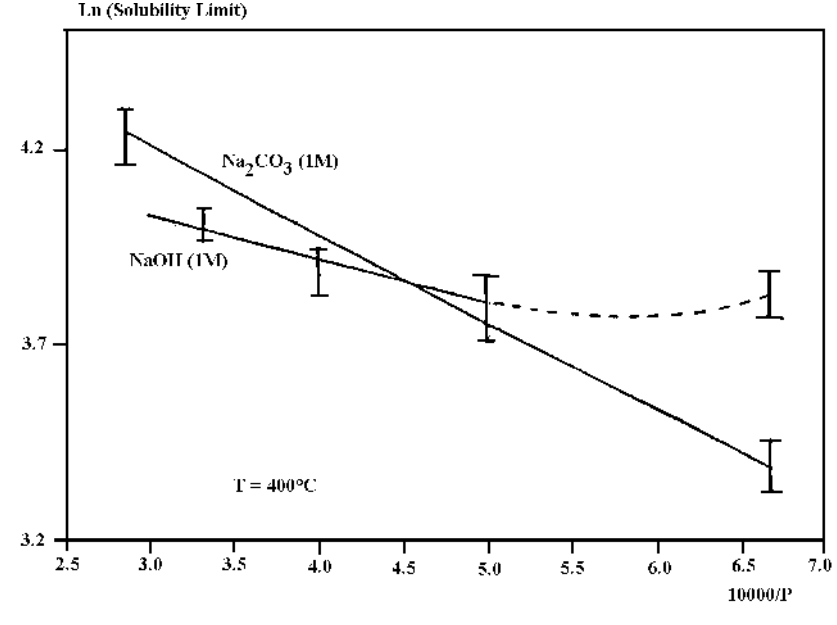

Figure 5.11. Log solubility (S_1) in NaOH (1M) and in Na_2CO_3 (1M) vs. $1/P$.[46]

Physico-chemical defects are mainly induced by the nature of the nutrient or the solvent and also by chemical contamination of the solution by the metal constituting the reaction vessel. Quite often, solid or liquid inclusions like $NaFe^{3+}Si_2O_6$ (acmite) are inserted in the α-quartz. The most important impurity in quartz is H^+, which easily fits interstitially in the large (1 Å) channels that lie parallel to the *c*-axis to charge compensate for Al^{3+} which goes to a Si^{4+}. It enters the lattice from the growth solutions as OH^-, the O^{2-} being incorporated in the SiO_2 lattice. In thermodynamical conditions, different cations (in particular Li^+) can be in the interstitial positions, in particular for compensating the $Si^{4+} \rightarrow M^{3+}$ cationic substitution into the α-SiO_2 lattice. Figure 5.12 shows the effect of growth rate on Al^{3+} concentration in the *Z*-region of grown crystals using hydroxide mineralizer.[47] Aluminum concentration was determined by EPR.[16] Similarly, Laudise has studied the dependence of the effective partition coefficient for OH^- impurity in quartz on growth rate (Fig. 5.13).[48] Lithium salt is added to the solvent to check the aluminum concentration in the grown crystal. The entry of Al occurs in the use of (OH) and (CO_3) based mineralizers. Table 5.3 gives the distribution of impurities in different sectors of synthetic quartz, which has been studied by Yoshimura et al. (1979), and Iwasaki and Kurashige (1978).[49][50]

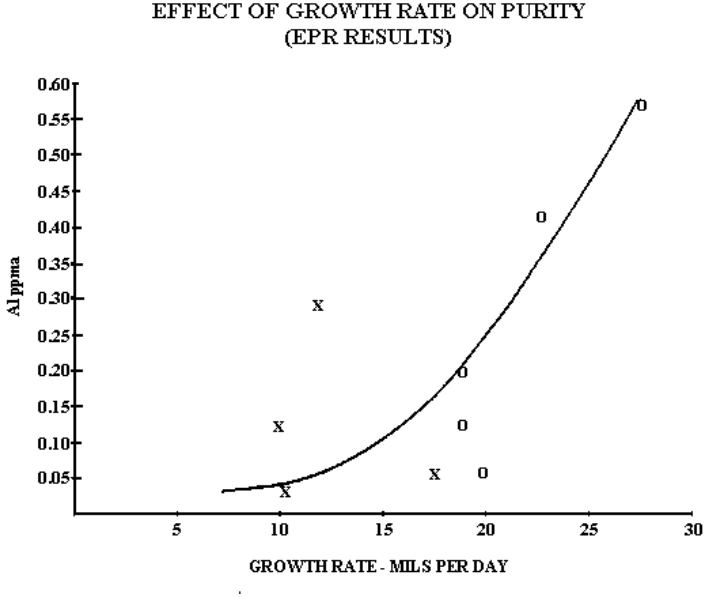

Figure 5.12. Effect of growth rate on $A1^{3+}$ concentration in the *Z*-region of growth crystals.[16]

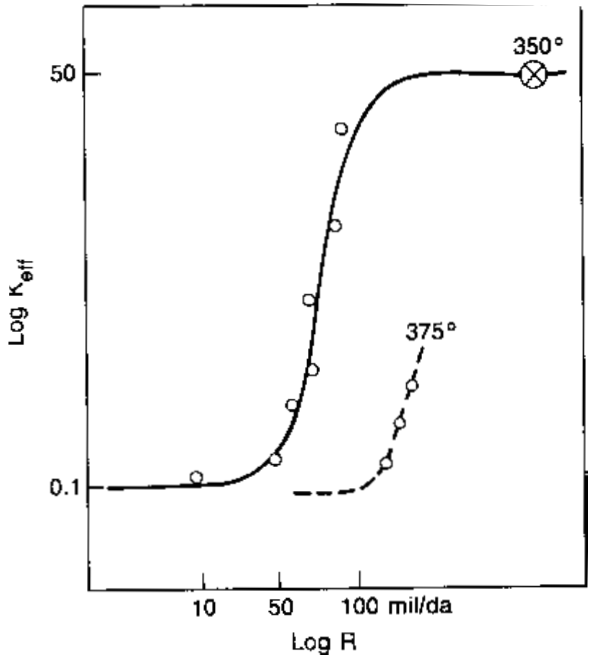

Figure 5.13. Effective partition coefficient for OH^- impurity in quartz on the growth rate.[48]

Table 5.3. Impurities in Synthetic Quartz Crystals (ppm)

Sector	Al	Na	Li
Z	5	1	0.5
+X	31	9	5
-X	122	40	5
S	85	26	16

The structural defects in quartz are basically the dislocations. Their origin can be due, generally, to foreign particles, thermodynamical parameters governing the crystal growth, or hydrodynamic conditions inside the reaction vessel.

5.2.6 Processing of α-quartz for High Frequency Devices

The study of the type of defects present on silica surfaces would be of great importance for a better understanding of electrical or piezoelectric properties. The development of high frequency devices (24 MHz $\rightarrow$ 100 MHz or more) induce some strong constraints concerning the shaping of the α-SiO_2 material. The low defect, high purity synthetic quartz should have the following characteristics:[51]

Parameter	Desirable	So far achieved
Etch channel density	< 10 / cm ^{2}	< 86
Inclusion density	< 10 / bar	
Impurity concentrations (ppb)		
Al	< 200	700
Li	< 300	300
Na	< 500	1640
K	< 40	300
Fe	< 100	1800
Q (3500/3800 cm^{-1})	< 2.5 x 10^6	> 2.5 x 10^6
Strain	none	variable
Fringe distortion	< 0.05 RMS	variable

The existence of defects, either physico-chemical or structural, in synthetic quartz crystals leads to the critical modifications of devices. There are three different parameters on which the quality of quartz depends:[52]

i. Chemical impurities, e.g., $(OH)^-$ distribution, induce a large decrease of the acoustic *Q*. The substitution $O^{2-} \rightarrow (OH)^-$ being coupled with the cationic one ($Si^{4+} \rightarrow M^{3+}$), the M^{3+} impurities can play an important role concerning the chemical aging of resonators and its behavior vs. ionizing radiations.

ii. Crystal defects like dislocations, etching channels, fractures, etc., which influence the acoustic distribution.

iii. Inclusions (iron, sodium, acmite, aluminum, etc.).

As the application of quartz goes to higher and higher frequency devices, the thickness of the quartz plate drops. For example:

24 MHz range applications: ~ 70 μm thickness

100 MHz range applications: ~ 6–7 μm thickness

The thinning down of the quartz plate depending upon the frequency measurements and can be expressed as

$$F(\text{MHz}) = \frac{K\left(\text{MHz}\,\mu\text{H}^{-1}\right)}{e(\mu\text{m})}$$

where *e* is the plate thickness, *K* is a constant characteristic of the material and of its orientation, and *F* is the resonance frequency.

Sweeping is one of the most popularly used techniques in recent years to enhance the performance of quartz resonators. Sweeping or solid state electrolysis or electro-diffusion is generally performed under vacuum or air or hydrogen or desired atmosphere.[53]-[55] During sweeping, the crystal is placed in an electric field and heated. Figure 5.14 shows the schematic diagram of the sweeping apparatus. Then, there is a migration of the impurities, and some modifications are induced within the crystal. According to the parameters used by the manufacturer during the sweeping process, and the quality of the as-grown crystals, the results could be very different. Sweeping reduces the formation of etch tunnels. The effect of sweeping is to remove lithium and sodium deposited interstitially during the growth. These ions are usually trapped along an angstrom-wide

tunnel, which is parallel to the *Z*-axis in the quartz crystal lattice. These ions, in an interstitial position, interact with aluminum impurities substitutional in the lattice to form Al-Li centers, which have shown to be weakly bonded and are the cause of low radiation tolerance in a resonator. In the sweeping process, these are replaced by Al-OH or Al-hole centers, which have a much higher radiation tolerance.

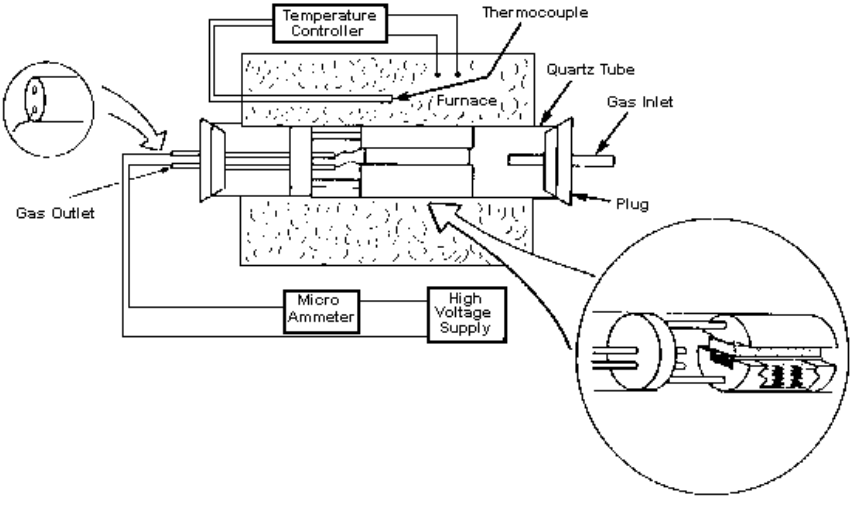

Figure 5.14. Schematic diagram of the sweeping apparatus.[55]

Sweeping is influenced by the electric field, strength, electrode type, and atmosphere. It takes less time in air due to the availability of water in the atmosphere.[56] Electrodes, usually platinum, or gold or aquadog are deposited on each of the *Z* surfaces of a lumbered bar. The crystal is then subjected to a field of 1000–2000 volts/cm (thickness) at temperature 500–550°C. The current is continuously measured and the sweeping is considered completed when the current has dropped to a constant value. It takes usually 5 to 7 days to remove alkalies. In some quartz, the sweeping may take 7 days or even more. Sweeping has also been used to dope quartz crystals in order to determine the effect of the dopant on the properties of the crystallization of quartz. A vast amount of literature data shows that sweeping can not become a routine process even

if all the same experimental conditions are ever applied. The quality of the swept crystal can change in such a way that the modifications are sometimes unexpected. So, each industrially swept crystal must be controlled before using. Some of the controlling techniques are the x-ray topography and the infrared spectroscopy. These techniques help to characterize the physico-chemical defects and the α_{3500} value (Q factor). The reader can refer to the works of Refs. 12, 57, and 58.

There are several other techniques employed for the fabrication of piezoelectric high- to ultrahigh-frequency devices based on quartz resonators. The important ones are chemical polishing and ion beam etching (IBE). The reverse thermodynamic relations are employed for the refinement of chemical polishing. Several solvents like HF and NH_4HF_2, NaOH, KOH. xH_2O, NaOH. xH_2O, etc.[59]

Similarly, the industrial chemical etching process is specially dedicated for large thickness removals without damaging the blank surface texture. This is most useful for frequency applications of quartz, because the mechanical grinding and lapping introduce surface stresses. Fluoride media is the most popularly one for this type of chemical polishing.[60] Recently, Cambon et al. (1994) have tried industrial chemical etching successfully in the temperature range of 150 to 180°C using concentrated NaOH solvents.[61] During the chemical etching process, several factors influence the process: kinetics, etching temperature, etching time, plate orientation, SiO_2 concentration, solvent concentration, wafer carrier geometry, and so on. Using this process, about 3200 quartz plates can be processed. The resonators manufactured by this process have demonstrated a high level of performance, even higher than those obtained by mechanical means.

Future avenues in this direction are: improvements on theoretical knowledge, improvements in the quality of solvents, nutrients, and seeds, autoclaves' technology, material used for autoclaves, dimensional ratio (diameter/length), crystallization zone/dissolution zone, basic questioning of the validity of presently used growth parameters (P,T), and better understanding of complementary treatments like sweeping, chemical etching, etc. Thus, any work on quartz is still a promising field, and it will have some important consequential effects on hydrothermal growth, in general, and facilitate the development of other materials production.

5.3 BERLINITE

Berlinite, $AlPO_4$ is named after N. J. Berlin (1812), a pharmacologist of the University of Lund. Its physical properties are shown in Table 5.4.[62] Berlinite replaces quartz in electronic devices because its large mechanical coupling factors are greater than α-quartz, and its resonant frequency is nearly independent of temperature for certain orientations.[63]–[65] Berlinite is also interesting because its presence in Ca aluminum phosphate bioglass ceramics is believed to lead to higher bioactivity of bone implants.[66][67] Table 5.5 gives a tentative comparison with quartz.

Table 5.4. Physical Properties of Berlinite and Quartz (Schwarzenbach, 1966)[62]

Properties	$AlPO_4$	Quartz
Density	2.64 (natural) 2.56 (artificial)	2.655
Hardness	6 – 7	7
n_e	1.529 ± 0.003	1.544
n_o	1.519 ± 0.003	1.535
Birefringence	+ 0.01	+ 0.009
a	4.94291	4.9138
c	10.94761	5.4052
c/*z*	5.4738 Å	
c/*a*	2.21481	1.10
c/2*a*	1.1074	
space group	$P3_121$ or $P3_221$	$P3_121$ or $P3_221$
z	3	3

Table 5.5. Tentative Comparison with Quartz (Thickness *Y* Rotated Resonators at Same Frequency)

Useful coupling coefficient (AT filter trapped resonators)	Enhanced by 1.4 – 1.5
Shift of oscillators or band width of filters (AT cut)	Twice
Angular sensitivity (1st order FTC)	Reduced
Thermal stability (higher order FTC)	Better
Q factor propagation losses	Already sufficient (may be comparable)
Thickness of plates (AT)	Reduced by 1.15
Electrode dimensions (AT)	Reduced by 1.32 (TT)
(Same plating 2D TT of TS)	Reduced by 1.23 (TS)
Nonlinear properties	To be determined
"Dry" berlinite has similar C, E, EPS constants, first order TC and much reduced higher order TC.	

Berlinite occurs in nature associated with augelite, attacolite, and other phosphates as small crystals at the Westana Iron mines near Nasum, Kristiaanstad, Sweden. However, the synthetic berlinite is more popular and abundant and it can be obtained as fairly big crystals. The first successful growth of berlinite crystals was by Jahn and Kordes (1953), followed by Stanely (1954).[68][69] Stanely carried out the experiments in a sealed borosilicate glass vessel placed in a low pressure environment. Mason (1950)[70] carried out the piezoelectric measurements for a small crystal of berlinite. However, the importance of berlinite only came into light in 1976 when Chang and Barsch[63] studied the piezoelectric properties of berlinite, and reported large mechanical coupling constants and that its resonant frequency was nearly independent of temperature for certain orientations.

The main problem connected with the growth of berlinite is the negative temperature coefficient of solubility, which insists on some special growth conditions, because of the lower solubility at higher temperatures, and higher solubility at lower temperatures. One of the principal problems in a systematic growth of $AlPO_4$ crystals is the growth rate relationship in H_3PO_4, and the lack of good solubility data (because of the negative temperature coefficient of solubility) at the constant fill conditions, which are essential for successful growth.[71]

Although so much of progress has been achieved in the growth of berlinite crystals, our knowledge on $AlPO_4$ is still comparable to that of quartz some thirty years ago, particularly with reference to solubility, reproducibility, crystal perfection, phase equilibria data, crystal size, etc.

Today it is possible to grow more than 500 kgs of dislocation-free high-purity quartz in a single experimental run. However, in the case of berlinite, it can not be more than a few hundred grams. The major problem is the highly corrosive phosphoric acid media in which the growth takes place.

5.3.1 Crystal Chemical Significance of the Growth of $AlPO_4$ Crystals

Berlinite is isostructural with quartz, $Si(SiO)_4$, and the artificial compound $AlAsO_4$. It shows the same thermal inversion as SiO_2,[72] although, at slightly lower temperatures, it crystallizes in hexagonal system—trigonal trapezohedral class-32. Artificial crystals are very similar to quartz with $(10\bar{1}1)$ $(01\bar{1}1)$ and (1011) faces. The natural crystals are massive and granular. As mentioned above, berlinite is isostructural with quartz but has a doubled *c*-parameter. It consists of alternating AlO_4 and PO_4 tetrahedra linked with vertices. Sosman[73] has reviewed all the forms of silica reported up to 1960. According to him, there are twenty-three polymorphic modifications of quartz, and eleven of them are the basic ones. Berlinite, although isostructural and isoelectronic with quartz, shows only six polymorphic modifications analogous to six major varieties of silica. Figure 5.15 shows six polymorphic modifications of berlinite analogous to six polymorphic modifications of quartz. The structure of all the six forms of berlinite can be described under three subgroups, i.e., quartz, tridymite, and cristobalite with higher and lower temperature forms.

The growth of any compound does not depend only upon the growth techniques and growth parameters like the starting materials, flux agents, mineralizer, temperature, pressure, rate of heating or rate of cooling, but also upon its crystal chemical parameters. A systematic study of the synthesis of ABO_4 compounds (A = Al, Fe, Cr, Co, Ga, B, Mn; B = P, As and V) and quartz with reference to their crystal chemical significance yields very interesting data which help to understand the growth technique of ABO_4 compounds.[74][75]

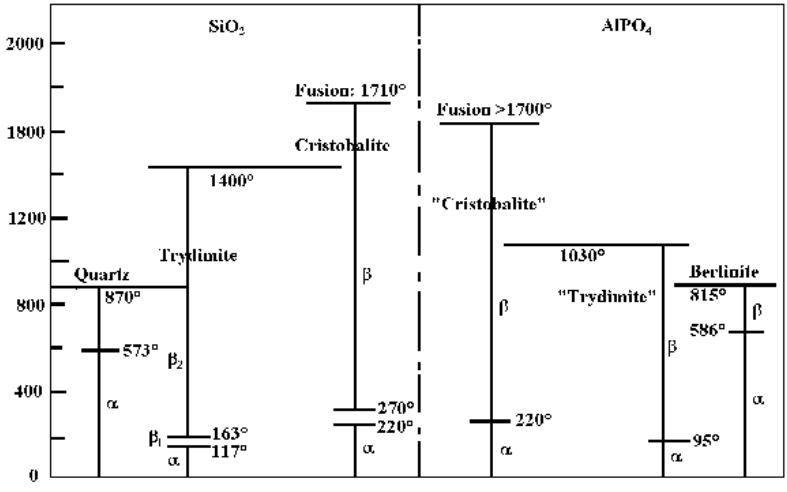

Figure 5.15. Six polymorphic modifications of berlinite analogs to six polymorphic modifications of quartz.

5.3.2 Solubility of Berlinite

Solubility is an important parameter in the successful growth of any compound in the form of large single crystals. The lack of solubility data is responsible for the earlier failures in the growth of $AlPO_4$ crystals. It was only in the late 1970s and early 1980s that reports on the solubility of $AlPO_4$ appeared in the literature. The problem associated with the growth of large single crystals of $AlPO_4$ is directly related to the lack of a

systematic study of the solubility and partly to the P_2O_5 pressure. Although, several reports have appeared on the solubility measurements with reference to various parameters, still there is no unanimity in the results. The solubility of berlinite was first determined by Jahn and Kordes (1950) in orthophosphoric acid above 300°C and it was found positive (Fig. 5.16).[68] Subsequently, Stanley (1954) reported a negative solubility for berlinite in 6.1 M H_3PO_4 (Fig. 5.17).[69] The solubility of $ALPO_4$ varies widely with the type of solvent used. Some authors claim that solubility of $AlPO_4$ in HCl is similar to that in H_3PO_4. The most important difference is the higher solubility at comparable mineralizer concentration.

The authors[76] have made an attempt to study the solubility of $AlPO_4$ in some new solvents like HCOOH, NH_4Cl, Na_2CO_3, $NH_4H_2PO_4$, NaF, KF, LiF, etc. The solubility of $AlPO_4$ (in wt %) as a function of temperature and at a pressure of 2 kpsi in 2M HCOOH solution is shown in Fig. 5.18.

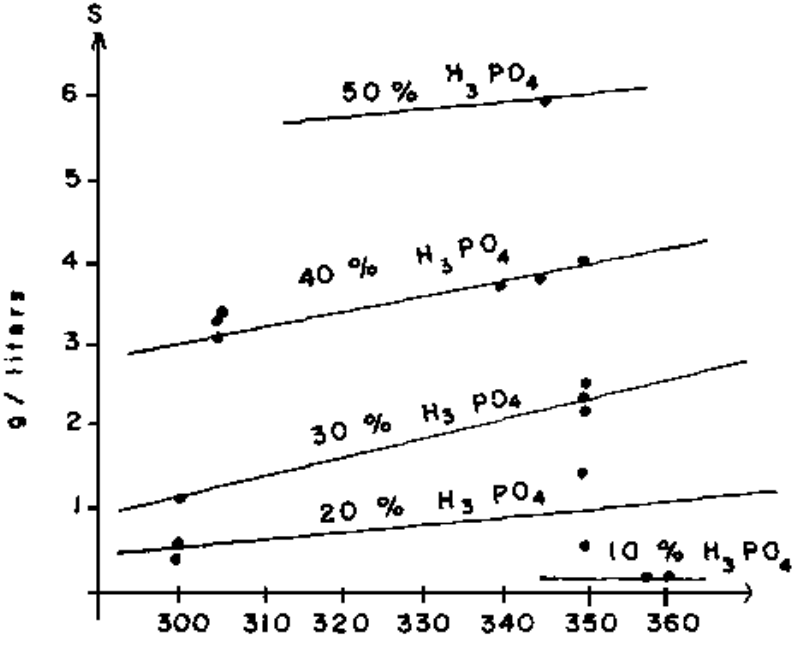

Figure 5.16. Solubility of berlinite in orthophosphoric acid above 300°C.[68]

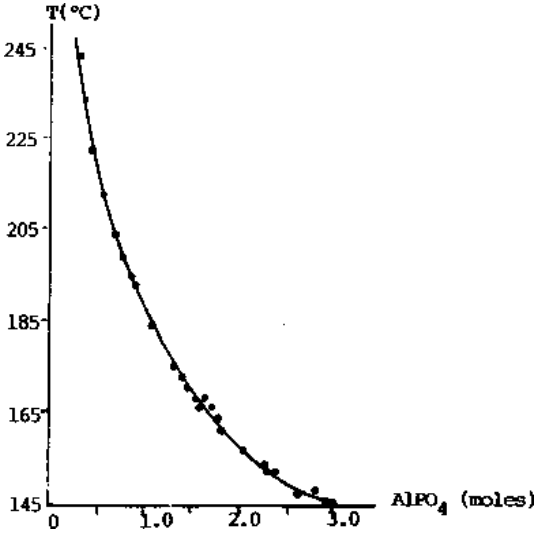

Figure 5.17. Negative solubility for berlinite in 6.1 M H_3PO_4.[69]

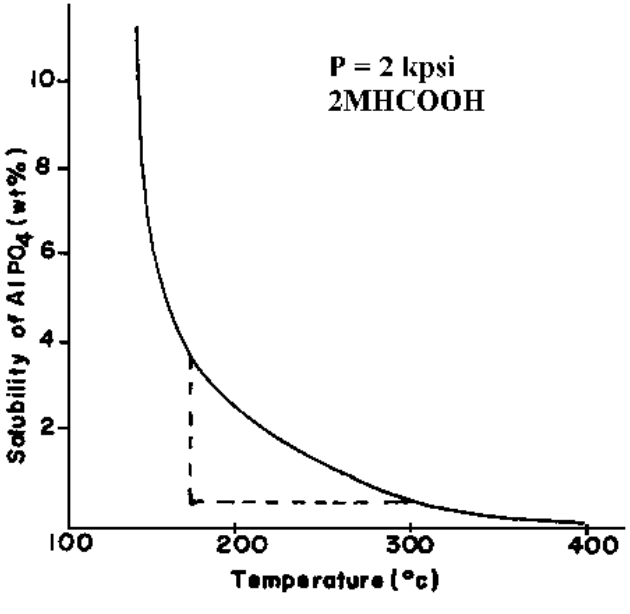

Figure 5.18. Solubility of $A1PO_4$ (in wt %) as a function of temperature.[76]

Recently, it has been shown that the solubility of $AlPO_4$ in H_2SO_4 is retrograde with respect to temperature and higher than in H_3PO_4 and HCl at comparable temperature, pressure, and acid molarity. However, the viscosity of sulphuric and phosphoric acid solutions is greater than that of HCl. Hence, the addition of HCl to H_2SO_4 would form a more efficient solvent for the growth of $AlPO_4$.[77] Figure 5.19 shows solubility as a function of temperature in H_2SO_4 + HCl mixtures. The authors have also carried out thermodynamic interpretation of the solubility data. The dissolution of berlinite in the mixtures of acids H_2SO_4 and HCl is a process of complex formation between Al^{3+} and the ligands present in the solution: OH^-, H_2O, Cl^-, HSO_4^-, SO^-_4, $H_2PO^-_4$. At low temperature, the complexes are similar to those of $AlPO_4$ in HCl; that is with Al-Cl complexes predominating. Even polynuclear complexes might form a broader metastable zone.

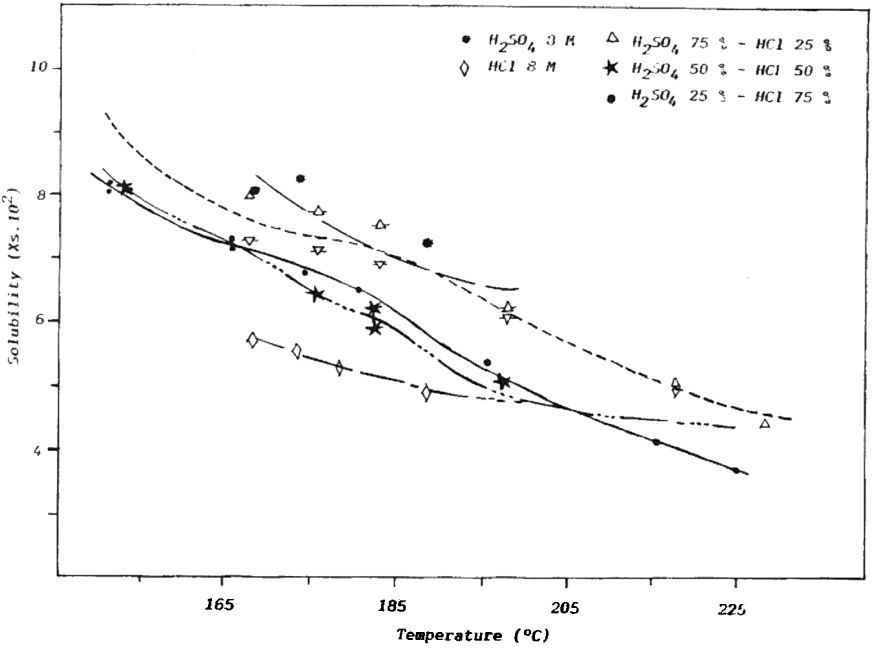

Figure 5.19. Solubility as a function of temperature in H_2SO_4 + HCI mixtures.[17]

With the rise in temperature, the association of Cl^- with H^+ increases the yield of HCl and destabilizes the $[Al^{3+}]$ complex. Under these circumstances, sulphate and monohydrogen phosphates replace chloride ligands and force a change in the coordination number of Al from six to four due to the steric effect. Similarly, H^+ also tends to destabilize the complex with sulphate and becomes $H_2PO^-_4$ hegemonic ligand as its association constant with H^+ does not vary significantly with a rise in temperature. Finally, the nucleation takes place by polymerization of tetrahedral $[Al^{3+}]$ complexes.

Table 5.6 gives comparative data of solubility of $AlPO_4$ obtained for various mineralizers under varying experimental condition.[76]

Table 5.6. Comparative Data of Solubility

Solvent	T (°C)	P (Kpsi)	Time (days)	Remarks
3M HCOOH	300	1	5	—
3.05M NaOH	170	10	3	Residue not $AlPO_4$
2M NH_4Cl	300	1	5	High solubility
4.62M Na_3PO_4	300	10	3	Residue not $AlPO_4$
2M HCOOH	300	11	5	Good solubility
3M Na_2HPO_4	300	10	5	1 % solubility
2.5M NH_4Cl	300	1	5	Fairly good solubility
3.05M CH_2COOH	170	10	3	Negligible solubility
2M $NaHCO_3$	300	1	5	Fairly good solubility
2M NaCl	300	1	5	Negligible solubility
3.05M NaCl	170	10	3	4 % solubility
2M NaF	300	1	5	Good solubility
2M KF	300	1	5	Good solubility
2M LiF	300	1	5	Good solubility
3.05M NH_4HF_2	300	10	5	Residue not $AlPO_4$
2M $NH_4H_2PO_4$	300	1	5	Negligible solubility
2M HCl	300	1	5	Good solubility
3.05M NH_4HF_2	170	10	5	Residue not $AlPO_4$
3.05M HNO_3	170	10	5	Negligible solubility
3.05M NaCl	300	10	4	Negligible solubility
1.0M Na_2CO_3	300	1	5	Negligible solubility

5.3.3 Crystal Growth

Berlinite could be best grown only by hydrothermal technique. The α-berlinite is stable up to 584°C, and below 150°C the hydrates and $AlPO_4.H_2O$ are stable. Therefore, the growth temperature should be greater than 150°C but less than 584°C. However, the solubility and *PVT* studies have clearly shown that crystal growth must be carried out at less than 300°C because of the reverse solubility. Several versions of the hydrothermal growth of berlinite single crystals have been tried to suit the solubility.

Nutrient Preparation. Berlinite in small crystal form can be obtained by hydrothermal reactions of H_3PO_4 with different chemicals containing aluminate.[69][78]–[80] Normally, high purity alumina is used as the nutrient, because of the purity of the grown crystals. The crystallization reaction is:

$$Al_2O_3 + 2H_3PO_4 \rightarrow 2AlPO_4 + 3H_2O$$

These fine crystals of aluminum orthophosphate are in turn used as the nutrient to grow bigger single crystals of berlinite.

The temperature coefficient of solubility of $AlPO_4$ is negative in the temperature-pressure range below 300°C. Thus, in the usual hydrothermal temperature gradient where the bottom of the autoclave is hotter than the top, $AlPO_4$ would be expected to nucleate preferably in the bottom region, so one would like to place the seed in the lower hotter region and nutrient in the upper cooler region.

The most important modifications suggested from time to time in the growth of berlinite crystals are as follows:

i. Crystal growth by slow heating method.

ii. Crystal growth by composite gradient method.

iii. Crystal growth by temperature gradient.

iv. Growth on seeds.

Chai[79] suggested the following nutrient preparation conditions for large (kgs) quantities, where the temperature is cycled:

Solvent H_3PO_4 (molar)	6.1
% Fill	81
$AlPO_4$ charge (gm)	45 presaturation at 25°C
Initial temperature (°C)	150
Final temperature (°C)	275
Differential temperature, dT (°C)	1 – 2
Heating rate (°C)/day	10
Method of heat rate increase	10
Yield (gm)	
> 60 mesh*	19.5 gm (70 % yield)
< 0 mesh	8.1 gm
Total yield	27.6 gm
Run duration (day)	15

* 60 mesh = 0.25 mm

Crystal Growth By Slow Heating Method. The method was previously described in Refs. 76 and 81–85, and it was mainly used for improving the quality of seeds and to enhance the size of the crystal with conditions similar to those used to obtain nucleations. A major drawback of this method is the impossibility of obtaining crystals of sufficient size in one operation due to the limited quantity of aluminum phosphate available in the solution.

Synthesis of berlinite crystals under lower temperature and pressure conditions using slow heating method was carried out using acid digestion bombs (T = 100–250°C; P = 100–300 atm) and smaller Morey autoclaves (T = 200–250°C; P = 300–1000 atm). The nutrient was taken in teflon liners.

The experiments at higher temperature (T > 500°C and P > 100 bars) yielded the β-berlinite. With an increase in the pressure, other high-pressure modifications of aluminum orthophosphate belonging to the cristobalite form were obtained.

Crystal Growth By Composite Gradient Method. In order to gain more flexibility in adjusting the growth rates for Z seeds and to avoid the preliminary work of crystal growth, nutrients of sufficient size (that did not cause crystallites to drop on crystals) needed to be obtained. A modification of the horizontal gradient method was originally proposed in Ref 87. Recently, berlinite crystals have been obtained by this method

successfully.[87] The autoclave used in the initial experiment is shown in Fig. 5.20. The following growth conditions were chosen by the authors[86][87] after experimental trials:

- Silica glass autoclave: 100 cm, diameter 30 mm
- Ratio hot/cold zone: *x* /1
- Solution: H_3PO_4, $H_2O/AlPO_4$ (6.5/1.1)
- Growth temperature: 170°C
- Horizontal temperature difference: $5 < T < 30$°C
- Construction diameter: 10 mm
- Powdered nutrient
- Filling: 80 %

Growth With Reverse Temperature Gradient. This is a more popular and widely used method in the growth of berlinite crystals. Here, the nutrient is kept in a casket at the upper portion of the autoclave, which is cooler. The nutrient is nothing but the crystalline powder or fine grains of $AlPO_4$ obtained by a slow heating method. The temperature of the bottom of the liner is kept at slightly higher temperature and this is the zone of crystallization, where berlinite can be crystallized either spontaneously or on seeds.[88]

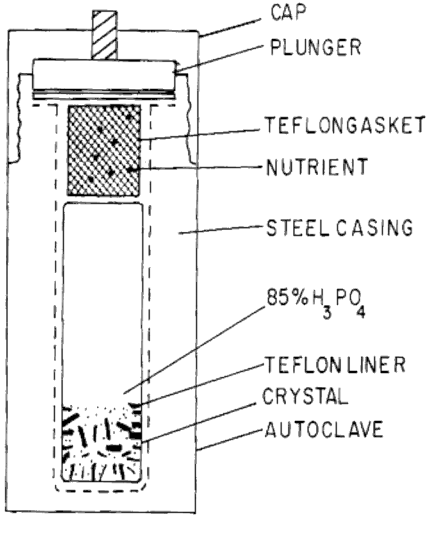

Figure 5.20. Autoclave used in the berlinite synthesis.[76]

Crystal Growth On Seeds. Spontaneously nucleated seeds and oriented seeds cut from grown crystals are mounted on a platinum frame which is placed in the bottom (hotter) region of an autoclave, and the nutrient (~ 60 mesh particle size prepared as described earlier) is placed above in a platinum gasket in the upper region (or in a teflon gasket). Thus, the seeds are in the warmer supersaturated region at the bottom of the autoclave and the temperature gradient achieved by cooling the top allowed proper convection. The schematic diagram showing the position of seeds, nutrient, and the baffle is represented in Fig. 5.21.

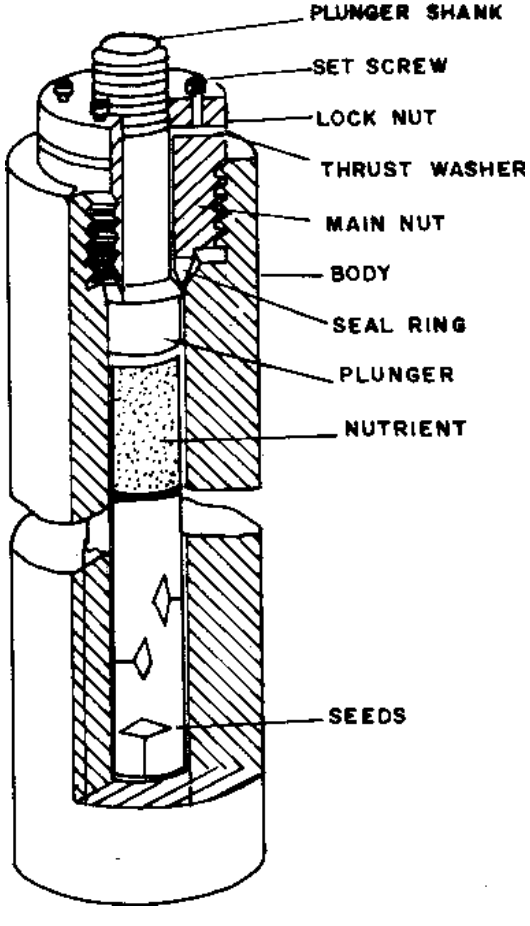

Figure 5.21. Schematic diagram showing the position of seeds, nutrient, and the baffle in the growth of berlinite crystals.[78]

In the growth of berlinite on seeds, the orientation of the seed is very important because the growth rate and perfection depend upon the seed orientation. According to Laudise (1985),[78] the growth rates are shown for seeds whose faces are indicated below:

(0001) (basal plane)	: :	0.25–0.50 mm/day
$(10\bar{2}\bar{1})$ (*X* cut)	: :	0.23–0.30 mm/day
$(10\bar{1}\bar{0})$ (*Y* cut)	: :	0.12–0.15 mm/day
$(01\bar{1}\bar{1})$ (minor rhombohedral face)	: :	0.12 mm/day
$(10\bar{1}\bar{1})$ (major rhombohedral face)	: :	0.15 mm/day

The relative growth rates are in general agreement with the morphology of the equilibrium form, as judged from observing spontaneously nucleated crystals, which are bounded by small prism $(10\bar{1}\bar{0})$ faces and terminated by minor and major rhombohedral faces. Thus, it would be expected that the rates on prism, major, and minor faces, are smaller than for $(11\bar{2}0)$ and (0001) faces, since the latter two do not exist as bounding equilibrium surfaces. In general, the morphology of the spontaneously nucleated crystals depends upon various parameters like pressure, temperature, volume, and composition of the nutrient and mineralizer.[89]–[91] For example, impurities in the powder come into the corresponding nutrient and caused twinning. The starting material like sodium aluminate or aluminum hydroxide gives needle-like crystals, whereas, pure $AlPO_4$ gives rhombohedral and pyramidal crystals.[76]

Yaroslavskii and Popolitov (1990) have studied the growth of berlinite on seeds in detail using fine crystalline charge and also aluminophosphate glass charge as nutrients.[92] They found that dissolution rate of aluminophosphate glass charge is three times greater than that of the crystalline charge. The solubility growth rate and crystal quality have been studied in great detail using different solvents like H_3PO_4, HCl, HNO_3, H_2SO_4. If the acid concentrations are increased above 2.5M, the spontaneous crystals form, and mother liquor is captured by the edges of the growing crystal. The growth rates differ greatly between the fine crystallization charge and aluminophosphate charge. The temperature gradient has been varied from 5–50°C. When the ΔT is high (40–50°C), it introduces macro inclusions and gas-liquid inclusions, and are clearly visible upon passing bright light through the crystal. The growth rates observed by the authors are rather high at 0.35–0.50 mm/day in H_3PO_4, 0.35–0.45mm/ day in HCl, 0.25–0.35 mm/day in HNO_3, and 0.2–0.3 mm/day

in H_2SO_4 solvent media. The growth rate of α-berlinite on $[10\bar{1}0]$ and [0001] seed plates against the solvent concentration, growth temperature and temperature gradient are shown in Figs. 5.22 *a, b,* and *c*. The growth rate from aluminophosphate glass is 1.5–2 times greater than that from fine crystalline charge under the same conditions for mild process parameters.

5.3.4 Morphology

Although $AlPO_4$ crystals obtained spontaneously are small in size, they exhibit distinct morphological features. The crystal size varies from 0.5 to 4 mm and the common forms are hexagonal, rhombohedral, rod shaped, needle-like, and occasionally rounded. The morphological forms of $AlPO_4$ mainly depend upon the nutrient composition and the solvent in action. Data on the dependency of the morphological features, and the nutrient composition, as well as the solvent used are given in Table 5.7.

A typical morphology of $AlPO_4$ is shown in the schematic diagram (Fig. 5.23) consisting of major and minor rhombohedral faces. Figures 5.24 *a* and *b* show the characteristic photographs of the berlinite crystals.

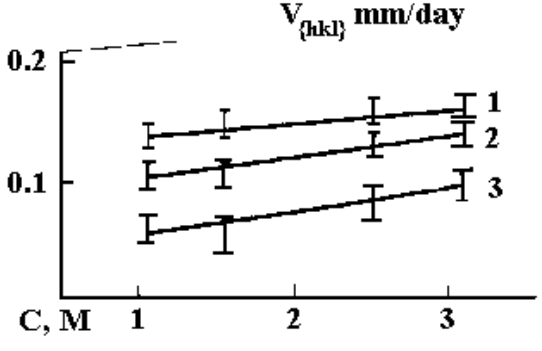

(a)

Figure 5.22. Solution concentration, growth temperature, and temperature gradient vs. growth rate *(a)–(c)*.[92]

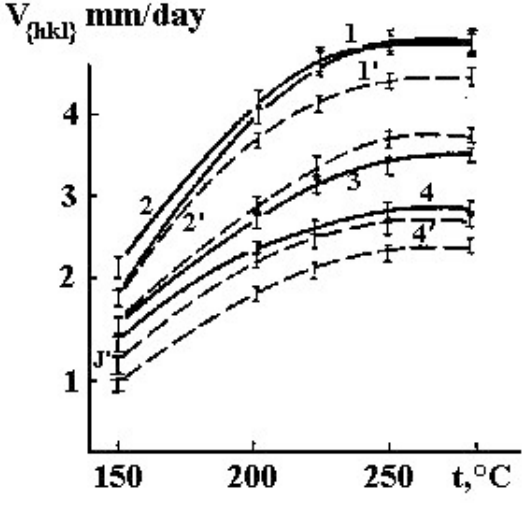

(b)

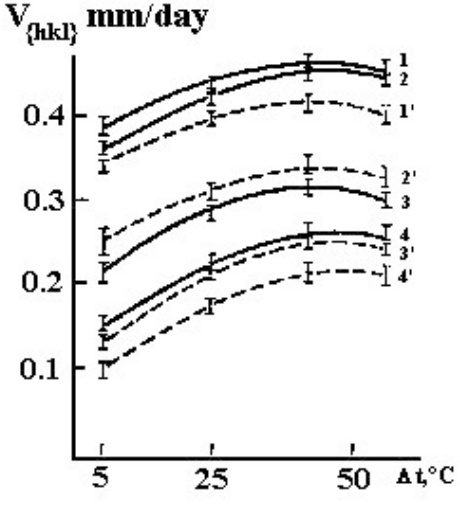

Figure 5.22. *(Cont'd.)*

Table 5.7. Morphology of Aluminum Orthophosphate Crystals

Nutrient composition	*T* °C	Morphology
$Al_2O_3 + H_3PO_4$ mineralizer HCl (1.5M)	280	Hexagonal and rhombohedral
$Al_2O_3 + H_3PO_4$ mineralizer NaCl (2M)	300	Rhombohedral
$Al_2(OH)_3 + H_3PO_4$ mineralizer NaF (2.5M)	300	Rods, needles or acicular
$Al_2O_3 + H_3PO_4$ mineralizer NH_4Cl (4M)	300	Small hexagonal, rhombohedral and equil-dimensional
$Al_2O_3 + H_3PO_4$ mineralizer HCOOH (2M)	280	Hexagonal and rhombohedral
$Al_2O_3 + H_3PO_4$ mineralizer $NaHCO_3$ (3M)	300	Hexagonal, rhombohedral and slightly irregular
$AlCl_3 + H_3PO_4$ mineralizer HCl (2M)	270	Hexagonal

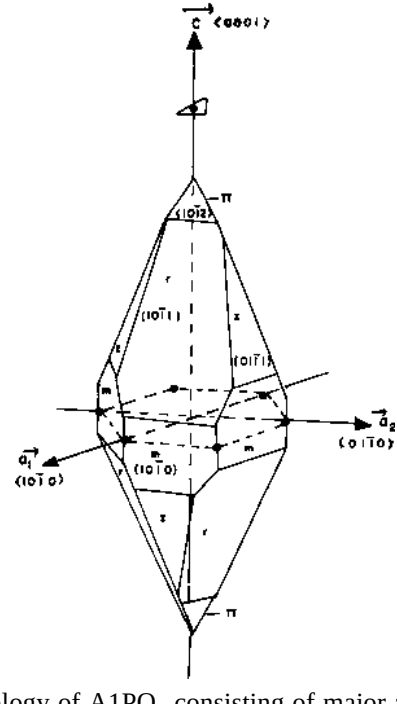

Figure 5.23. Morphology of $A1PO_4$ consisting of major and minor rhombohedral faces.[83]

It is observed that these admixtures play an important role in the process of crystallization of $AlPO_4$. In the actual experiments without any admixtures, well-developed rhombohedral and hexagonal crystals have been obtained, but with the addition of various admixtures the crystal changes to fibrous, rod shaped, acicular, massive, equi-dimensional and irregular shapes (Figs. 5.24 *c, d*). In the case of Zr and Ti as the admixtures, fibrous or acicular crystals of berlinite have been obtained; such results were earlier obtained only in experiments containing $Al(OH)_3$ as the starting component.[76][91]

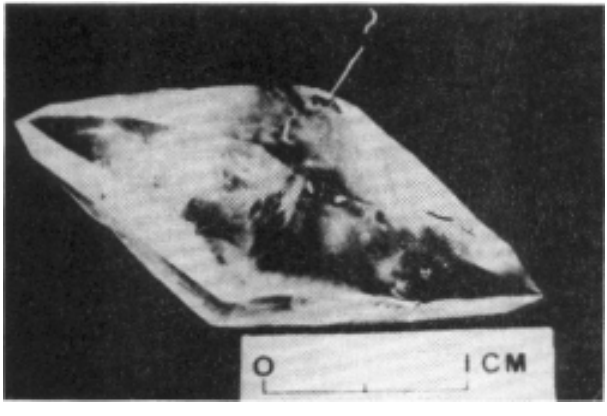

(a)

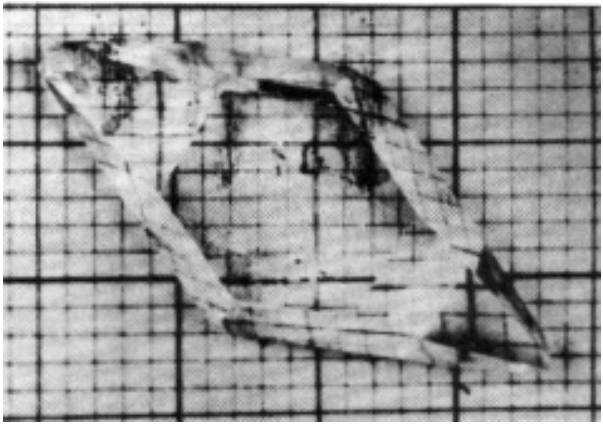

(b)

Figure 5.24. Characteristic photographs of the berlinite crystals *(a-d)*.[76][83]

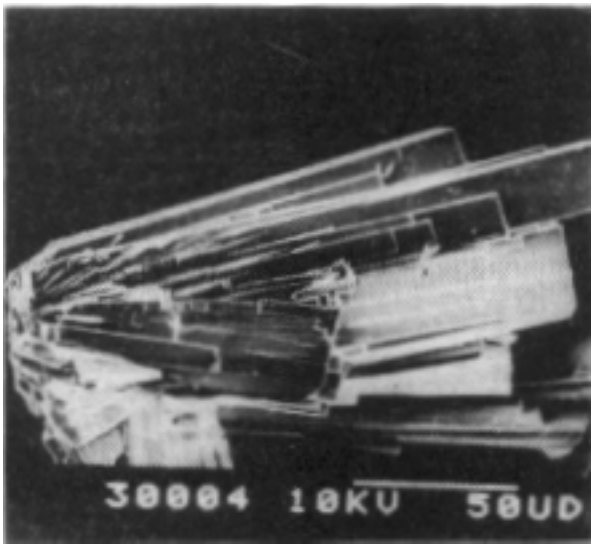

(c)

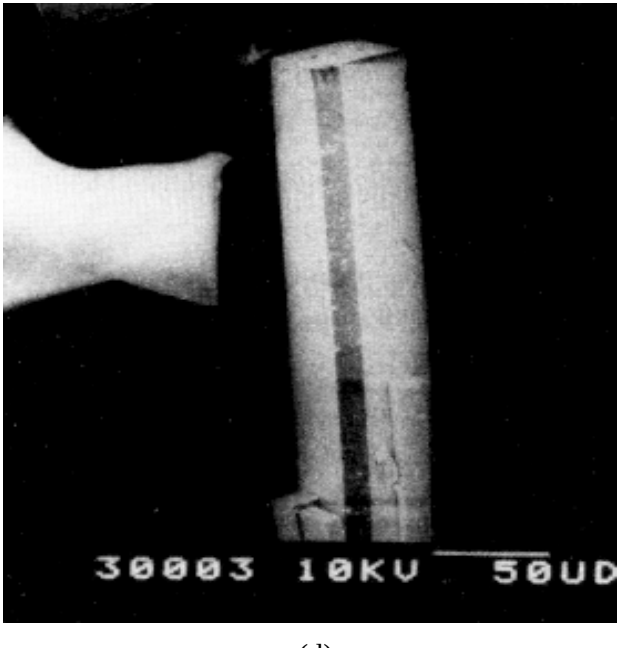

(d)

Figure. 5.24. *(Cont'd.)*

Growth defects in synthetic berlinite samples have been studied by several workers through x-ray topography.[89][93] The berlinite crystals, in general, show internal structural defects along with a high density of defects on x-ray Lang topography. It can be seen that crystals which appear transparent from outside contain many internal defects. Figure 5.25 shows a typical Lang x-ray topograph taken in (2110) face.[83] Line defects were attributed to the disorder in crystal structure and more likely to the impurities existing in the boundary of repetitive overgrowth. However, it is possible to distinguish various types of contrasts that differ by their temperature behavior. Dislocation-related contrasts vary slightly with temperature, but they appear more strongly, especially after the second thermal cycle. The variation of contrast present in the topography for the growth bands can be interpreted in terms of localized variations of the deformation in the sample with temperature. These variations appear in the same temperature range as the anomalies observed in propagation loss, frequency, and temperature characteristics. These anomalies have been attributed to water impurities in these hydrothermally grown crystals.[94][95] This explanation is qualitatively valid and in good agreement with the changes of the deformation contrast observed during the thermal cycles. The contrast due to the water impurity content is observed in selected areas and is predominantly located at growth bands that correspond to the adsorption of water on some growing faces during the cycle.

Figure 5.25. Lang x-ray topograph taken in (2110) face.[83]

A combination of selected growth conditions reducing the water content and using heat treatment to control the water distribution could be of great interest for improving the piezoelectric device application of berlinite. The choice of the seed is fundamental for the production of good crystal and a selection of excellent slices for this use is absolutely necessary when this condition is fulfilled. The x-ray topographs obtained on different crystals have shown that the quality was improved but the remaining defects could be classified into two classes. This is due to the defects present in the seed which have been developed in the grown crystals (dislocations and sometimes twins) and those which were carried during the start of the growth (bundles of dislocations) or during the growth (growth bands).

No fundamental differences were found by x-ray topography between the horizontal gradient, vertical gradient, and slow heating methods, when good seeds and optimized conditions were used.[92] The two principal imperfections readily observable are *crevice flawing* and *cracks*. When growth is on a non-equilibrium face, there is a tendency for higher growth rates and the formation of *hillocks* which tend to protrude across the solute-depleted diffusion layer near the growing face. The tips of such hillocks experience a high supersaturation and tend to grow faster than the regions between hillocks. This phenomenon is the hydrothermal analogue of constitutional surpercooling and may be viewed as a kind of dendritic growth.[96][97] Entrapment of solution between hillocks leads to bubbles of solutions in the grown material, which are observed as *viels*. Thus, growth at slower rates and on equilibrium faces produces a greatly reduced tendency for crevice flawing.

Cracks are often observed in hydrothermally grown material. In the case of quartz[25][98] we found that they were associated with strain caused either by strain in the seed propagating into the grown crystal or by strain associated with dislocations arising at inclusions in the new growth. It was further observed in quartz that disorder regions in seeds propagated into crystals and strain free seeds were much less likely to produce cracked growth.

At an annealing temperature which is high enough, berlinite becomes milky, and in TEM pictures one observes a large density of bubbles with a mean size of about 1000 Å; while in untreated, as-grown berlinite no such bubbles are visible. Further more, the growth of these bubbles is accompanied by a severe increase in the dislocation density of the order of 10^5 cm^{-2} or less, but in the heat treated crystals this density

reaches 10^9 cm^{-2}. An increase of at least six orders of magnitude is produced, like for wet quartz, which exhibits the same dramatic dislocation multiplication. This situation can be observed in berlinite, where bubbles with a mean diameter of 250 Å can be observed together with a very high density of dislocation.[94][98] Recently, Morris and Chai (1998) have studied the imperfect low-angle boundaries and fracture in hydrothermally grown berlinite crystals obtained on multiple-seed plate arrays.[99]

5.3.5 Thermal Behavior

The stability range of any material with a device potential is an important parameter. Byrappa et al. (1986) have reported the differential thermal analysis for containing various admixtures (Fig. 5.26).[100] For pure berlinite, the inversion temperature was reported to be at 586°C and this is similar to that reported by Beck (1949).[72] However, there are reports fixing this transition temperature at 581°C[101] and at 579°C.[102] Such a variation in the α-β inversion temperature can be explained by the effect of the starting materials, the presence of admixtures in the final products, and even the metals from the mineralizers which also act as admixtures.

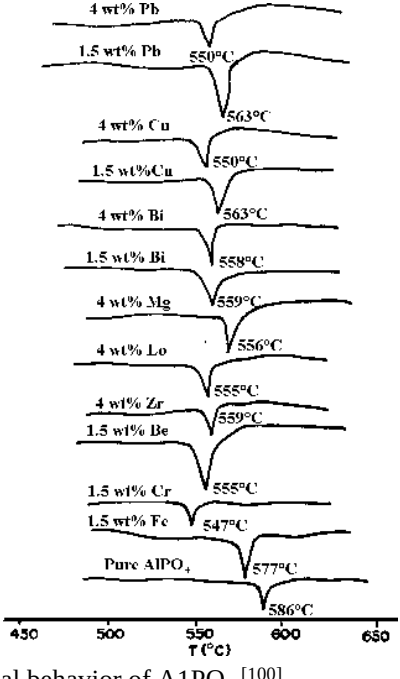

Figure 5.26. Thermal behavior of $A1PO_4$.[100]

Studies on the thermal expansion of berlinite have not been reported much in the literature. Byrappa and Prahallad (1989) have reported the thermal expansion of berlinite in detail.[103] The thermal expansion values vary depending upon the percentage of concentration of impurities in the crystal.

The values of thermal expansion for α-berlinite containing various admixtures are given in Table 5.8, and the values are, in general, very low for these materials because of the covalent bonding. Alpha-berlinite is relatively stable compared to β-berlinite with reference to the action of the dopants. The difference in α_a (max) - α_a (min) = 0.39 $\times 10^{-5}$ and α_c (max) - α_c (min) = 1.572 x 10^{-5} C^{-1}, which shows that the *c*-axis is more susceptible to thermal expansion than the *a*-axis. The coefficient of thermal expansion is quite high when rare earths are used as admixtures.

Table 5.8. Thermal Expansion of α-Berlinite Containing Admixtures[103]

Admixture	Ionic radii	Atomic weight	a	c	v
—	—	—	1.63×10^{-5}	1.068×10^{-5}	4.38×10^{-5}
Sr	0.63	51.996	1.90×10^{-5}	1.89×10^{-5}	5.77×10^{-5}
Fe	0.64	55.847	1.98×10^{-5}	1.13×10^{-5}	5.16×10^{-5}
Cu	0.72	63.546	1.76×10^{-5}	1.81×10^{-5}	5.39×10^{-5}
Nd	0.99	144. 24	2.02×10^{-5}	2.64×10^{-5}	6.78×10^{-5}
La	1.016	138. 905	1.75×10^{-5}	2.64×10^{-5}	6.22×10^{-5}

- concentration of the admixture in the nutrient was 1.5 wt %

5.3.6 Piezoelectric Properties of Berlinite

The piezoelectric properties of berlinite have been studied in detail by several authors. Chang and Barsch (1976),[63] and Ballato and Iafrate (1976)[104] pointed out attractive properties of *Y* rotated and doubly rotated cuts of berlinite in terms of its large coupling coefficient (twice that of quartz), with a constraint of zero first order frequency temperature coefficient (FTC). Several groups appeared throughout the world immediately to study the growth and characterization (with reference to its first, second

and third order frequency temperature coefficient) of berlinite. Figure 5.27 shows the comparison of *Y* quartz and *Y* berlinite resonators. It can be noticed that the *Q* factor is greater by an order of magnitude than for resonators. In Fig. 5.27, also given the frequency response of the *Y* quartz plate of similar design whose *Q* factor is not so different and whose coupling coefficient is smaller. The higher order temperature coefficients measured with different crystals, even with different plates of the same crystal, show values much larger than for quartz resonators of the corresponding orientation. Table 5.9 gives the comparison between quartz and berlinite. However, it has been demonstrated that the water dissolved in berlinite crystal induces low values of two factors and impairs significantly the intrinsically very favorable thermal behavior of this material.

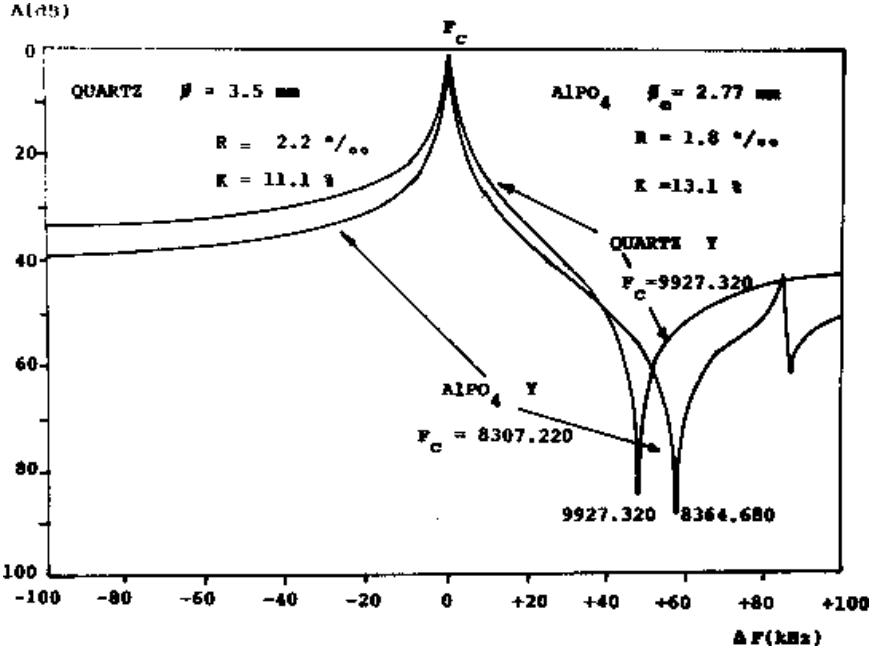

Figure 5.27. Frequency response of the *Y* quartz plate.[63]

Table 5.9. Tentative Comparison with Quartz (Thickness *Y* Rotated Resonators at same Frequency)

Useful coupling coefficient (AT filter trapped resonators)	Enhanced by 1.4 – 1.5
Shift of oscillators or band width of filters (AT cut)	Twice
Angular sensitivity (1^{st} order FTC)	Reduced
Thermal stability (higher order FTC)	Better
Q factor propogation losses	Already sufficient (may be comparable)
Thickness of plates (AT)	Reduced by 1.15
Electrode dimensions (AT)	Reduced by 1.32 (TT)
(Same plating 2D TT of TS)	Reduced by 1.24 (TS)
Nonlinear properties	To be determined

"Dry" berlinite has similar C, E, EPS constants, first order TC and much reduced higher order TC.

Jumas et al. (1987) gave an excellent comparison of piezoelectric properties of $AlPO_4$ to quartz.[92] According to them, the coupling coefficients measured with AT resonators with filter type response were about 11%. For quartz, the maximum values were 7.4%, and this permits one to obtain filters with twice the bandwidth. The electric constant of berlinite is lower by a factor of 1.2 to 1.35 than the corresponding constant of quartz, but the density is very similar. The frequency constants Nfa and Nfr (Nfa = 4 hx; Nfr = 4hxfr, where 2h is the thickness of the plate) are lower than those for the corresponding orientation of quartz by a factor 1.1 to 1.7; for the AT cuts the factor is 1.15.

The first, second, third, etc., order frequency temperature coefficients of berlinite are mostly dependent on the temperature coefficient (TC) of the pertinent elastic constants and the dilation coefficient.[105] As the latter are similar to those of quartz,[63] most of the better thermal behavior observed with "dry" berlinite, as compared to quartz, results from smaller values of the TC of elastic constants. For some other constants, similar things may also be expected. In Fig. 5.27, the results of Poignant are given, indicating a similar behavior of the TC of C33 for quartz and berlinite.[83] It is also expected that for other analogues of quartz with similar α-β phase transition and reduced elastic constants, similar or better thermal behavior of resonators could be obtained.

This point is of great importance for frequency generation and filtering applications of resonators, for which it is fundamental to obtain a frequency response free of unwanted (unharmonic) modes. For identical cut, resonant frequency, and plating, it can be shown that smaller dimensions of electrodes are required for berlinite than for quartz to obtain a frequency response without spurious unharmonic modes (trapping of only one mode).

Shannon and his group (1993) have studied in detail the dielectric properties of berlinite with reference to the presence of $(OH)^-$.[106][107] It has been well established that water in berlinite is found in both macroscopic and microscopic inclusions. Because crystals are grown from H_3PO_4 or H_3PO_4/HCl solutions, it is likely that the inclusions also contain this acidic solution and consequently, high concentrations of H_2PO_4, HPO^-_4 and /or Cl^- ions. Quantitative NMR determination of proton content unequivocally determines the H_2O and hydroxyl content, whereas complementary IR absorbency studies of the 3300 cm^{-1} band confirm the molar absorption coefficient of 81 $l mol^{-1}$ cm^{-1} originally determined for liquid H_2O by Thompson (1965).[108] The dielectric constant variability of berlinite prepared by different investigators is believed to result from *(i)* a variation in H_2O content in microscopic and macroscopic inclusions and *(ii)* unidentified crystalline defects.

5.4 GALLIUM PHOSPHATE, $GaPO_4$

Gallium phosphate, like aluminum phosphate, belongs to the family of quartz and quartz-like MXO_4, where M = B, Al, Ga, Fe, Mn, and X = P, As.[109] Amongst them, $AlPO_4$ and $GaPO_4$ have been studied

extensively with reference to their crystal growth, crystal chemistry, and physical properties, especially piezoelectric properties.[75][110]–[114] Both $AlPO_4$ and $GaPO_4$ exhibit piezoelectric characteristics which are superior to those of conventional α-quartz. As evident from Table 5.10, for the same AT cut, $GaPO_4$ exhibits larger coupling coefficient which makes $GaPO_4$ a most promising material in the field of wide band filters. In addition to this, the $\alpha - \beta$ phase transition for $GaPO_4$ occurs at 976°C, and hence, it can be used in a very wide range of temperatures for filters and sensor devices.[115]–[118]

Table 5.10. Comparison of Some Piezoelectric Characteristics[109]

Parameter	Quartz	Aluminum Phosphate (Berlinite)	Gallium Phosphate
Coupling coefficient* K%	8.5	11.0	> 16.0
Surtension coefficient* Q	3.10^6	10^6	$> 5.10^4$
α - β Phase transition °C	573	584	No

* AT cut

5.4.1 Crystal Growth of Gallium Phosphate

The synthesis of gallium orthophosphate does not differ much from the synthesis of berlinite. It is usually carried out by the hydrothermal technique at temperatures less than 250°C. On the whole, the growth of aluminum and gallium phosphates is carried out using reverse temperature gradient, or slow temperature, increasing essentially in the acid media like H_3PO_4,[119] H_2SO_4, HCl + H_2SO_4, H_3PO_4 + H_2SO_4,[113][117][118] HCl,[117][120] KF, NaOH.[120] The starting material/ nutrient for $GaPO_4$ growth is prepared usually by solid state reactions with Ga_2O_3 and $NH_4H_2PO_4$, twice at 1000°C for 24 hours and subsequently hydrothermally treated at 150°C for 30 hours in 4M H_3PO_4 solution. The resultant product is generally a single phase of $GaPO_4$. Like berlinite, the gallium phosphate also shows a retrograde solubility in all the solvents

below 400°C, and above this temperature, the solubility becomes positive.[110][114][120] Hence, the nutrient is kept at the low-temperature zone (i.e., dissolution region), and the seed crystal is kept at higher temperature zone (i.e., crystallization region). The temperature gradient (5 to 40°C) is selected according to the quality and the growth rate required. Figure 5.28 shows the schematic representation of the growth of berlinite crystals and the same experimental setup can be used for the growth of gallium orthophosphate crystals. The growth of gallium orthophosphate can be carried out at 180°C for seven to ten days. By this arrangement, it was expected that the dissolved nutrient would be efficiently used to grow single crystals on the seed without the occurrence of spontaneous nucleation. As the lattice parameters of both berlinite and gallium phosphate are very close, some authors have used even berlinite crystals with a definite orientation/cut as seeds, and obtained $GaPO_4$ epitaxy on $AlPO_4$ seeds using 6M H_2SO_4 solvent, at a temperature greater than 200°C.[117] The experimental temperature is critical in the case of gallium phosphate because the crystals obtained at a temperature less than 200°C show the presence of water, which deteriorates the piezoelectric characteristics. Hence, it is advisable to use acid mineralizers with a boiling temperature of 225–240°C. Practically, there is no water in such a solvent, and it consists of orthophosphoric acid (90%) and pyro-phosphoric acid (10%). The solubility is presaturated with $GaPO_4$ to avoid the dissolution of the seeds. To keep the solution from boiling during the crystal growth, inert gas is pumped into an autoclave up to 50 bars.[121]

Cochez et al. (1994) have proposed the following scheme for the growth of α-$GaPO_4$ as the best method:[117]

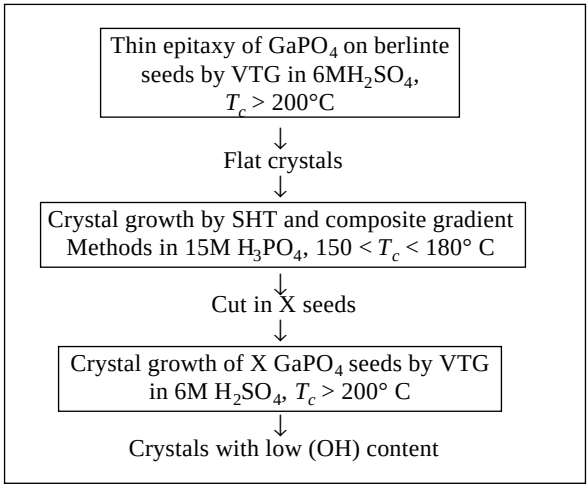

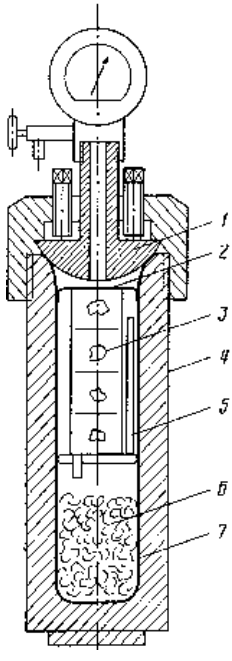

Figure 5.28. Schematic representation of the growth of berlinite crystals.[119]

The first stage of $GaPO_4$ crystal growth process is the epitaxy of $GaPO_4$ on berlinite seeds. The second stage consists of growing 2–d crystals through the slow heating method, or the horizontal gradient method, or the composite method (i.e., the combination of the first two). In the third stage, the X seeds are grown which helps in reducing the $(OH)^-$ content in the crystals.

Popolitov and Yaroslavskii (1990) have studied the crystallization processes of α-$GaPO_4$ under hydrothermal conditions.[120] They have studied the rate of crystallization, (i.e., the amount of $GaPO_4$ crystals formed per unit time), action of solvent, its concentration and the temperature regime. Gallium phosphate glass (prepared by sol-gel method) has been used as the nutrient with Ga:P ratio = 1: 1.5. The experiments were carried out in the temperature range 200–300°C, P = 20 – 35 MPa using teflon liners, with a temperature gradient of 4–5°C. The yield of $GaPO_4$ single crystals as a function of growth temperature and concentration of different solvents used is shown in Figs. 5.29 and 5.30. All the curves shown in Figs. 5.29 and 5.30 are described by a simple exponential

equation: $M = KC^n$, where K is the rate of bulk crystallization, C is the solvent concentration, and n is the formal order of bulk crystallization. Table 5.11 gives the values of K, C, and n for aqueous HCl, HNO_3, KF, and NaOH at 200, 250, and 300°C.

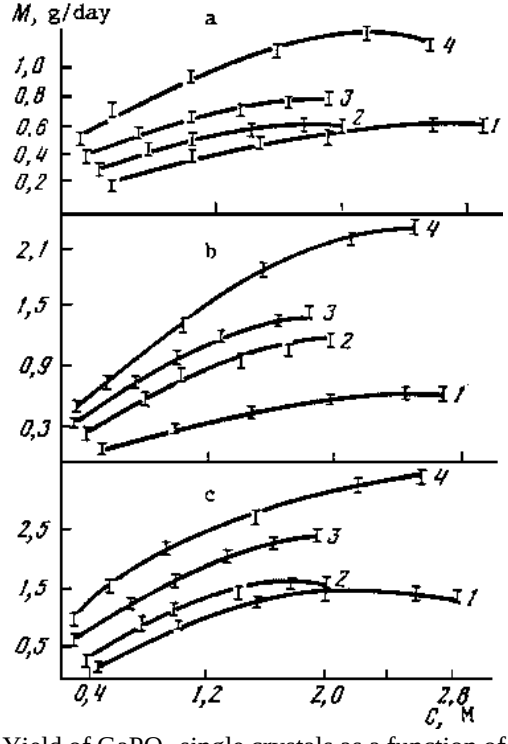

Figure 5.29. Yield of $GaPO_4$ single crystals as a function of growth temperature and concentration of different solvents.[120]

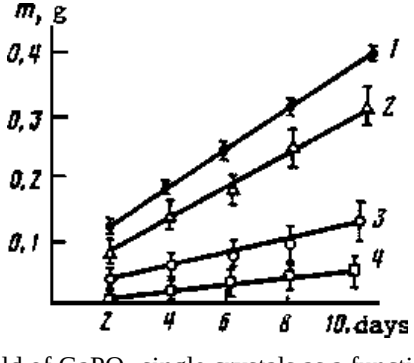

Figure 5.30. Yield of $GaPO_4$ single crystals as a function of time.[120]

Table 5.11. Crystallization Kinetics for $GaPO_4$

Solvent	HCl			HNO_3			KF			NaOH		
T, °C	200	250	300	200	250	300	200	250	300	200	250	300
K	0.22	0.48	0.76	0.11	0.28	0.41	0.09	0.14	0.26	0.04	0.05	0.15
n	0.61	0.58	0.57	0.58	0.50	0.47	0.20	0.22	0.18	0.30	0.28	0.27

Also, the authors[120] have calculated the activation energy for the formation of $GaPO_4$ single crystals from the Arrhenius equation. Similarly, the solubility of α-$GaPO_4$ has been studied by several workers within a wide range of *PT* conditions (T = 200–500°C, P = 50–1000 atm).[112][114][117][122] Figure 5.31 shows the solubility of $GaPO_4$ in the phospho-sulphuric acid solution 15M H_3PO_4 + 9M H_2SO_4 in terms of % in H_2SO_4. There is an increase in the solubility with a progressive enrichment in H_2SO_4 in the solvent. However, it always remains lower than in pure H_2SO_4. The solubility remains retrograde in all the studies up to 400°C.

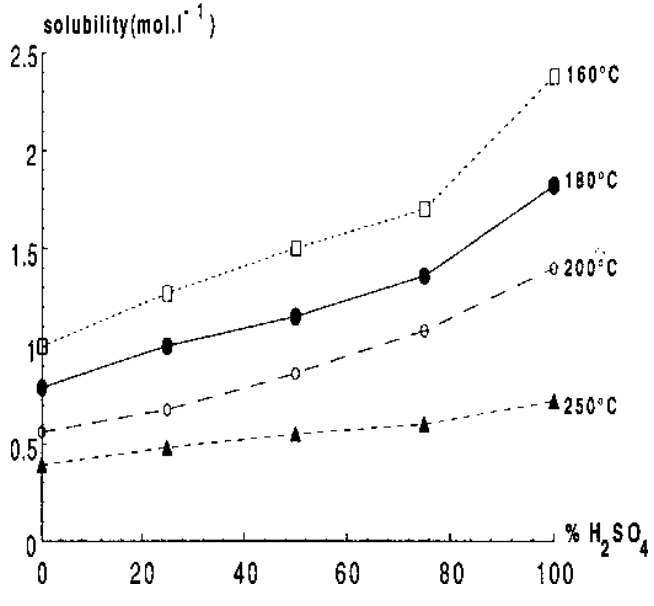

Figure 5.31. Solubility of $GaPO_4$ in the phospho-sulphuric acid solution 15M H_3PO_4 + 9M H_2SO_4.[114] *(Courtesy of the Gauthier-Villars/ESME, Paris.)*

5.4.2 Morphology

The morphology of the $GaPO_4$ single crystals is shown in Fig. 5.32.[120] The commonly appearing faces are $[10\bar{1}1]$, $[01\bar{1}1]$, $[10\bar{1}0]$, $[10\bar{1}2]$. Figure 5.33 shows the characteristic photographs of $GaPO_4$ crystals obtained by hydrothermal method. The growth rates along various crystallographic directions decrease in the following sequence:

$$\gamma(0001) >> \gamma(01\bar{1}2) > \gamma(10\bar{1}0) > \gamma(01\bar{1}1) > \gamma(10\bar{1}2) > \gamma(10\bar{1}1)$$

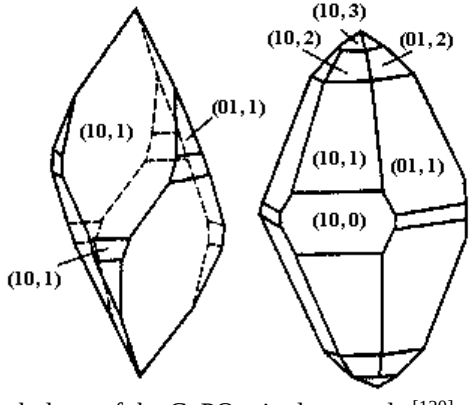

Figure 5.32. Morphology of the $GaPO_4$ single crystals.[120]

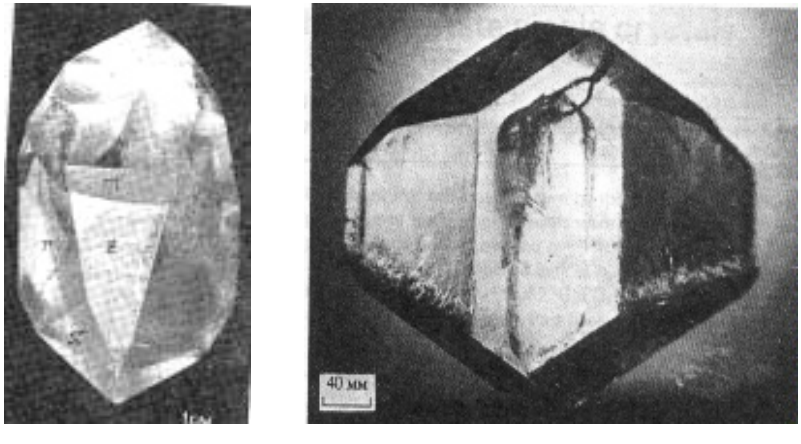

Figure 5.33. Characteristic photographs of $GaPO_4$ crystals obtained by the hydrothermal method.[121]

The common twins observed in $GaPO_4$ are according to the Dauphine, Brazil and Laydolt's twinning laws. This has been discussed in great detail in Ref. 121. The x-ray topographic studies on $GaPO_4$ have been carried out by Capelle et al.[118]

5.4.3 Dielectric Properties of Gallium Phosphate

The influence of the growth rate on the quality of the $GaPO_4$ crystals has been studied through infrared spectrometry by Cochez et al. (1993).[114] As conventionally done for quartz and berlinite, the $(OH)^-$ impurity content was monitored by infrared measurements in the wave number range of 4000 to 2500 cm^{-1}, using the relation:

$$\alpha = {}^1/_d \text{ cm log } (T_{3800}/T_{3167})$$

where T_{3800} and T_{3167} are respectively the transmittances at 3800 and 3167 cm^{-1} respectively. The strongest absorption band of Al-OH for berlinite appears at 3291 cm^{-1} and it is shifted to 3167 cm^{-1} for Ga-OH in case of $GaPO_4$ (Fig. 5.34). The α values obtained by the authors are 1.6 and 2.2 for two of their characteristic $GaPO_4$ samples. It can be observed that the $(OH)^-$ content increases with the temperature gradient.

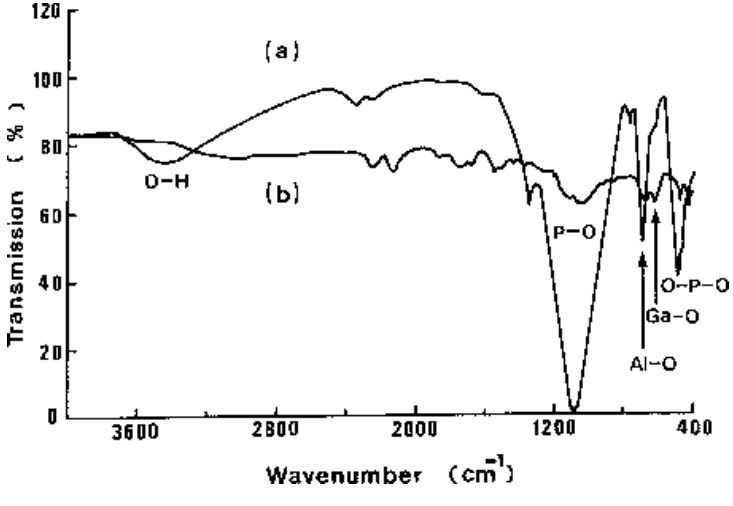

Figure 5.34. FT-IR spectra of *(a)* $A1PO_4$ (wet) and *(b)* as-grown single crystals of $GaPO_4$.[114] *(Courtesy of the Gauthier-Villars/ESME, Paris.)*

The dielectric properties have been studied in detail by Hirano et al. (1990) for $GaPO_4$ crystals.[75] According to the authors, the frequency independence of $\in'$ at room temperature in this crystal indicates that mainly electronic ionic polarizations contribute to the dielectric constant of $GaPO_4$. These two polarizations always exist below 10^{13} Hz.

Figure 5.35 shows the extrapolation of possible piezoelectric properties to other quartz-like materials.[109] Table 5.12 gives the extrapolation of AT cut characterizations from well-known quartz and quartz-like materials.

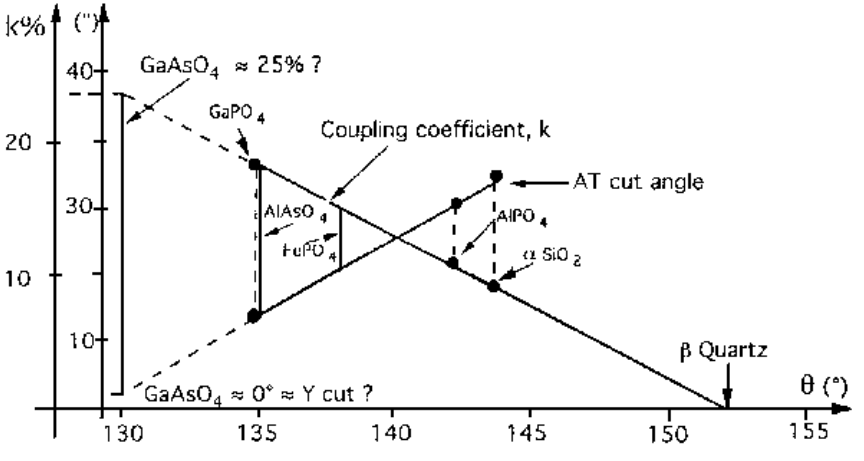

Figure 5.35. Extrapolation of possible piezoelectric properties to other quartz-like materials.[109] *(Courtesy of the Academic Press, Orlando, Florida.)*

Table 5.12. Extrapolation of AT Cut Characteristic from Well-known Quartz and Quartz-like Materials

Material	SiO_2	$AlPO_4$	$FePO_4$	$AlAsO_4$	$GaPO_4$	GeO_2	$GaAsO_4$
AT cut angle (°)	-35.25	-33.02	≈ -20	≈ -15	≈ -15	≈ 0	≈ 0
coupling coefficient *k* (%)	8.5	11.0	≈ 15	≈ 18	≈ 18	≈ 25	≈ 25
c/a	2.20	2.22	2.23	2.23	2.26	2.27	2.28

Cochez et al. (1994) have well-studied and extrapolated the relations that exist between the crystal structure distortions, expressed in terms of the M-O-X angle (where M = B, Al, Ga, Fe, Mn, and X = P, As) value and different physical properties.[117] For instance, piezoelectric characteristics of the AT cut and dielectric constant anisotropy of three known materials (SiO_2, $AlPO_4$, and $GaPO_4$) have been linearly related to their M-O-X angle value successfully. Conversely, knowledge of the M-O-X value allows prediction of physical properties for quartz-like crystals that have not been synthesized. Consequently, using only M-O-X angles, one can describe the structural strains, the α-β transition existence, and some physical properties, such as density, piezoelectric characteristics, and elastic constants.

Based on this reasoning, $GaAsO_4$ and GeO_2 appear to be the most promising materials for piezoelectric applications, unfortunately, the concomitant increase in structural distortions from quartz to $GaAsO_4$ and GeO_2 make their crystal growth very difficult. Thus, from the crystal growth point of view, $GaPO_4$ seems to be the best compromise for industrial development because of its high AT cut coupling coefficient and large temperature range stability with a few drastic packing distortions. If the size of the $GaPO_4$ crystals grown by the hydrothermal technique is increased at least by one fourth the value of the quartz, then $GaPO_4$ would be the best piezoelectric material of the 20th century and probably of the early 21st century as well.

5.5 POTASSIUM TITANYL PHOSPHATE (KTP)

Potassium titanyl phosphate, $KTiOPO_4$ (*KTP*) is one of the best nonlinear optical materials increasingly being used commercially for the second harmonic generation (*SHG*) and parametric oscillation since its discovery and introduction in 1976.[123] It all began when there was a search for a suitable crystal to convert efficiently the near-infrared light at 1.06 μm, which is useful in laser surgery. However, from the surgeon's point of view there is a difficulty as the near-infrared is not visible clearly. Thus, the solution for this problem was to use a second crystal which efficiently converts the near-infrared to the visible—a harmonic generator crystal.[124][125] The requirement was for a material with high conversion efficiency and appropriate index of refraction characteristics to allow phase matching. The AT & T Bell Labs group[124] tried with $LiNbO_3$.

Subsequently, the DuPont group discovered KTP to be phase matchable most efficiently at 1.064 μm to easily visible green light at 0.53 μm. It has very high laser damage resistance, coupled with low optical losses and it is transparent over a wide range of wavelengths with favorable angular, spectral and temperature bandwidthsn and has high conversion efficiencies.[123][126][127] Also, it was found that KTP's conversion efficiency was twice that of $LiNbO_3$ and hence is the most commonly used 0.53 μm harmonic generator. The additional advantage is that the preparation of $LiNbO_3$, which could be grown from the melt, was very expensive. Also, the starting materials for the growth of $LiNbO_3$ were equally expensive. In contrast to this, the starting materials for the growth of KTP are rather cheaper and the growth techniques are relatively inexpensive. The lower cost preparative methods could have an impact on its use, and indeed, more generally on the commercialization of nonlinear optical materials and electrooptic devices and systems on the whole. KTP crystals are mechanically, chemically and thermally stable and non-hygroscopic. It is remarkable for both high nonlinear optical coefficients and high conversion efficiency. The material has excellent physical properties, and can be used in a type II phase-matching configuration. In the recent years, KTP has been developed for quasi-phase-matched guided-wave devices to access the visible spectrum.

KTP belongs to the family of compounds that have the formula unit $MTiOXO_4$, where M = K, Rb, Tl, NH_4 or Cs (partial) and X = P or As. All members belong to the orthorhombic space group, $P_{na21,}$ point group, mm2, with the following lattice cell parameters: a = 12.814, b = 6.404, c = 10.616 Å, V = 371.115 $Å^3$. An important crystallographic property with reference to the optical, chemical and solid-state behavior of KTP is that there are two formula units in the asymmetric unit so that the proper solid-state formula is $K_2(TiOPO_4)_2$. The structure of KTP is composed of helices of TiO_6 octahedra linked via phosphate bridges. This leads to an open framework structure in which the charge-balancing cations are incorporated within the channels (Fig. 5.36).[128] The nature of the $KTiOPO_4$ host framework suggested the possibility that modification of the internal structural characteristics, and hence the electro-optic properties, might be achieved by gas-phase absorption and description. The K-ion exists in a high-coordination number site and is weakly bonded to both the Ti octahedral and P-tetrahedral channels existing along the *Z*-axis [001] direction, where K can diffuse with a diffusion coefficient several orders of magnitude greater than in the *X*-*Y* plane.

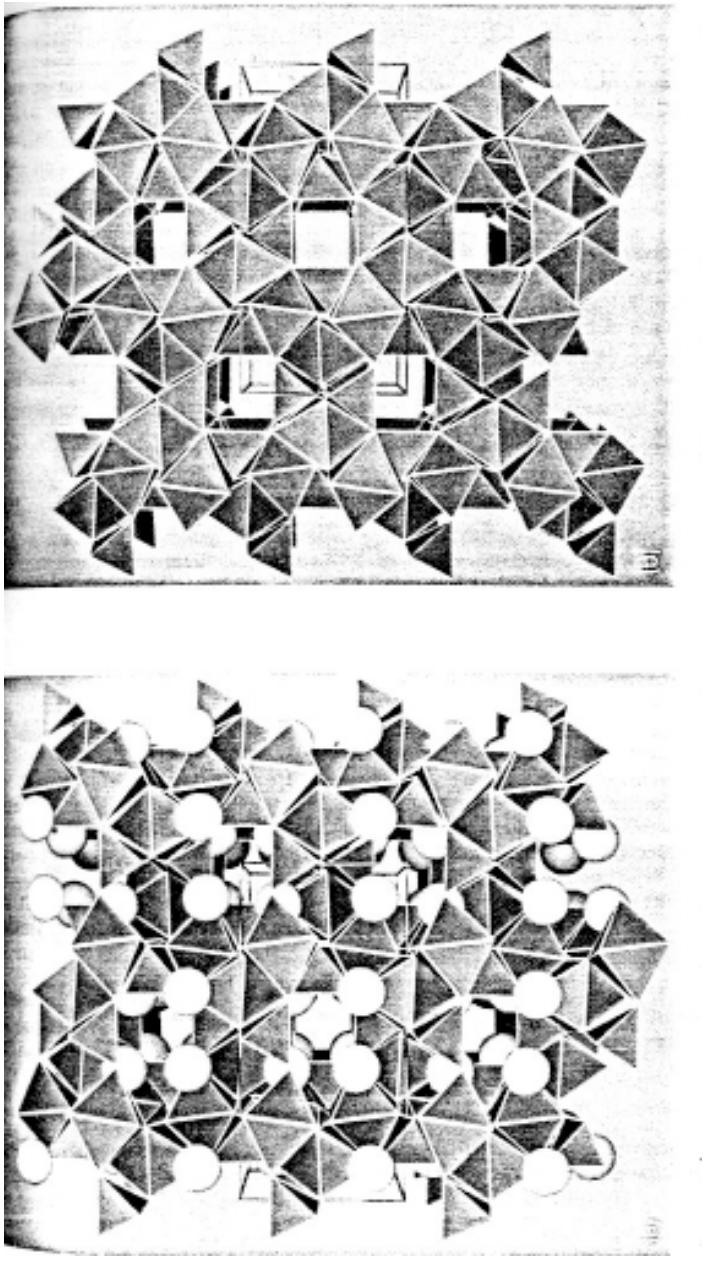

Figure 5.36. Structure of $KTiOPO_4$.[128]

In spite of the above-mentioned unique properties of KTP, its application has been limited by a shortage of crystals of sufficient size and quality. In particular, the crystal growth processes have tended to be plagued by spurious nucleation problems and the inclusions of the solvents. The first attempt to prepare KTP crystals was by Ouvard during 1890, who melted TiO_2, $K_4P_2O_7$ and K_3PO_4.[129] Masse and Grenier (1971) prepared KTP in the polycrystalline form.[130] However, the single crystals of KTP were first obtained by Zumsteg et al. (1976) at the DuPont Experimental Station.[123]

5.5.1 Crystal Growth of KTP

KTP decomposes before melting at 1148°C. Thus, incongruent melting and glass formation make it impossible to grow KTP crystals directly from the melt. Similarly, growth from aqueous solution at low temperature (less than 300°C) is impossible because of the low solubility of KTP. Therefore, large single crystals of KTP can be grown by both high temperature and pressure hydrothermal and flux techniques. There are several problems with reference to the quality of the crystals grown by the flux method. When pure phosphate self-fluxes are used, the main problem is the high melt viscosity. Its tendency to spuriously nucleate and also to leave behind major structural defects in the crystals has motivated the researchers to look for better fluxes. We have summarized the advantages and disadvantages of both flux and hydrothermal methods and quality of KTP crystals in Table 5.13. Similarly, the main problem with the use of the hydrothermal technique for the growth of KTP crystals is the higher pressure-temperature conditions of growth. In fact, when Zumsteg et al. (1976)[123] and Berlien and Gier (1976)[131] synthesized KTP by the hydrothermal method, the pressure-temperature conditions were quite high (P = 1.5 to 3 kbar, T = 650° to 700°C). The crystal size was not more than a few millimeters since the experiments were carried out in small platinum or gold capsules. Liu et al. (1982, 1984) have reported the growth and properties of hydrothermally grown KTP.[132][133] They prepared nutrient by the reaction of KH_2PO_4 and TiO_2 at 1250°C. The hydrothermal "flux" was 1.5 KH_2PO_4, 1.0 TiO_2 in Ag^- or Au^- lined autoclaves at a pressure of 24–28 kpsi (1.66-1.93 kbar) and 520–560°C in a gradient of 30–70°C. Growth rate on (011) was 0.2–1.8 mm/week. The higher pressure-temperature conditions do not yield large size crystals and the cost of the experiments involved is rather high. This led to the serious

Table 5.13. Difference Between Flux and Hydrothermally Grown KTP Crystals

Flux Grown KTP	Hydrothermally Grown KTP
- Temperature is constantly lowered and crystals grow through continuous change in solubility	Temperature is constant, and crystal growth occurs through continuous transport of nutrient by convection currents.
- Growth temperature is high (> 950°C)	Growth temperature is moderate (< 500°C)
- Pressure atmospheric	Pressure < 1.4 bar
- Growth rate is ≥ 1 mm/day	Growth rate < 0.6 mm/day
- Experimental duration: 7 to 10 days	Experimental duration several weeks (~ 30 days)
- Incorporation of fluxes into the lattice, & concentration of nonstoichiometric defects occurs	Incorporation of $(OH)^-$ into the lattice, as crystals are grown at lower temperature
- Reduced stoichiometry, thermooptic effect, poorer quality, susceptible to optical damage (less damage resistant)	Increased chemical stoichiometry, uniform refractive index, high quality, higher resistance to optical damage (most damage resistant)
- Cost of production-less expensive	Cost of production-very expensive
- Limited or slow incorporation in laser devices	More useful for laser applications
- Poor in perfection, purity and homogeneity	Better, perfect, purity and homogeneity
- Suffers from blackening at the end part of the negative pole when placed in DC field	Does not
- Higher ionic conductivity	Lower ionic conductivity
Growth morphology is more or less the same	

efforts from several groups, particularly with reference to the *PVT* relations in several related systems like K_2O-TiO_2-P_2O_5, which ultimately brought down the pressure-temperature conditions to the tune of $P = 700$ bars, $T = 375$–$425°C$. The credit goes to Laudise and Belt for contributing extensively on the *PVT* relations of the KTP systems and also for growing large size single crystals of KTP by the hydrothermal technique.[134]–[137] The earlier hydrothermal experiments on KTP were carried out using platinum or gold lined autoclaves with Tuttle seals (cold-cone seal closures). The crystalline KTP nutrient in appropriate dimensions and quantity was introduced into the bottom part (dissolution zone), and the seeds (cut in proper directions) were suspended on a frame in the upper part (growth zone) of the liner cavity. A baffle separated them so as to control the solution convection for establishing a suitable temperature gradient. The mineralizers used in the earlier experiments were usually KF and K_2HPO_4 taken with a definite molarity. The percent fill (70–80%) and percent open area of the baffle (5 to 10%), temperature gradient (Δt = 10–80°C) were selected appropriately. Under such experimental conditions, the crystals are usually $16 \times 15 \times 7$ mm^3.

At present, several variants of hydrothermal growth of KTP single crystals are known.[134][135][138] Laudise et al. (1990) have carried out *PVT* measurements on 2M K_2HPO_4 and 2M K_2HPO_4 saturated with KTP (Figs. 5.37*a* and *b*).[138] It was important that growth be conducted in the absence of a gas-liquid interface, otherwise seeds in the gas phase do not grow, and bubbling, boiling, and bumping contribute to poor quality deposition. They made nutrient by the reaction of KH_2PO_4 and TiO_2 in platinum at 1250°C. The hydrothermal flux was 1.5 KH_2PO_4-1.0TiO_2 in gold or silver lined autoclaves at $P = 1.66$–1.93 kbar, $T = 520$–$560°C$ and $\Delta T = 30$–$70°C$. Growth rates on (011) were 0.2–1.8 mm/week. Laudise and co-workers have discovered much lower *PT* conditions for KTP growth, permitting the use of ordinary, unlined steel autoclaves in a K_2HPO_4 solvent. By using the reaction $KH_2PO_4 + TiO_2 \rightarrow KTiOPO_4 + H_2O$ to form KTP, they carried out a phase stability study, the results of which are shown in Fig. 5.38. Figure 5.38 shows only the water-rich corner of the complete ternary. Everywhere along the line A-H_2O, mole ratio KPO_3/TiO_2 = 1.00, the same as in KTP. Arrow 1 in Fig. 5.38 at $\cong$ 65 mol % $KPO_3/KPO_3 + TiO_2$ ($KPO_3/TiO_2 \cong 1.8$) is at or close to the boundary of the phase fields α + KTP and KTP at 600°. Alpha *(α)* is not a completely characterized phase, probably less K than in KTP. The boundary is probably nearly the same position at 500°C. Arrow 2 in Fig. 5.38, approxi-

mately 50 mol % $KPO_3/KPO_3 + TiO_2$ ($KPO_3/TiO_2 \cong 1.0$), is the boundary between the phase fields KTP and KTP + TiO_2 (anatase) at 600°C. It coincides with the line A-H_2O. Arrow 3, at approximately 58 mol % $KPO_3/KPO_3 + TiO_2$($KPO_3/TiO_2 \cong 1.4$), indicates that the boundary between the phase fields KTP and KTP + TiO_2 (anatase) at 500°C and lies at stoichiometry: richer in KPO_3 than A-H_2O. It moves to the left at lower temperatures. Assuming the validity of the boundaries defined by the arrows 1, 2 and 3, the appropriate phase boundaries have been drawn in Fig. 5.38 so as to terminate in the complete phase diagram on the KPO_3-TiO_2 axis at K(TiO)PO. Thus, the lines EC(1)G, F(3)H and D(2)A terminate at KTP. The line EF schematically represents the solubility of KTP at 500°C. It does not intersect A-D-H_2O, so KTP is incongruently saturating at 500°C, i.e., the mole ratio of KPO_3/TiO_2 in the liquid, where KTP is the only stable solid phase, ≠ to the ratio in KTP. Somewhere in the TiO_2-rich part of the diagram, anatase would probably be the sole stable phase and, in the KPO_3-rich region, E would probably be the sole stable phase. The authors did not try to find these boundaries because they are not directly relevant to KTP growth.

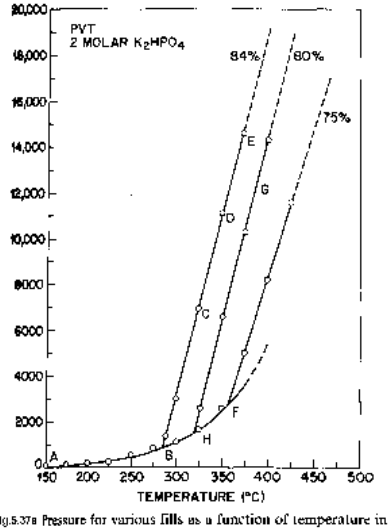

Fig.5.37a Pressure for various fills as a function of temperature in 2M K_2HPO_4.

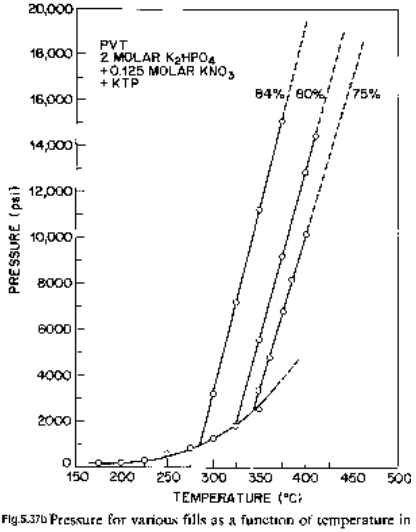

Fig.5.37b Pressure for various fills as a function of temperature in 2M K_2HPO_4 + 0.125M KNO_3 saturated with KTP.

Figure 5.37. PVT relations in KTP system.[138]

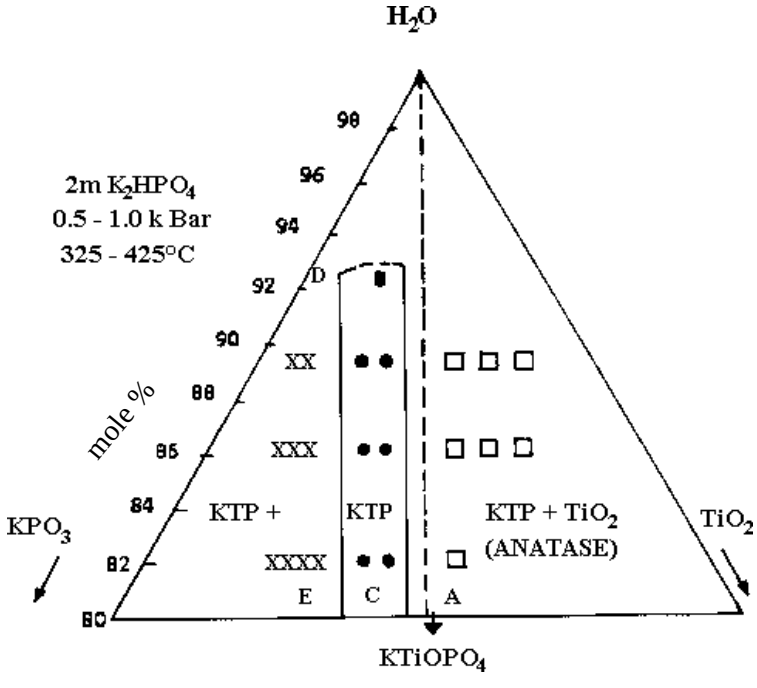

Figure 5.38. Phase diagram for KTP system.[138]

Typical conditions used in growth runs are as follows:

Autoclave:	- Pt lined, 1" ID x 6" IL (2.5 cm × 15 cm)
Mineralizer:	- 2 m K_2HPO_4 + 0.5 m KPO_3
% Fill:	- 75 %
Crystallization temperature:	- 375°C
Nutrient (dissolving) temperature:	- 425°C
Temperature differential (ΔT):	- 50°C
Seed orientation (201), (011):	- rates from 2.6 to 5.7 mil/day (~ 0.07–0.14 mm/day), (010) rate generally higher, quality good
(Seed orientation based on a = 12.80 Å, b = 6,400 Å, c = 10.580 Å)[138]	
Spontaneous wall nucleation:	- moderate; crystals clear but not too well formed

The growth rates are for the total increase in crystal thickness or time of the run. Increasing ΔT to 75°C and increasing KPO_3 decreased the growth rate, but growing without KPO_3, i.e., with the mineralizer (2 m K_2HPO_4) alone, did not markedly effect the growth rate or quality. Growth in KH_2PO_4 or KPO_3 alone was very slow.

In the growth of KTP, like quartz, the seed orientation is very important. The growth rates are different in different seed orientations and the highest rate for KTP has been obtained on (011) seed crystal.[139]

The crystals grown at lower growth rates are superior in quality. Therefore, proper care has to be taken to achieve the optimum growth rate under hydrothermal conditions by selecting appropriate growth parameters, because a combination of several growth parameters act upon the growth rate and crystal quality of KTP.

5.5.2 Solubility of KTP

The solubility of KTP is an important aspect. The higher experimental temperature pressure adopted in the earlier works were due to lack of accurate data on the solubility of KTP and added to that the solubility of KTP is rather low in most of the conventional solvents.

The solubility of KTP in 1M K_2HPO_4 + 0.5 KPO_3 solutions has been studied in detail.[138] Figure 5.39 shows the solubility of KTP (in wt%) in 1M K_2HPO_4 + 0.5 KPO_3 at 10 kpsi. The solubility data indicate good solubility for growth at 600°C and a positive temperature coefficient.

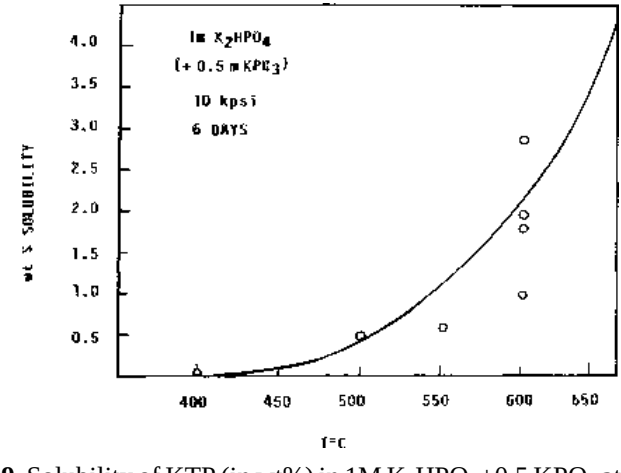

Figure 5.39. Solubility of KTP (in wt%) in 1M K_2HPO_4+0.5 KPO_3 at 10 kpsi.[138]

KTP crystals, using a complex mixture of water soluble phosphate glasses, KTP, solvents and water, have been obtained by several researchers. The glass composition is K_2O (42–70), TiO_2 (1–18), P_2O_5 (26–55) (mol%). The optimum ratio K/P is equal to 0.8–2.5, optimum glass composition is K_2O (55–60), P_2O_5 (38–42), (TiO_2 (1–5) (mol%).

Byrappa (1996) has carried out an extensive study on the solubility of KTP.[140] The main objective of this study was to find a suitable mineralizer solution in order to increase the growth rate, solubility, and crystal quality, but at reduced *PT* conditions. As well-known from the literature survey, the hydrothermal technique is most suitable for the growth of KTP crystals as it produces high-quality defect-free crystals. However, the main problem with the use of the hydrothermal technique for the growth of KTP crystals is the higher *PT* conditions of growth. In fact, when the early hydrothermal experiments were carried out, the *PT* conditions were rather high (P = 1.5 to 2 kbar; T = 650° to 700°C). The higher *PT* conditions do not yield large size crystals and the cost of the experiments involved is rather high. Subsequently, the inflow of the research data particularly on the *PVT* relations in several related systems of K_2O-TiO_2-P_2O_5, has brought down the *PT* conditions to the tune of P = 10 kpsi and T = 375–425°C.

Investigators have carried out hydrothermal experiments within a wide range of *PT* conditions using Morey and Tuttle type autoclaves. The nutrient materials were taken in teflon liners for experiments at lower *PT* conditions (using Morey type of autoclaves) and in platinum liners for experiments at higher *PT* conditions (using Tuttle type of autoclaves). A series of mixed mineralizers like H_2SO_4 + KOH, KF + HCl, HF + KF, H_2SO_4 + HCl + KF in different ratios were tried in order to bring down the *PT* conditions of crystallization of KTP crystals. The pressure in the system was calculated from *PVT* relations. In the case of lower *PT* experiments, the temperature was 275°C and the pressure was approximately 100 bars. The experiments were carried out for 8–10 days and spontaneously nucleated small crystals of KTP were obtained. The resultant product was washed thoroughly in distilled water to remove the excess solvents and the crystals were collected and dried. The size of the crystals were around 1 mm, colorless, transparent, and exhibited vitreous luster. The faces were developed in most of experiments. The solubility measurements were carried out on KTP crystals using the above said mixed mineralizers under hydrothermal conditions. Figure 5.40 shows the solubility curves for KTP. Figure 5.41 shows a representative photograph of a KTP crystal obtained by the hydrothermal method. Similar experiments

were carried out under elevated *PT* conditions (P = 500 bars and T = 325°C). The crystals were better in quality compared to the crystals obtained under lower *PT* conditions.

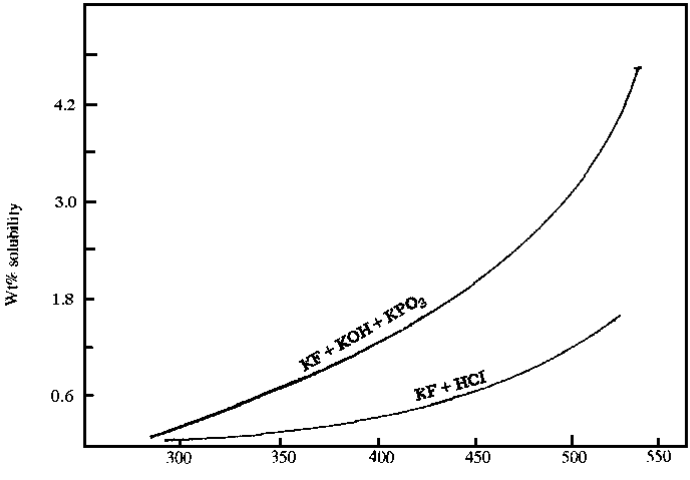

Figure 5.40. Solubility curves for KTP.[140]

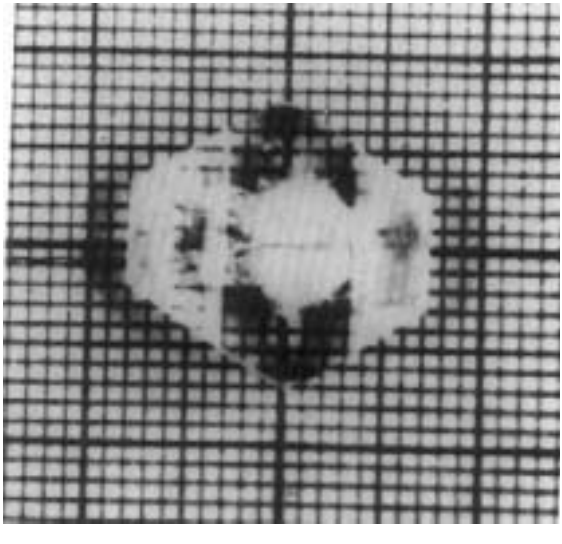

Figure 5.41. Representative photograph of a KTP crystal obtained by the hydrothermal method.[138]

Belt et al. (1989) have reported the growth of KTP single crystals in 4-liter capacity autoclaves at temperatures of 475°C and 1.5 kbar.[139] Gold liners were used here exclusively as corrosion resistance to the phosphates. Baffle openings were adjusted in the range of 20% with T = 30–40°C and the total run durations were 40–50 days. The growth rates sustained were 0.5–1.0 mm/side/week on (011) seed crystals.[126]

Belt and his group from Airtron Division of Litton Systems have increased the autoclave volume further and developed the low-temperature hydrothermal process in 5-liter systems. These large autoclaves have produced the largest KTP single crystals available in the world, see Fig. 5.42. These crystals are typically 4 × 5 × 8 cm and easily provide finished parallelpipeds of 1–1.5 cm^2 apertures and up to 2 cm long when material is extracted from either side of a seed. The schematic diagram of the large KTP crystals grown in 5-liter autoclaves is shown in Fig. 5.43. The rectangle in the center is seed plate, and the numbers identify prominent planes.[137] A successful large-scale hydrothermal growth process affects the size, cost, yield, and quality of KTP crystals. The cost of an autoclave is governed by its size, the type of alloys used, and availability of heat-treated billets from which the autoclaves are fabricated. Thus, lower-temperature experiments can use autoclaves made from more-common steel alloys, in turn lowering the cost.

The darkening of KTP crystals caused by the lack of oxygen in the growth process can be overcome by introducing an oxidizing agent, for example, 1–5 wt% of H_2O_2, into the mineralizer solution.

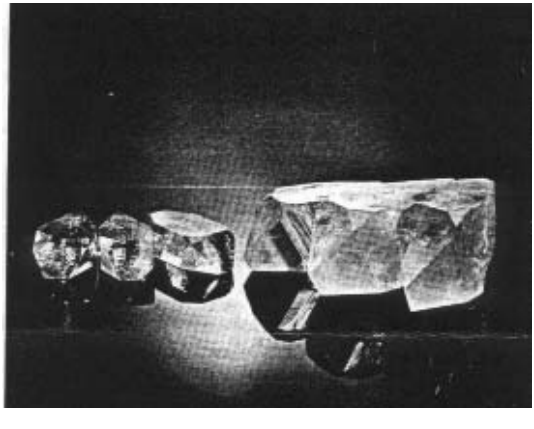

Figure 5.42. KTP single crystals grown using large autoclaves (5 liter). *(Photo courtesy of R. F. Belt.)*

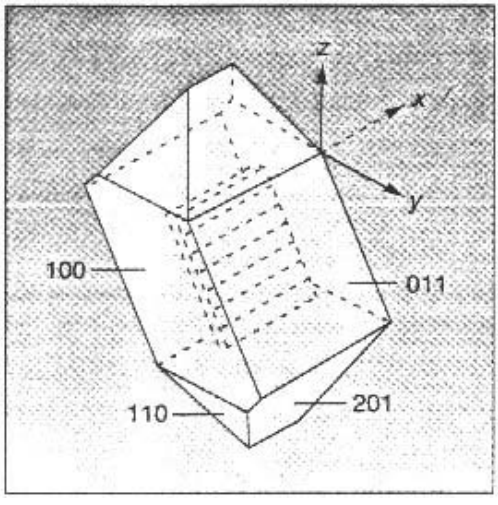

Figure 5.43. Schematic diagram of the large KTP crystals grown in 5-liter autoclaves.[137] *(Courtesy of the PennWell Publishing Co., USA.)*

5.5.3 Morphology

The morphology of KTP crystals is quite interesting and it does not vary much from flux-grown to hydrothermally grown. KTP usually grows as multifaceted crystal with fourteen faces typical for the KTP structure. The commonly seen crystal faces are {100}, {011}, {201} and {110} faces. These faces possess different growth rates and their relative sequence remains constant, even though the absolute growth rate of each face may vary with growth temperature gradient, solvent concentration, and so on. The average growth rates for various faces of hydrothermal KTP are given in Table 5.14.

Table 5.14. Average Growth Rate for Various Faces of Hydrothermal KTP

Growth Rate (10^{-3} mm/day)			
{100}	{201}	{011}	{110}
90	97	123	156
65	72	88	110
40	45	53	71

The {100} face has the largest area and, thus, the smallest growth rate among the faces. The width and height of the steps in KTP are inversely proportional to the growth rate or to the ΔT in different runs. Since KTP grows as multifaceted crystal, cutting and polishing of the crystal are quite cumbersome. Therefore, the growth of KTP with increased volume at lower cost is (very important) most desirable.

As shown in Table 5.13, the properties of KTP crystals vary with the growth method. Hydrothermally grown KTP crystals generally show an absorption band between 3550–3600 cm^{-1} due to the presence of $(OH)^-$. Generally, if a crystal used for a nonlinear interaction has even a small amount of absorption, the efficiency of the nonlinear interaction will be decreased. Absorption of the laser radiation occurs through the volume of the crystals illuminated by the laser beam. Thus, heating of the crystal occurs through this volume also. Cooling, on the other hand, occurs by conduction. Consequently, heating the surface of the crystal establishes thermal gradients within the crystal. As the refractive index depends on the temperature through the thermo-optic effect, gradient variations in the refractive index will also be generated. Variations in the refractive index will result in non-ideal phase matching throughout the volume of the nonlinear interaction. As the nonlinear interaction is quite sensitive to the variations in phase matching, the heating of the crystal can cause a significant degradation in the efficiency of the nonlinear interaction.[141]

Several authors have measured the ionic conductivity in pure and doped KTP crystals.[142][143] The ionic conduction property of these crystals allows ion-exchanged wave-guides to be formed readily in them.

5.6 POTASSIUM TITANYL ARSENATE

Recently, it has been shown that the nonlinear optic and electro-optic coefficients of potassium titanyl arsenate (KTA) crystals are significantly superior to those of KTP crystals.[144] Similarly, the arsenate isomorphs, like KTA, RTA, and CTA, unlike the phosphate isomorphs, are prone to ferroelectric multi-domain formation which renders these crystals useless in practical applications. KTA belongs to the class of forty compounds which are all structurally characterized by corner-linked octahedrally coordinated titanium chains connected with tetrahedrally coordinated phosphorus or arsenic bridges.

KTA can be prepared by methods analogous to those used for KTP. Brahmani and Durand (1986) have reported the structure of KTA

crystals[145]. The reputed effective nonlinear coefficient (d_{eff}) of KTA is 1.6 times that of KTP. This favorable property has encouraged several groups to carry out the hydrothermal growth of KTA at temperatures less than 600°C. Belt and Ings (1993) have hydrothermally grown KTA crystals using KH_2AsO_4 and KOH mineralizers. Flux grown KTA crystals were used as the seed crystals by these workers.[146] These authors have also studied the *PVT* relationship, solubility, and the growth rates and growth morphology in detail; with the pressure balancing method, growth rates of 0.2–0.4 mm/side/day can be achieved on {011} seeds. The experiments have been carried out in large size autoclaves of 4- to 5-liter capacities. Figure 5.44 shows the characteristic photographs of KTA single crystals obtained by Belt and Ings under hydrothermal conditions. The ideal morphology of KTA crystals is shown schematically in Fig. 5.45. The experimental conditions are given in Table 5.15.

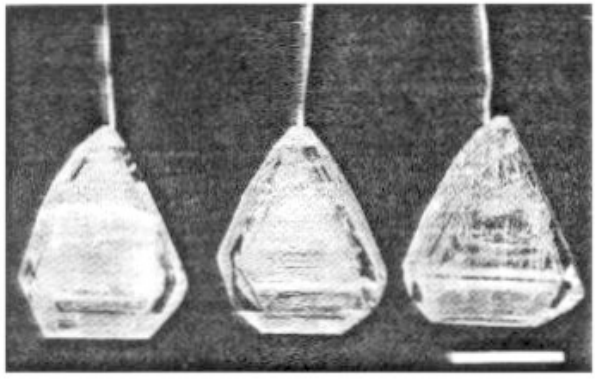

Figure 5.44. Characteristic photographs of KTA single crystals obtained by Belt and Ings under hydrothermal conditions.[146]

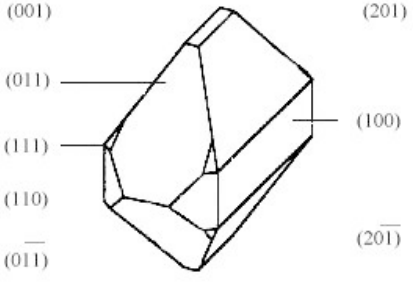

Figure 5.45. Ideal morphology of KTA crystals is shown schematically.[146]

Table 5.15. Summary of the Experimental Parameters of the Hydrothermal Growth Experiments in Production-Sized Autoclaves

Run No.	Mineralizer	% Fill		Nutrient	Nutrient temp. (°C)	Pressure (atm)	Seeds	Gradient (°C)	Run time (weeks)	Results
		Inner	Outer							
1	4M KH_2ASO_4	80	57	Flux grown KTA	560	1700	Unoriented flux growth KTA	28	2	Slight growth on KTA seeds
2	4M KH_2ASO_4	78	58	Flux grown KTA	590	1820	(201), (011) and (100) flux grown KTA	50	1.5	0.1 mm/side/week on (201) and (011) seeds, 0.2 mm/side/ week on (100) seeds
3	4M KH_2ASO_4	77	57	Flux grown KTA	590	1700	(201) and (011) flux grown KTA	30	2	0.2 mm/side/week on (201) and (011) seeds
4	4M KH_2ASO_4	77	57	Flux grown KTA	590	1700	(201) flux grown KTA	40	4	0.4 mm/side/week on (201) and (011) seeds, 0.2 mm/side/week on (100) seeds

Some authors have studied the ionic conductivity in KTA crystals and usually the ionic conductivity is one order of magnitude lower than KTP crystals. The ionic conductivity is found to be one-dimensional, i.e., along *Z*-direction only.

The structure of KTP family has the typical formula $\{K^+\}$ $[Ti^{4+}]O$ $(P^{5+})O_4$, where the flower brackets indicate nine- or eight-fold coordination, the square brackets six-fold octahedral coordination and the parentheses four-fold tetrahedral coordination. Different isovalent and aliovalent substitutions in a given structure are quite interesting, and could, perhaps, result in different structural and optical properties. Cheng et al.[147] have found that stability of KTA crystals is higher compared to other KTP-like compounds, Nb-doped KTP crystals are observed to be stable, and K_{1-x} Ti_{1-x} Nb_xO PO_4 single crystals with $x \approx 0.25$ have been obtained without any charge compensator. Partial charge compensation of Nb^{5+} in K_{1-x} Ti_{1-x} Nb_xO PO_4 crystals by Ga^{3+}, Fe^{3+} and Mg^{2+} has been reported. However, complete substitution of Ti^{4+} in single crystals of KTP with any aliovalent cation pair has not been achieved by any method.

On the contrary, complete substitution of Ti^{4+} with Nb^{5+}-Mg^{2+} and Nb^{5+}-Zn^{2+} cation pairs was reported to be possible in the case of KTA crystals. This result, suggested Chani et al. (1997), that it might be possible to prepare new aliovalent analogous of KTA containing Nb^{5+}-M^{3+} (M = Al, Cr, Ga, Fe, In) cation pairs in octahedral positions of KTP structure.[148] KTA crystal was the chosen basic material for this purpose as it was noted to be most stable compared to KTP.[147]

Lattice parameter values, in general, were found to increase with increasing M^{3+} cation radius, as expected. The results of compaction measurements indicate that Ti-free crystals with the structure of KTP have tendency to create potassium vacancies. This result is in good agreement with that reported for nonsubstituted KTP crystals. Structural analogues of KTP corresponding to K [Ta, M]O AsO_4 were prepared by solid-state reaction. However, no KTP phase formation was observed in K [Nb, M]O PO_4 and K [Ta, M]O PO_4 systems.

The growth of KTP family of materials on the whole is fascinating and challenging for both technologists and academicians.

5.7 CALCITE

Calcite, $CaCO_3$ is an important carbonate mineral and it occurs commonly in nature both as well-developed crystals and amorphous material. The pure and optically clear calcite is called Iceland spar. Calcite is polymorphous and exists in at least five modifications. The two polymorphs commonly found in nature are calcite and aragonite. In addition, there are two synthetic forms known only at high pressures: calcite II and calcite III. Vaterite (γ-$CaCO_3$) is a metastable hexagonal form which crystallizes at ordinary temperatures and pressures.[149]

Calcite single crystals form an important optical material owing to its large birefringence and transparency over a wide range of wavelengths. This property makes it one of the significant materials for polarized devices such as optical isolaters and *Q* switches. It also exhibits antiferromagnetic properties. Although there are many deposits of calcite in the world, the optically clear quality calcite (for example, Iceland spar) has been depleted in recent years, leading to its shortage in nature. However, the demand for optically clear calcite single crystals is increasing greatly with the development of laser devices such as optical isolators,[150][151] and similarly, the chemical impurities and growth defects depend upon the geological settings and often lead to variations of refractive index and internal light scattering centers, and low optical damage resistance. Hence, the artificial means of obtaining optically pure calcite is becoming very popular. Many laboratories throughout the world have attempted to obtain calcite, but most of them have suffered from size or quality problems. In fact, the first publication on the synthesis of calcite appeared in 1883. Lemberg[152] heated basalt for six months with distilled water. It took up 2.43 % H_2O, which was not removed over H_2SO_4 in two weeks; the solution remaining in the tube had a slightly alkaline reaction. The same basalt heated with K_2CO_3 solution for nine months gave a glass rich in H_2O, and $CaCO_3$ crystals. A glass made from palagonit from Vidoe heated for three months with distilled H_2O was little attacked, but the product contained 8.61 % H_2O. Similarly, melted labradorite, heated for thirteen months with K_2CO_3 solution gave a glass rich in K, and the Ca replaced had formed $CaCO_3$. Further Lemberg obtained $CaCO_3$, while the MgO remained combined with the SiO_2 after heating augite with K_2CO_3 solution for one year at 100°C. When anorthite, with a little augite, was heated for 189 hours at 180–190° with Na_2CO_3 solution, the product consisted of calcite crystals, amorphous substances, and a

columnar mineral similar to cancrinite. Later, Friedel and Sarasin (1885) obtained small calcite crystals by heating $CaCl_2$, precipitated $CaCO_3$, and 60–70 cc H_2O for ten hours at 500°C; with 20 gms $CaCl_2$ and a few grams $CaCO_3$ the crystals were large enough for goniometric measurements. Crystals obtained were simple rhombohedra.[153] There was no aragonite in the product. However, all these earlier works on the synthesis of calcite were purely of geological/mineralogical interest, and the size of the crystals obtained was in no way nearer to the fabrication of devices. The most significant problem for the growth of calcite crystals is that the growth techniques are restricted due to the dissociation of $CaCO_3$ at high temperatures. Several techniques have been employed to grow calcite single crystals like low temperature solutions,[154][155] gels,[156][157] fluxes or eutectics,[158][159] top seeded solution growth,[160] travelling solvent zone melting,[161] hydrothermal hot pressing,[162]–[164] and hydrothermal.[150][151][165]–[170] Calcite crystals grown by most of these methods encounter several problems including the presence of large thermal stress, CO_2 dissociation, and alkaline carbonate flux inclusions which cause serious defects and contamination by metal ions. On the other hand, the hydrothermal method is one of the most promising techniques for growing unstable crystals such as a carbonate compound, with the advantage of suppressing the dissociation of CO_2 and yielding high quality crystals in a homogeneous ambient at relatively low temperatures.[171] Also, this technique is closer to the conditions in which calcite grows in nature.

Many researchers have tried to grow calcite single crystals at relatively low temperatures since calcite crystals dissociate to form CaO and CO_2 above 900°C under atmospheric pressure. Varieties of solvents have been used for hydrothermal growth of calcite, but none of them have succeeded in growing large single crystals. The solubility of calcite is very interesting. It has been studied in water under various CO_2 pressures.[172][173] The CO_2 pressure would be concerned with dissolution and precipitation of calcite in nature. Thus, hydrothermal growth under variable CO_2 pressures is also very interesting from the point of view of geochemistry. The solubility is positive for increasing CO_2 pressure and negative for increasing temperature. This behavior of calcite has posed a real problem in the search for a suitable solvent to obtain higher/optimum growth rates. Despite this, a large number of reports concerning calcite growth, hydrothermal reaction of calcite in chloride, and other chloride solutions have appeared. Because natural calcite crystals are formed in both chloride and carbonate hydrothermal solutions and these chloride solutions are almost

analogous to natural carbonate thermal springs. Ikornikova has done an extensive work on the aspects of solubility, designing an apparatus to grow calcite crystals with changing CO_2 concentration as the pressure is reduced at constant temperature, crystal growth kinetics, and mechanism.[166]

For hydrothermal crystal growth of calcite, several inorganic solvents like NaCl, LiCl, $CaCl_2$, $NaNO_3$, $Ca(NO_3)_2$, NH_4NO_3, K_2CO_3, and carbonic acid have been employed as mineralizers. The growth conditions vary from 150°C and 15 MPa, to 600°C and 200 MPa. No one has used organic salt solutions to grow calcite crystals under hydrothermal conditions. Yamasaki and his group have tested the solubility of calcite in ammonium acetate solution.[170] However, there is no unanimity with respect to solubility owing to the change in the sign of the temperature coefficient of CO_2 solubility in H_2O, as shown in the isobaric diagram Fig. 5.46. The diagram clearly shows two regions: I and II, lying on the two sides of the 200 bar isobar, which is close to the isobar of the critical pressure of water. The pH of the system falls with increasing P_{CO_2} under standard conditions. This is connected to the fact that with increasing CO_2 solubility, the concentration of both the hydrocarbonate and the hydrogen ions increases. The solubility of calcite in aqueous solutions of carbon dioxide was studied between 10–300°C and 1–100 bar.[172][173] At the same time, for T = constant, the solubility rises exponentially with increasing P_{CO_2}. Later experiments at 200–600°C and 200–1400 bar in solutions of 10–100 mg/ml CO_2 showed that absolute solubilities of calcite at high temperatures and pressures were almost an order of magnitude lower than those measured at pressures up to 100 bar.[174] The following groups have carried out extensive studies on the solubility of calcite: *i)* Ikornikova of Russia, during 1960s and 1970s—using chloride solutions; *ii)* Belt, USA, during 1970s—using carbonate solutions; *iii)* Hirano, Japan, during 1980s and early 1990s—using nitrate solutions; *iv)* Kodaira, Japan, during 1990s—using H_2O-CO_2; *v)* Yamasaki, Japan, during 1990s to date—using ammonium acetate and other organic solvents. Each one of the last three groups claims superiority of their solvents over the others. Figures 5.47 and 5.48 show the solubility curves for calcite in different solvents. Yanagisawa et al. (1996) have studied the effect of pH of CH_3COONH_4 on the growth of calcite.[170] It was found that calcite crystals could not grow in the CH_3COONH_4 solutions with a low pH. This has been explained by the change in the existing ion species in the solution. A high growth rate was obtained in the solutions with a pH of 7.0–7.5. Beyond a pH of 7.5, the

growth rate falls again. The pH of solution decreased with the increase in temperature, and it reached 6.0 at 200°C. This result suggested that H_2CO_3 was the main dissolved species in the solution at 250°C. When calcite dissolves in water, the carbonate ion must change its ionic form to HCO_3^-, which is very essential for the crystal growth of calcite, whereas H_2CO_3 does not contribute to the growth of calcite crystals. The formation of the ionic species HCO_3^- has been noticed by several workers like Kikuta and Hirano in the NH_4NO_3 solutions from FT-IR studies.[174] This suggests that calcite dissolves in the solvent below 200°C as follows:

$$NH_4NO_3 + CaCO_3 + H_2O \rightarrow Ca^{2+} + HCO_3^- + NO_3^- + NH_4^+ + OH$$

$$2NH_4F + CaCO_3 + H_2O \rightarrow CaF_2 + HCO_3^- + 2NH_4^+ + OH^-$$

$$(NH_4)_2\,SO_4 + CaCO_3 + H_2O \rightarrow CaSO_4 + HCO_3^- + 2NH_4^+ + OH^-$$

This work strongly confirms that a small amount of additives such as phosphate, sulphate, borate, and ethylene glycol effectively arrested the growth of calcite.

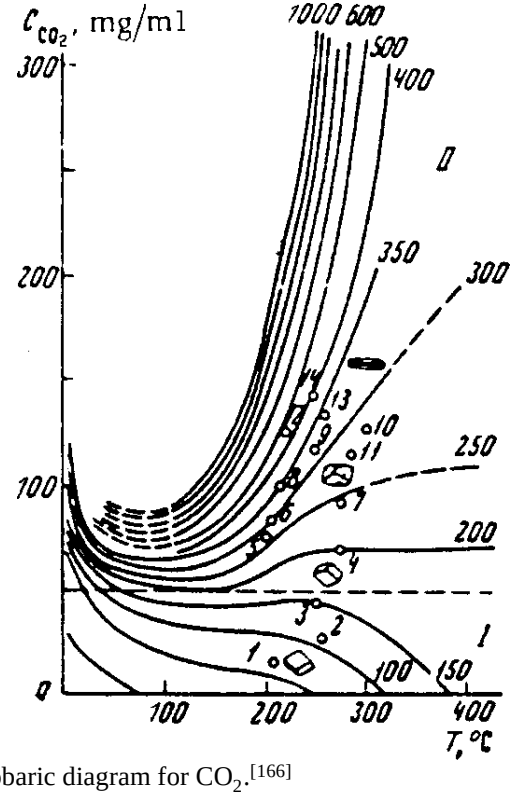

Figure 5.46. Isobaric diagram for CO_2.[166]

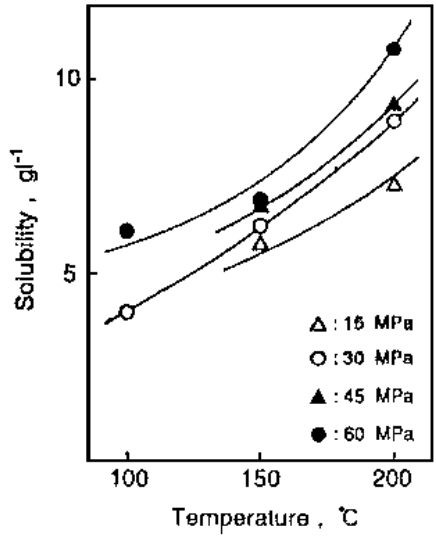

(a)

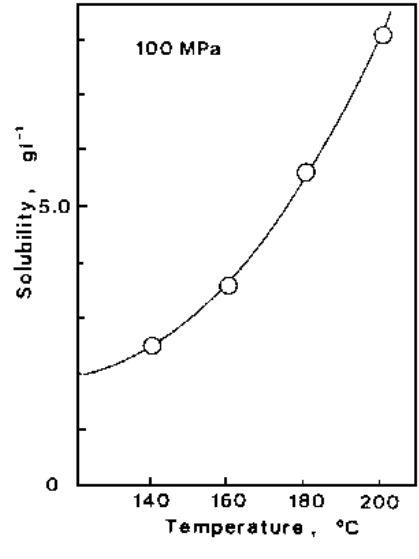

(b)

Figure 5.47. Solubility curves for calcite in different solvents, *(a)* in 1mNH_4NO_3 and *(b)* in 3mNH_4NO_3.[171]

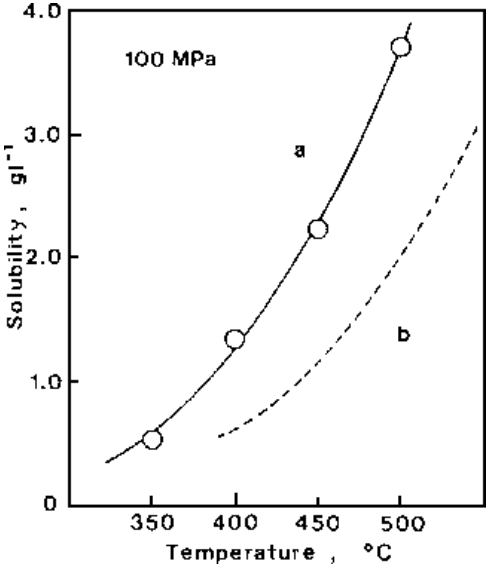

(a) 1.5mCa$(NO_3)_2$
(b) 3mNaCl

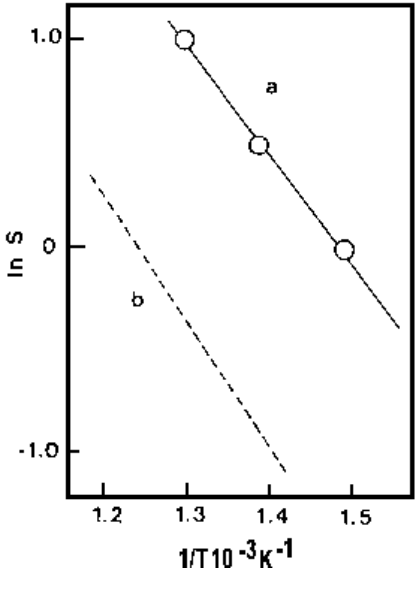

(a) 1.5mCa$(NO_3)_2$
(b) 3mNaCl

Figure 5.48. Solubility curves for calcite in different solvents.[168]

5.7.1 Crystal Growth

Solubility of calcite can be both positive and negative for increasing CO_2 pressure and increasing temperatures, respectively. Therefore, the growth of calcite crystals insists on a special experimental setup. Figure 5.49 shows the arrangement of the apparatus designed by Ikornikova for growing calcite crystals in aqueous solutions of CO_2 with a negative temperature coefficient of solubility, together with curves illustrating the height distribution of temperature and CO_2 concentration.[166] The crystals obtained by this means, with seed crystals at the bottom and nutrient at the top followed by a temperature gradient between the two zones separated through a baffle, have rhombohedral faces covered with stepped pyramids. Similarly, Ikornikova has designed another apparatus for synthesizing calcite crystals in aqueous solutions of carbonic acid under isothermal conditions. The autoclave used is a rocking autoclave. Figure 5.50 shows the schematic diagram of the apparatus used in the synthesis of calcite. The autoclaves in both the cases are either glass or teflon lined.[166][169] In this case, usually at pressure under 150 kg/cm^2, rhombohedral calcite crystals without any pinacoid are formed. The pinacoid appears on crystals formed at pressures greater than 200 kg/cm^2.

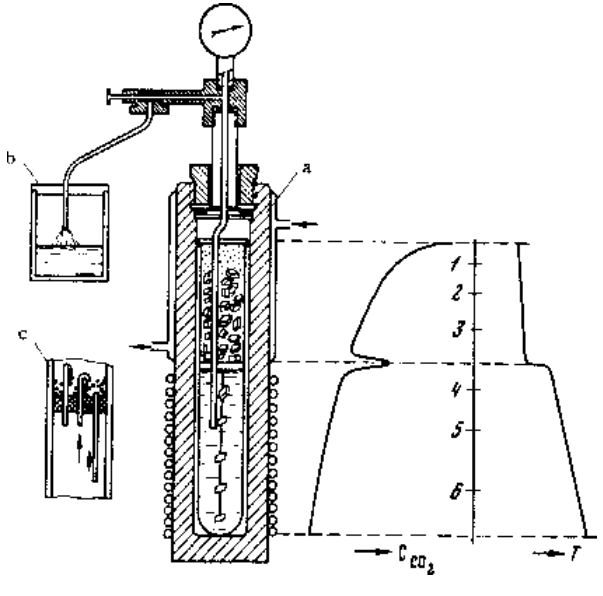

Figure 5.49. Arrangement of the apparatus for the growth of calcite.[166]

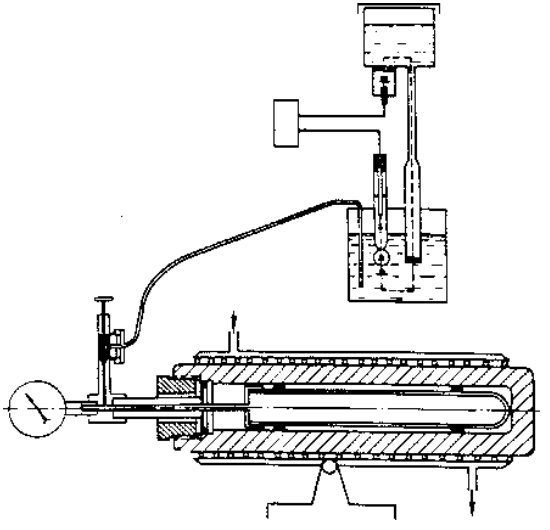

Figure 5.50. Schematic diagram of the apparatus used in the synthesis of calcite.[166]

Kinloch et al. (1974) have obtained calcite single crystals in large autoclaves (23 cm internal diameter × 280 cm length)—commercial production using 6 M K_2CO_3 mineralizer. As K_2CO_3 attacks autoclaves made of ferrous alloys, the autoclaves were provided with cylindrical silver and platinum cans.[150] The following are the experimental conditions used by these workers:

Nutrient:	-	45 Kg. of optical grade crystals of Mexican origin
Seeds:	-	Natural calcite crystals cutting rhombohedra with 10–20 cm^2 surfaces and 1–2 cm thick
Solvent :	-	6 m K_2CO_3
Nutrient temperature:	-	435–445°C
Seed temperature range:	-	410–425°C
% Fill:	-	86 % (1.72 Kbar)
Baffle opening:	-	8 %
Temperature gradient:	-	5 to 10°C
Experimental duration:	-	30 to 50 days
Growth rate obtained:	-	50 μm/day/face for {1011} face

Much of the recent works on the growth of calcite single crystals are being carried out under moderate to lower temperatures (200–150°C) using several new solvents like ammonium nitrate, ammonium acetate, and so on. The results are far better than crystals obtained under higher temperatures because of the reduced thermal strain. Recent workers use teflon liners. A considerable amount of progress has been achieved in the single crystal growth of calcite with reference to the solubility, growth rate, reaction kinetics, seed orientation, morphology, surface morphology, optical and laser quality, and so on. Figure 5.51 shows the schematic diagram of the autoclave for hydrothermal crystal growth of calcite commonly used in recent years. It is well confirmed that the ammonium nitrate and acetate solvents are more effective than chloride solvents from the viewpoint of calcite crystal growth. The calcite crystals dissolve in ammonium nitrate or acetate solutions, accompanied by the evolution of ammonia. This reaction increases the dissolution of calcite in the hydrothermal solution which gives an advantage of lowering the pressure, temperature conditions of the growth, and in turn facilitates the use of teflon liners. Great improvements are achieved by using a baffle plate and band heater to control the temperature gradient and the transport behavior. Higher temperature gradients give higher growth rates, especially at higher growth temperatures. Usually the growth rate varies from 25 μm/day to 213 μm/day. The rhombohedral face (1011) is the fastest growing face. Hence, natural calcite crystals cleaved at (1011) plane are used generally as seed crystals. Yanagisawa et al. (1996) have obtained the highest growth rate reported so far, for calcite, 213 μm/day using ammonium acetate solvent at 230°C and a temperature gradient of 20°C. However, the optical quality of the calcite crystal was relatively poor. Only under experimental conditions, such as temperature gradient of 15°C and growth temperature of 235°C, was the growth of transparent calcite crystals achieved at 57 μm/day. Figure 5.52 shows the hydrothermally grown calcite crystals by different authors. When as-cleaved crystals are used, the calcite crystals obtained are usually opaque or not transparent, and the surfaces show a greater degree of defects like growth hillocks, a lot of small secondary grown crystals, and strains. The crystals grown on the etched seed crystals are usually transparent and the surfaces are very smooth. Figure 5.53 represents the characteristic photographs of calcite single crystal grown in NH_4NO_3 solution using as-cleaved and etched seeds. Similarly, Figure 5.54 represents the surface morphology of the calcite crystals using as-cleaved and etched seeds. Recently, Lee (1998)

has re-attempted the solvent NH_4Cl, first reported by Ikornikova,[165] to obtain calcite single crystals[175] to suppress the spontaneous mineralizer. It was observed that the addition of such an organic additive played an important role in suppressing the formation of spontaneous nuclei; usually higher % fill (81–83%) was selected in all the experiments and the pressure-temperature conditions were kept low. Hence, teflon was used as the liner.

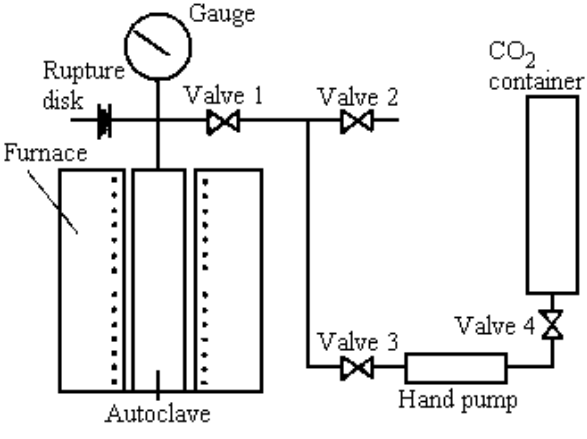

Figure 5.51. Schematic diagram of the autoclave.[169]

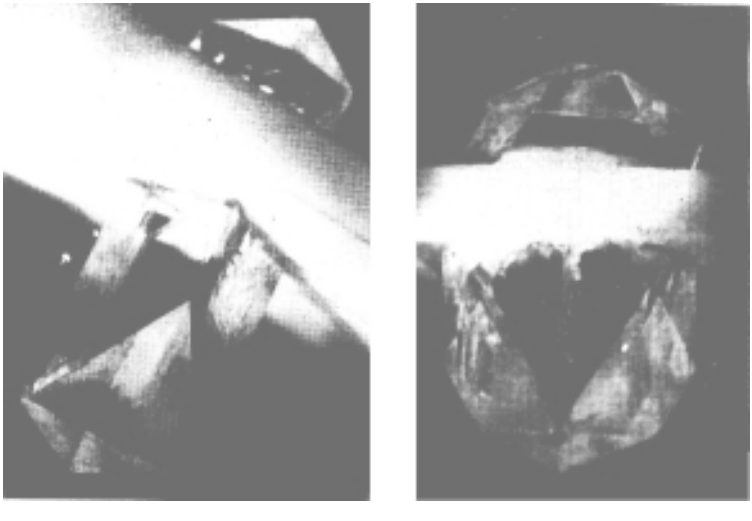

Figure 5.52. Hydrothermally grown calcite crystals.[166]

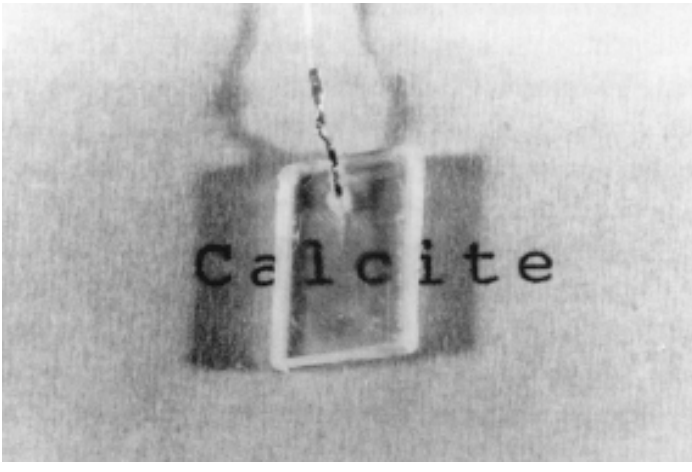

Figure 5.53. Characteristic photograph of calcite single crystal grown in NH_4NO_3 solution.[168]

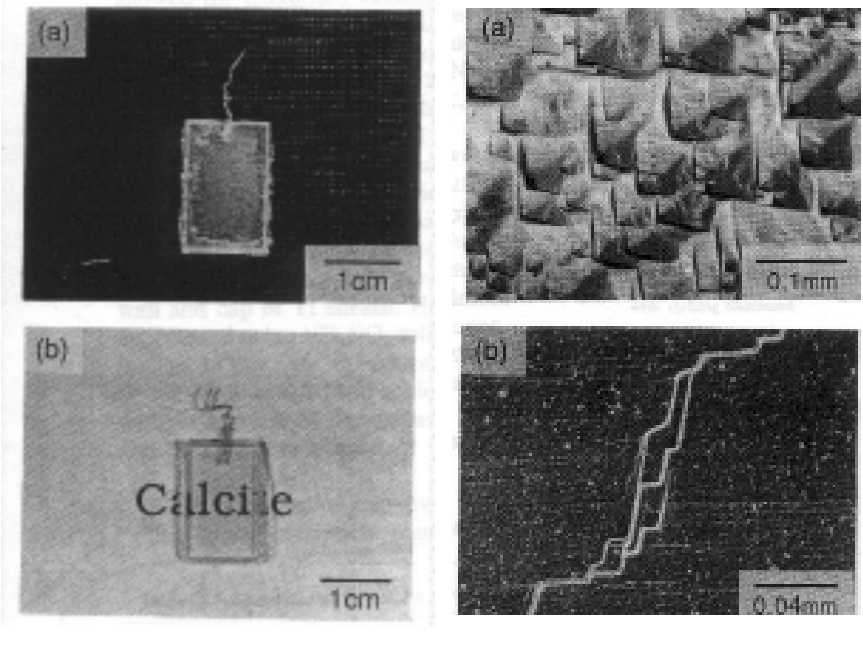

Figure 5.54. Surface morphology of the calcite crystals using as-cleaved and etched seeds.[168]

5.7.2 Hydrothermal Hot Pressing of Calcite

The hydrothermal hot pressing is being applied in recent years for the solidification of $CaCO_3$. The hydrothermal hot pressing (HHP) technique is a method by which hard solid bodies of powders can be produced in a short time and at a relatively low temperature under saturated vapor pressure. This process is very similar to diagenesis[176] in geology, therefore, a diagenesis process, such as for limestone, may be resurrected by using this technique. The results, using the hydrothermal hot pressing technique, may bring in some new information to the sedimentary process and a new technology of forming fabrication processes. Yamasaki and Weiping (1993) have obtained $CaCO_3$ by hydrothermal hot pressing with sea water, and they have designed a "quasi-diagenesis" experiment. Initially, the $CaCO_3$ powder was synthesized in seawater, and this powder was then solidified by the hydrothermal hot pressing technique. Various ions of sea water, Cl^-, Na^+, K^+, SO^{2-}_4, etc., were absorbed on the surface of the synthesized $CaCO_3$ sample powder during the precipitation process, and these ions formed soluble salts such as NaCl and $CaSO_4$ under hydrothermal hot pressing conditions, that is, the solubility of the synthetic $CaCO_3$ powder surface may have increased rapidly in the presence of $CaSO_4$, and NaCl solution under hot pressing conditions. Consequently, it was revealed that the small grains were dissolved, and then recrystallization occurred, or the grains adhered to the surface of larger grains and formed large grain growth during hydrothermal hot pressing. The solidification process was carried out by a dissolution-recrystallization mechanism during the hot pressing process.

Yamasaki et al. (1993) have solidified the powders of calcium carbonate with sodium carbonate by mechanical compression under hydrothermal conditions. The effects of hydrothermal conditions such as temperature, pressure, and ratio of Ca/Sr on the reaction process and microstructure of the solidified bodies have been studied.[163]

The growth of calcite single crystals is becoming very popular in recent years with the fast decrease in the availability of natural calcite. Although the growth of calcite has been better understood in the last five to six years, still there is no unanimity with reference to the solvent and experimental conditions. There is no doubt that calcite crystal growth is one of the flourishing and challenging topics.

5.7.3 Growth of Related Carbonates

There are several works in the literature dealing with the growth of other carbonates like $MnCO_3$ (rhodochrosite), $FeCO_3$ (siderite), $CaCO_3$ (spherocobaltite), $CdCO_3$ (otavite), $NiCO_3$, and so on. Most of these are the important carbonate minerals, and their growth carries a great significance to the geological literature.

$MnCO_3$ (Rhodochrosite). The crystallization of rhodochrosite crystals takes place in LiCl solutions (1–25 wt%) at temperatures 400–450°C, and pressure 680–2500 atm., the ΔT = 10–50°C.[177] In the experiments with 20–25% LiCl solutions at ΔT = 10°C, T = 430°C, and P = 960 atm, Ikornikova has obtained transparent crystals of rhodochrosite with a size of 5–7 mm.

$FeCO_3$ (Siderite). The synthesis of siderite is slightly more difficult than $MnCO_3$ having to do with the stability during the variation in the oxygen potential. Ikornikova (1970) has obtained transparent crystals of $FeCO_3$ in NH_4Cl solutions at T = 300–350°C, P = 600–800 atm and P_{CO_2}–300 atm.[178]

$CaCO_3$ (Spherocobaltite). The growth of spherocobaltite crystals has been carried out on the seeds in the LiCl solution. Autoclaves of 300 cm^3 using titanium liners have been used. Separate experiments have been carried out in 1.2–1.7 liter autoclaves with platinum liners. Spontaneously grown crystal was used as a seed crystal. However, detailed studies on the growth of spherocobaltite are not known.[177][178]

$CdCO_3$ (Otavit). Monocrystals of otavit were first obtained by Ikornikova.[177] Crystals were grown in LiCl (5–20%) and NH_4Cl (1–5%) solutions in the temperature interval 300–550°C, ΔT = 15–20°, P = 700–900 atm. The size and quality of the crystals in the growth zone were regulated through the concentration of solution and temperature gradient.

$NiCO_3$. Monocrystals of carbonate of nickel could be obtained at T > 150–500°C and P > 1500 atm using $NiCO_3$, $Ni(OH)_2$. During the evolution of CO_2 in the autoclave, the crystallization of $NiCO_3$ takes place at much lower pressure and NH_4Cl (2–10%) solution.[179]

Figures 5.55, 5.56, and 5.57 show photographs of some selected hydrothermally synthesized carbonates in the hydrothermal laboratory of K. Byrappa.

The growth of carbonates, in general, is quite interesting academically, technologically, and geologically.

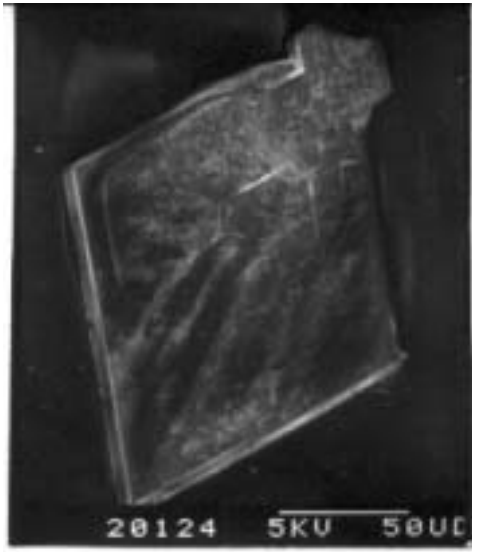

Figure 5.55. $ZnCO_3$ crystal.

Figure 5.56. $SrCO_3$ crystal.

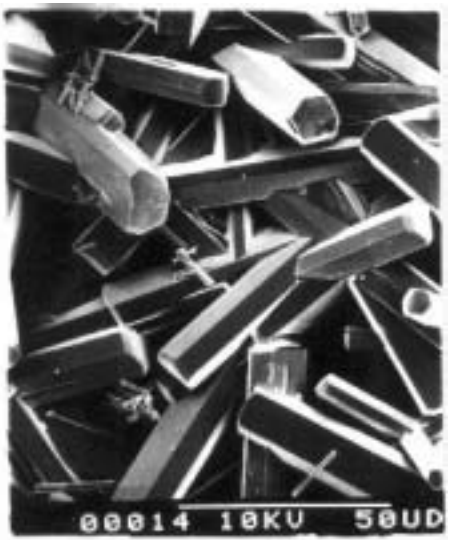

Figure 5.57. $BaCO_3$ crystal.

(Photographs courtesy of J. A. K. Tareen and B. Basavalingu.)

5.8 HYDROXYAPATITE (HAp)

Apatite is a common mineral in igneous, sedimentary and metamorphic rocks,[180] which has the general chemical formula of $A_{10}(BO_4)_6X_2$, where A = Ca, Sr, Ba, Fe, Pb, Cd, and many rare earth elements; BO_4 = PO_4^{3-}, VO_4^{3-}, SiO_4^{4-}, AsO_4^{3-}, CO_3^{2-}; X = OH^-, Cl^-, F^-, CO_3^{2-}. Water exists in different forms.[181][182] The presence of the elemental phosphorus, which is a major component of apatite, was first reported in the 17th century and the phosphorus in mineral pyromorphite (lead apatite) was discovered in 1779.[183][184] Since the first synthesis of apatite done in the middle of 19th century,[185] a lot of studies in the geochemical, crystallochemical, biological, and other fields have been carried out. In fact, most of the geochemical and crystallochemical studies were carried out on natural apatites, whereas biological or other recent studies were mainly done using synthetic apatites. However, many efforts have been made to prepare large single crystals of HAp with only limited success. The interest in the synthesis of hydroxyapatite is linked with its importance as a major constituent of the inorganic component in bones and teeth where it occurs as tiny crystals. Since it has been recognized to be one of the best biocompatible materials, there have been many reports on the biological aspects.[186]–[188] HAp crystals have selective adsorption ability of proteins depending on crystal planes and are used as an adsorbent in liquid chromatography.[189] Recent interest in the material has spread to the fields of electronics and surface science (or adsorption chemistry), where sintered or powder HAp is expected to function as, for example, gas sensors, catalysts, and chromatographic absorbers. The fabrication processing of HAp has also progressed with the growing importance of the biological applications of HAp as artificial bone and teeth.[190] Table 5.16 gives the physico-chemical properties of apatites.[191] However, a detailed knowledge of chemical and physical properties of HAp, including those relevant to the behavior in a biological environment, depends on the availability of sufficiently large single crystals of known chemical composition. Even today most of the studies on chemical properties, mechanical properties, biological responses and the prosthetic application of HAp are based on polycrystalline bodies with random crystal arrangement including sintered bodies, powders, granules and coatings.

Table.5.16. Physico-chemical Properties of Synthetic Hydrothermal or Natural Fluorapatite[191]

Properties	Values	Comments
Theoretical Formula	$Ca_{10}(PO_4)_6(OH)_2$	composition varies with sample preparation
Space Group	$P6_{3/m}$ (hexagonal) $P2_{1/b}$ (monoclinic)	mono. ↔ hexa. transition may occur at ca. 200°C
Lattice Parameters (LP)	a = 9.41-9.44 Å c = 6.84-6.94 Å	large discrepanices in L.P. of *'Wet Chemically'* HAp
Theoretical Density	3.16 g/cm^3	varies with composition
Moh's Hardness	3(CO_3-Ap) 5(HAp)	water and CO_3 in apatite lattice lower hardness
Heat Capacity	184.07 cal/K.mol at 298.16 K 950°C 180.16 cal/K.mol at 298.15 K	"wet" HAp following calcined at "wet" HAp following calcined at 1100°C
Thermal Expansion Coefficient	11-14 x 10^{-6} K^{-1}	*'wet'* HAp expands non-linearly
Melting Point	1614°C	'synthetic' HAp, hot-stage microscope method
Surface Energy	S(001)=95±25MPa	Natural FAp, slow cleavage method
Stiffness Coefficient at room temp (Mbars)	C11=1.434, C33=1.805 C44=0.415, C12=0.445 C13=0.575, C66=0.495	Natural FAp, ultrasonic pulse superposition
Dielectric Constant	7.40-10.47	varies with composition
Refractive Indices	n_w=1.649-1.651, n_c=1.642-1.644	relationship between indices & composition is shown in Ref. 1
Optical Frequency	2.71 (‖c) 2.69 (⊥c)	varies with composition

Daubrée (1851) was the first to synthesize apatite by passing phosphorus trichloride vapor over red-hot rime.[185] Since then a number of reports on the preparation of HAp by various methods have appeared in the literature, and the results prior to 1951 have been reviewed by Jaffe (1951).[186] Yoshimura and Suda (1994) have reviewed the preparation methods for HAp and grouped all the methods into three categories, as given in Table 5.17.[191] First is the conventional *solid state reaction method* at high temperature, the second is the *wet chemical method* at relatively low temperature and the third, which is a very important method today, is the *hydrothermal method* using high-temperature–high-pressure aqueous solutions.

Table.5.17. Preparation Techniques for Hydroxyapatite[191]

Techniques	Starting Materials	Synthetic Conditions	Comments
Solid State Reaction	$Ca_3(PO_4)_2$+ $CaCO_3$ $Ca_2P_2O_7$+ $CaCO_3$	900-1300°C, usually with water vapor	Ca/P-1.67, large grain size, irregular forms, inhomogeneous flowing
Wet Chemical Method	$Ca(NO_3)_2$+$(NH_4)_2$ HPO_4 $Ca(OH)_2$+ H_3PO_4	R.T.-100°C pH: 7-12	Ca/P < 1.67 fine irregular crystals with low crysatllinity inhomogeneous
Hydro-Thermal Method	wet chemically prepared HAp, other calcium phosphates, seeding	100-200°C (1-2 MPa), 300-600°C (1-2 Kbar)	Ca/P=1.67 homo-geneous, fine single crystals or large crystals
Gel Growth Method	Gel + Ca^{2+} + PO_4^{3-}	R.T.-60°C, pH: 7-10	large Monetite, Brushite, OCP, but small HAp
Flux Growth Method	CaF_2, $CaCl_2$ as flux $Ca(OH)_2$ as flux	1325°C (FAp,ClAp) HAp	large crystals with little lattice strain

The solid state reaction method has generally been used for processing ceramic powders and for studying phase stabilities. The powders prepared by this method, however, usually have irregular forms with a large grain size, and often have heterogeneity in composition due to incompleted reaction resulting from small diffusion coefficients of ions within solids.

The wet chemical method is a relatively easier method for obtaining HAp. Besides, the reaction in any living organisms may occur in aqueous solutions at low temperatures. Many experiments on the preparation of HAp by this method have been reported which investigate the formation mechanism of any calcium phosphates *in vitro*, in addition to *in vivo*. The powders prepared by this method, however, do not seem to be appropriate as the starting materials for ceramics because they are usually less crystallized, heterogeneous in composition, and irregularly formed. Sol-gel, alkoxide, and other chemical methods have also been used. CVD, plasma spray method and other (electro) chemical methods have been mainly used to form HAp layers on substrates.

The hydrothermal method enables us to prepare well crystallized, compositionally homogenous, uniform and easily sinterable powders due to great effects of the high-temperature–high-pressure aqueous solutions.

The growth of HAp crystals has been carried out by several other methods like the gel growth method.[192] There are several reports on the melt growth and flux growth of apatites of different compositions. Johnson (1961) has used the melt growth for the preparation of single crystals of apatite from the stoichiometric melt. These crystals grown from the melt at high temperatures, however, are usually severely strained due to the large temperature gradients existing during the growth.[193] Prener (1967) used the flux growth method, which is an excellent method since the fluxes like CaF_2, $CaCl_2$, and $Ca(OH)_2$ mixed with the starting apatite powders make lower liquidus temperature, far below needed for the melt growth method, resulting in the production of less strained apatite crystals.[194] Recently, Oishi and his group have obtained chlorapatite and fluorapatite crystals by the flux method using NaCl, KF and Ca_2ClPO_4 fluxes.[195]–[197] Masuda et al. (1990) have used the sol-gel method to obtain HAp from metal alkoxides.[198] Brendel et al. (1992) have used the polymerized method to achieve HAp coatings.[199] Likewise, many other methods are utilized in the processing of apatites. Thus, for the growth of HAp, the volatility of water at the necessary high temperatures makes hydrothermal conditions unavoidable.

5.8.1 Crystal Structure of Apatite

Most of the studies concerning the crystallochemical, geochemical and phase stability related aspects of apatite have been carried out on natural or hydrothermally synthesized large single crystals. The crystal structure of fluorapatite (FAp) was first determined by Naray-Szabo (1930) and by Mehmel (1930) independently.[200][201] Followed by these, several publications appeared on the structure of various forms of apatite.[202]–[204] The general agreement on the crystallographic aspects is as follows:

a) Apatite shows ionic bonding character, and it is made up of a close packing of large oxygen ions, resulting in the hexagonal crystal system.[205]

b) The space group of fluorapatite (FAp) is $P6_{3/m}$.[200]–[204]

c) Although the space group of HAp is believed to be $P6_{3/m}$, HAp prepared at high temperature is P 21/b (monoclinic) at room temperature,[200] nearly identical with chlorapatite (ClAp).

d) A phase transition in HAp is suggested to occur at ~ 200°C, probably due to the order-disorder orientation at $(OH)^-$ ions along the *c* axis.[206][207]

5.8.2 Phase Equilibria

The phase equilibria in the system $CaO\text{-}P_2O_5\text{-}H_2O$ have been extensively studied by the solid state reactions method under atmospheric pressure of water vapor by Van Wazer (1958),[208] and in aqueous systems at temperatures lower than 100°C by Brown et al. (1991, 1992).[209][210] Biggar (1966) has studied the phase equilibria in the system $CaO\text{-}P_2O_5\text{-}H_2O$ in the temperature range 700 to 950°C, and *P* of 1 kbar.[211] Feng and Rockett (1979) have studied the system $CaO\text{-}P_2O_5\text{-}H_2O$ at 200°C.[212] Figure 5.58 shows the $Ca(OH)_2\text{-}Ca_3(PO_4)_2\text{-}H_2O$ at 1000 bar with 50 wt% H_2O. Skinner (1974) found that the field of stability of hydroxyapatite alone with water in the triangle $CaO\text{-}P_2O_5\text{-}H_2O$ was confined to a narrow band joining the representative point of stoichiometric hydroxyapatite to the water representative point of the phase diagram.[213] There are several other phase equilibria studies on the apatite system and the reader can refer to the works.[191][214] Andrade et al. (1997) carried out a detailed

thermodynamic analysis of the system Ca-P-H_2O based on the development of the Eh-pH and Pa_C-pH (where $Pa_{Ca} = -\log_{10} a_{Ca}$) diagrams at different temperatures and different activities of phosphorous and calcium in aqueous solution. The hydroxyapatite precipitated at ambient temperature (30°C) was hydrothermally treated at 150°C.[215] Figures 5.59–5.63 show the Eh-pH diagrams of the Ca-P-H_2O system at 25°C and 300°C, for 1.67 molal activity of the Ca and 1 molal activity of pressure in the aqueous solution. Figures 5.61 and 5.62 present the Pa_{Ca}- pH diagrams (where $Pa_{Ca} = -\log_{10} a_{Ca}$), for the same system with $a_{Ca} = 1.67$ aP and show that the pH value for the point of minimum solubility of the hydroxyapatite clearly decreases with an increase in the temperature of the system. At each temperature level, HAp predominates in the higher pH range, while $Ca_3(PO_4)_2$, $Ca_2P_2O_7$ and $CaH_6P_2O_9$ have their predominate pH range successively in the more acid direction. The stability of the calcium phosphates at higher temperatures can be seen in Fig. 5.63. The equation numbers indicated in Fig. 5.63 refer to the following reactions:

(1) $3CaHPO_4\,(c) = Ca_3(PO_4)_2\,(c) + H_3PO_4\,(c,l)$

(2) $3CaH_2PO_4\,(c) = Ca_3(PO_4)_2\,(c) + 4H_3PO_4\,(c,l)$

(3) $Ca_{10}H_2P_6O_{26}\,(c) = 3\,Ca_3(PO_4)_2\,(c) + CaO\,(c) + H_2O\,(g)$

(4) $CaH_5PO_6\,(c) = CaHPO_4\,(c) + 2H_2O\,(g)$

(5) $CaH_6P_2O_9\,(c) = Ca(H_2PO_4)_2\,(c) + H_2O\,(g)$

The Eh-pH and Pa_{Ca}-pH diagrams have shown that HAp may be obtained at both atmospheric and hydrothermal conditions.

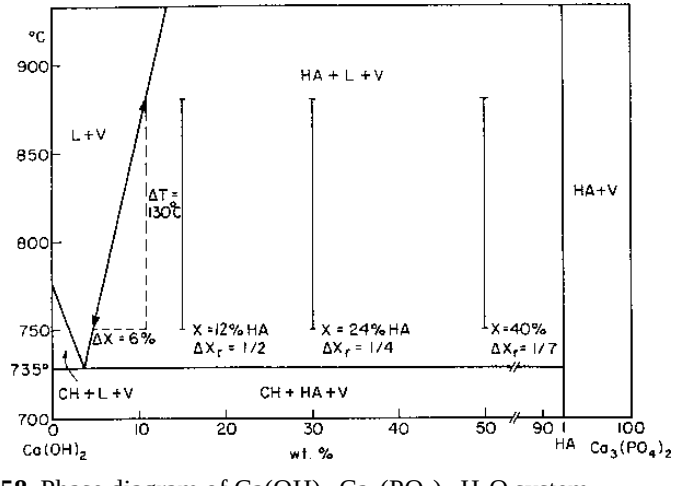

Figure 5.58. Phase diagram of $Ca(OH)_2$-$Ca_3(PO_4)_2$-H_2O system.

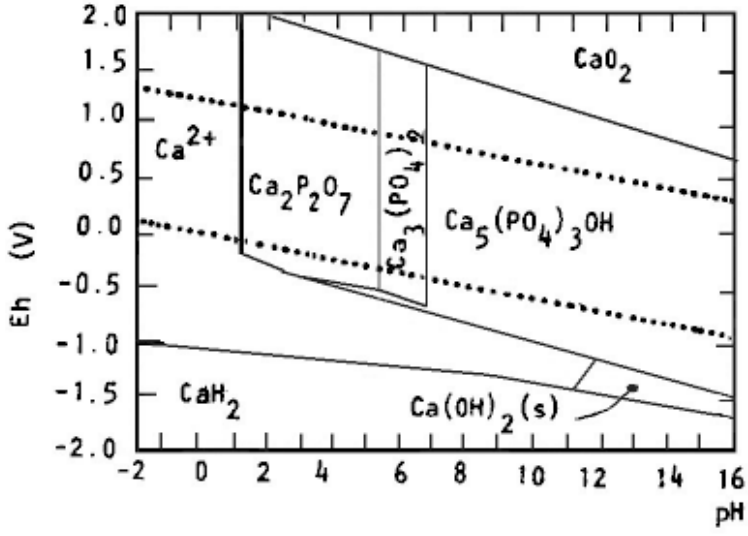

Figure 5.59. Eh-pH diagram of the Ca-P-H_2O system at 25°C for 1.67 molal activity of Ca and a_{Ca}=1.67 a_P.[215]

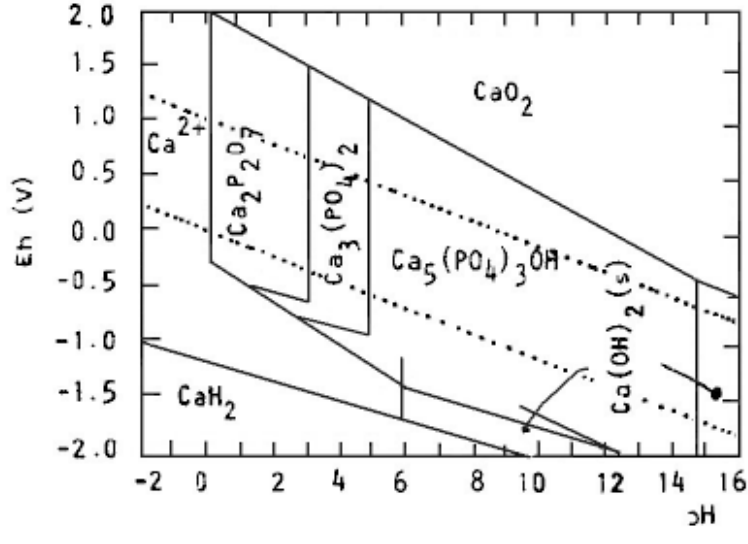

Figure 5.60. Eh-pH diagram of the Ca-P-H_2O system at 300°C for 1.67 molal activity of Ca and a_{Ca}=1.67 a_P.[215]

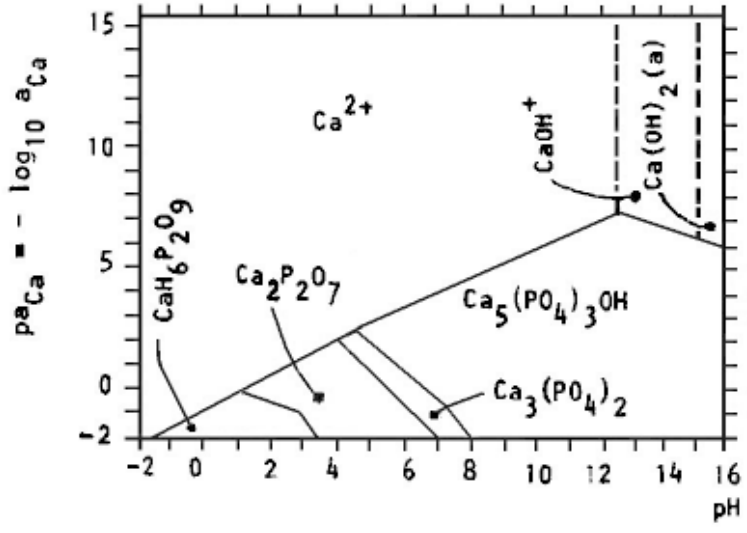

Figure 5.61. Pa_{Ca}-pH diagrams of the Ca-P-H_2O system at 25°C for a_{Ca}=1.67 a_P.[215]

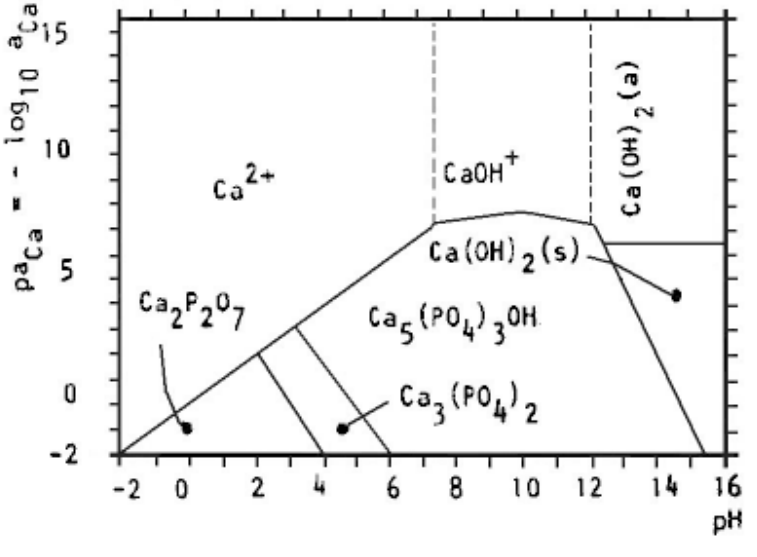

Figure 5.62. Pa_{Ca}-pH diagrams of the Ca-P-H_2O system at 300°C for a_{Ca}=1.67 a_P.[215]

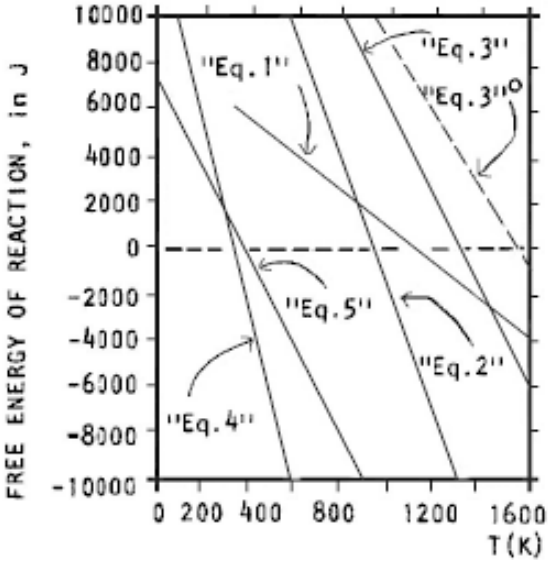

Figure 5.63. Free energy of reaction against temperature for some calcium phosphates according to Eq. (1) to Eq. (5) for water vapor fugacity equal to 0.03 atm, except for the dashed line, Eq. (3), which corresponds to water vapor fugacity equal to 1.0 atm.[215]

5.8.3 Crystal Growth

There are a large number of publications on the preparation of large HAp single crystals. Table 5.18 gives the representative works on the hydrothermal synthesis of HAp large single crystals.[218]–[225] Morey and Ingerson (1937) first attempted the hydrothermal synthesis of HAp crystals.[216] Since then, several reports have appeared in the literature. Roy (1971) grew prismatic single crystals of HAp, up to 4 mm length hydrothermally, from melts in the system $3CaO\text{-}P_2O_5\text{-}Ca(OH)_2$ and $3CaO\text{-}P_2O_5\text{-}Ca(OH)_2\text{-}H_2O$.[221] Mengeot et al. (1973) first succeeded preparing HAp single crystals of up to 7 × 3 × 3 mm in size by controlling the temperature gradient.[222] This work also revealed for the first time that HAp exhibited retrograde solubility in hydrothermal fluids between 300°C and 670°C under pressure of 3 kbar to 4 kbar. With the appearance of this report, most of the researchers placed nutrients at the cooler zone. Here, dissolution occurs and HAp crystals grow at the hotter region where the seed crystals are placed. This arrangement facilitated the growth of larger

HAp single crystals. However, the preparation of large single crystals of HAp has encountered several difficulties such as the tendency to incorporate impurities, the stability of nonstoichiometric composition, and the restricted field of crystallization in the phase diagram $CaO-P_2O_5-H_2O$, where HAp and H_2O only exist.

Table 5.18. Hydrothermal Synthesis of Hydroxyapatite Large Single Crystals[191]

Starting Materials	Synthetic Conditions	Comments
$CaHPO_4$	300°C 1250 lb/in^2,	0.3 mm in length
wet chemically prepared HAp	for 10 days 500°C, 354 bars,	2.35 mm in length, 0.2 mm in diameter
	for 10 days	
$CaHPO_4$	350°C, 100 MPa	2 mm
$Ca_3(PO_4)_2{\cdot}Ca(OH)_2$	15000 psi,	4 mm in length
or	held at 850-900°C,	
$Ca_3(PO_4)_2{\cdot}Ca(OH)_2$	then cooled 20°C/h.	
$-H_2O$ system	to ~750°C, quenched	
synthesized HAp	300-670°C,	7 × 7 × 3mm, identify
as nutrient & HAp	45000-60000 psi	the retrograde solubility
seed		of HAp
$Ca_3(PO_4)_2{\cdot}Ca(OH)_2$	oscillating temperature	8 × 0.5 mm
$-CaCO_3-H_2O$	technique, 750-800°C,	
system, $Ca(OH)_2$	14500-17500 psi	
as flux		
$CaHPO_4{\cdot}2H_2O$	100-300°C, 2 kbar	0.1 mm
wet chemically,	430-500°C, 2 kbar	3.5 mm, check the
followed by		retrograde solubility
Soxhlet extracted		of HAp
HAp		

In the recent years, Ito and his group have done excellent work on the single crystal growth of HAp.[226][227] Single crystals of carbonate-containing HAp have been grown hydrothermally by gradually heating with a temperature gradient applied to the vessel, using $CaHPO_4$, H_2O and carbon dioxide as dry ice. The hydrothermal reaction for the formation of HAp can be written as follows:

$$10CaHPO_4 + 2H_2O \rightarrow Ca_{10}(PO_4)_6(OH)_2 + 4H_3PO_4$$

Crystal growth experiments were performed, slowly hydrolyzing $CaHPO_4$ by gradually heating a pressure vessel with a temperature gradient applied.

Kikuchi et al. (1994) have obtained Sr-substituted HAp crystals of size $0.2 \times 0.2 \times 5$ mm^3 under hydrothermal conditions.[228] The starting materials such as calcium and strontium hydrogen phosphate ($SrHPO_4$) were gradually heated with a temperature gradient. The crystal growth occurred at low pH.

In most of the works, the effects of CO_3^{2-} on the morphology of the crystals have been reported: needle-like crystals are predominant if the carbonate content is higher than 0.1%, whereas equiaxial crystals occur if the carbonate content is below 0.1%. Hata et al. (1983) synthesized Cd hydroxyapatite single crystals, partly substituted with the first series transition elements for Cd ion, to investigate the substitution effects on the crystal growth and structural changes.[229] These crystals form a superstructure of pure Cd HAp. Nagata et al. (1995) have studied the synthesis of HAp crystals in the presence of methanol and studied the morphological variations in HAp crystals.[230] It was found that the products obtained from the slurries without methanol were rod-like or granular crystals. Addition of methanol to the slurries caused an increase in the ratio of plate-like crystals to rod-like crystals or granular crystals. When the weight of methanol added was equal to the weight of the slurries, only plate-like crystals were obtained.

Although several workers have reported a negative temperature coefficient of soluble for HAp, but there is no systematic study either on the experimental or theoretical side. In this respect, Vereecke et al. (1990) reported the calculation of the solubility diagrams and the effects of some parameters such as T (< 100°C), pH; partial CO_2 pressure, and ionic strength.[231] According to this report, the solubility of HAp is lowered with temperature indicating the retrograde solubility of HAp below 100°C.

Onuma et al. (1998) and Kanzaki et al. (1998) have carried out the direct growth rate measurement of HAp single crystals by Moire phase shift interferometry and AMF.[232][233] They carried out direct investigations of the growth kinetics for each crystal face of HAp. It was found that the *a*-face grew by step-flow combined with two-dimensional nucleation, and the rate-determining process of the growth was found to be the incorporation of a growth unit at the step front, from the measurement of step velocities. The growth rate of the *a*-face was estimated to be of the order of 10^{-4} nm/s from the step advancing rate. This value is about 3–4 orders of magnitude smaller than those for soluble inorganic crystals.[232] In contrast, the growth kinetics of HAp (0001), *c*-face, remain unclear. These authors have concluded that the volume diffusion process for growth is strong during the initial stages. It is believed that a strong bond site exists in the [0001] direction and there is no strong bond site in the $[10\bar{1}0]$ direction, which makes the rate-determing process between *c*- and *a*-faces different. Figure 5.64 shows the carbonate-containing hydroxyapatite single crystals grown on the polycrystalline hydroxyapatite disk and Fig. 5.65 shows carbonate-containing hydroxyapatite single crystals.

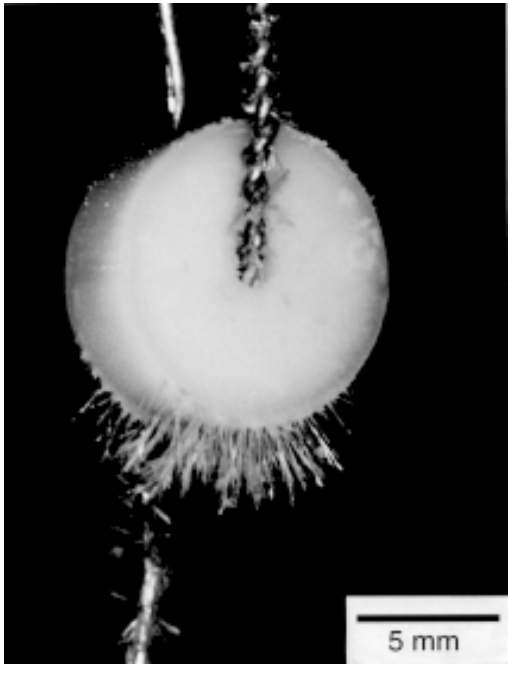

Figure 5.64. Carbonate-containing hydroxyapatite single crystals grown on the polycrystalline hydroxyapatite disk. *(Photo courtesy of A. Ito.)*

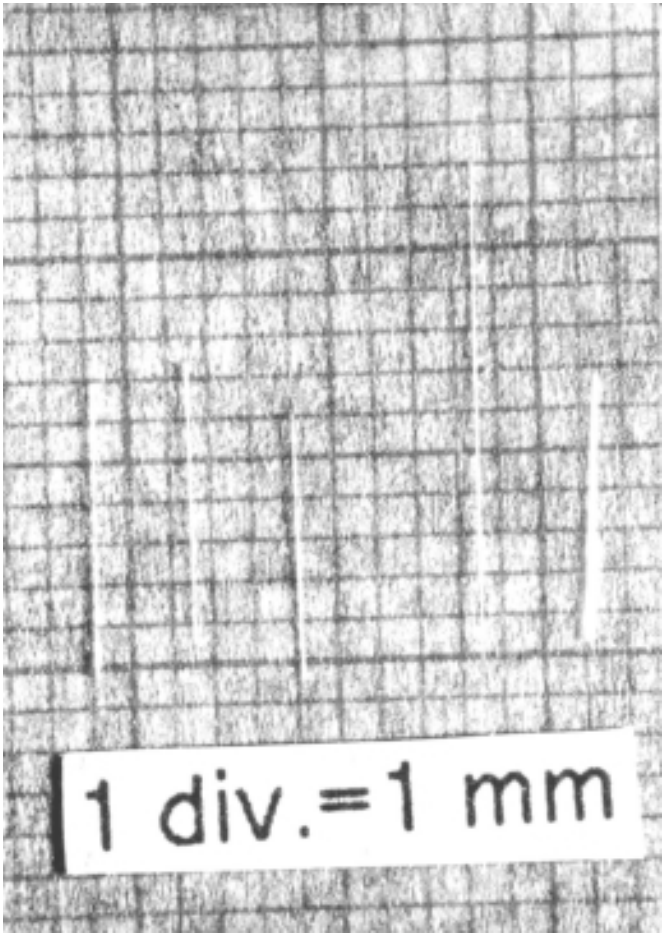

Figure 5.65. Carbonate-containing hydroxyapatite single crystals. *(Photo courtesy of A. Ito.)*

Like zeolites, hydroxyapatite is also an important technological material owing to its widespread applications attracting the attention of sicentists from interdisciplinary branches of science—including physicists, chemists, ceramists, medical doctors, engineers, and so on. Also, three International Symposiums on Apatite have been held. The importance of this material as a biomaterial, composite material, whiskers, fine particles, and so on, are discussed in Ch. 10.

REFERENCES

1. Tomkeieff, S. I., On the origin of the name "Quartz," *Min. Mag*., 26:172 (1942)
2. Sosman, R. B., *The Properties of Silica*, New York (1927)
3. Chao, E. C. T., Fahey, J. J., Littler, J., and Milton, D. J., Stisshovite, SiO_2, A Very High Pressure New Mineral from Meteor Crater, Arizona, *J. Geophys. Res.*, 67:419–423 (1962)
4. Ramsdell, C. S., The Crystallography of "Coesite," *Amer. Min*., 40:975 (1955)
5. Wei, P., The Structure of α - Quartz, *Zeit. Krist*., 92:355 (1935)
6. Bragg, W. H., The X-ray Spectra Given by Crystals of Sulphur and Quartz. *Proc. Roy. Soc.*, 89:575 (1914)
7. Hosaka, M., Miyata, T., and Sunagawa, I., Growth and Morphology of Quartz Crystals Synthesized Above the Transition Temperature, *J. Crystal Growth*, 152:300–306 (1995)
8. Arndt, J. and Rombach, N., Synthesis of Coesite from Aqueous Solutions, *J. Crystal Growth*, 35:28–32 (1976)
9. Dyuzheva, T. I., Lityagina, L. M., Bendeliani, N. A., Nikolaev, N. A. and Dorokhova, G. I., Hydrothermal Synthesis of Coesite (SiO_2), Crystallography Reports, 43:511–513 (1998)
10. Barth, T. F. W. The Cristobalite Structure: I High-Cristobalite; II Low-Cristobalite., *Amer. J. Sci.*, 23:350; 24:97 (1932)
11. Buisson, X and Arnaud, R., Hydrothermal Growth of Quartz Crystals in Industry, Present Status and Evolution, *J. de Phesique* IV, 4[C_2]:25–32 (1994)
12. Taki, S., Improvement of Growth Process and Characterization of Quartz Crystals, in: The Role of Crystal Growth for Device Development (N. Nizeki, ed.) *Prog. Crystal Growth Charact. Mat.*, 23:313–339 (1991)
13. Laudise, R. A. and Nielsen, J. W., in: *Solid State Phys*., (F. Seitz and D. Turnball, eds), 12:149, Academic Press, New York (1961)
14. Ballman, A. A. and Laudise, R. A., in: *Art and Science of Growing Crystals* (J. J. Gilman, ed.), p. 231, Wiley, New York (1963)
15. Kuznetsov, V. A. and Lobachev, A. N., Hydrothermal Method for the Growth of Crystals, *Soviet Physics-Crystallography*, 17:775–804 (1973) (Translated English edition)
16. Armington, A. F., Recent Advances in the Growth of High Quality Quartz, in: *Hydrothermal Growth of Crystals* (K. Byrappa, ed.), *Prog. Crystal Growth Charact. Mat*., 21:97–111 (1990)

17. Byrappa, K., Hydrothermal Growth of Crystals, in: *Handbook of Crystal Growth* (D. T. J. Hurle, ed.), Vol. 2, Elsevier Science Publishers, The Netherlands, 464:562 (1994)
18. Schafhaul, K. F. E., *Gelehrte Anzeigen Bayer, Akad*., 20:557 (1845)
19. Nacken, R., Hydrothermal Syntheses als Grundlage fur Zuchtung von Quarzkristallen, *Chem. Z.*, 74:745–749, (1950)
20. Nacken, R., Artificial Quartz Crystals, etc., U.S. Office of Technical Services Report, PB-6948 (1946)
21. Nacken, R., Artificial Quartz Crystals, etc., U.S. Office of Technical Services Report, PB-18-748 and 28-897 (1946)
22. Laudise, R. A., Ballman, A. A., and King, J. C., Impurity Content of Synthetic Quartz and Its Effect Upon Mechanical Q, *J.Phys. Chem. Solids*, 26:1305–1308 (1965)
23. Laudise, R. A., Hydrothermal Crystal Growth—Some Recent Results, in: *Advanced Crystal Growth* (P. M. Dryburgh, B. Cockayne, and K. G. Barraclough, eds.), Prentice Hall, NewYork, 267–288 (1987)
24. Laudise, R. A. and Sullivan, R. A., Pilot Plant Production of Synthetic Quartz, *Chem. Engg. Prog.*, 55:55–59 (1959)
25. Barns, R. L., Kolb, E. D., Laudise, R. A., Simpson, E. E., and Kroupa, K. M., Production and Perfection of *'Z-face'* Quartz, *J. Crystal Growth*, 34:189–197 (1976)
26. Kirov, G. K., Initial Growth Stages of Man-made Quartz Crystals and Growth Mechanism of their (0001) Face, *Cryst. Res. Technol*., 27:335–342 (1992)
27. Brown, C. S., Internal Friction in Synthetic Quartz, *Proc. Phys. Soc*. (London), 75:459 (1960)
28. Chakraborty, D., Dependence of Mechanical Q on Growth Rate of Quartz Single Crystals, *J. Crystal Growth*, 41:177–180 (1977)
29. Lias, N. C., Grudenski, E. E., Kolb, E. D., and Laundise, R. A., The Growth of High Acoustic Q Quartz at High Growth Rates, *J. Crystal Growth*, 18:1–6 (1973)
30. Lipson, H. G. and Armington, A. F., Aluminum a-d Hydroxide Distribution in Cultured Quartz Grown from $^{+}$x Seeds, *J. Crystal Growth*, 80:51–59 (1987)
31. Christie, I. R. A., Croxall, D. F. and Isherwood, B. J., UK Patent 2079175B, (Dec. 7, 1983)
32. Armington, A. F., Larkin, J. J., O'Conner, J. J., Cormier, J. E., and Horrigan, J. A., *Proc. 35th Annual Frequency Symposium*, E1A, p. 297, Washington, D.C. (1981)
33. Armington, A. F. and Larkin, J. J., The Growth of High Purity, Low Dislocation Quartz. *J. Crystal Growth*, 71 :799–806 (1985).

34. Kolb, E. D., Nassau, K., Laudise, R. A., Simpson, E. E., and Kronpa, K. M., New Sources of Quartz Nutrient for the Hydrothermal Growth of Quartz, *J. Crystal Growth*, 36:93–100 (1976)
35. Hosaka, M. and Miyata, T., Hydrothermal Growth of α-Quartz Using High-Purity α-Cristobalite as Feed Material, *Mat. Res. Bull.*, 28:1201–1208 (1993)
36. Avakov, V. A. and Vinogradov, B. N., Solubility of SiO_2 Polymorphs, *Izv. Vyssh. Ucheb. Zaved., Khim. Teknol.*, 17:879–882 (1972)
37. U.S. Patent No. 4853198 (Aug. 1, 1989)
38. Hosaka, M., Synthesis of Micro α-Quartz Crystals by Hydrothermal Hot-Press Method, *J. Crystal Growth*, 112: 291 (1991)
39. Wooster, N. and Wooster, W. A. Preparation of Synthetic Quartz, *Nature*, 157:297 (1946)
40. Spezia, J. G., La Pressione e Chimicament Inattiva Nella Solubilita e Ricostituzione del Quarzo, Atti Accad. Sci. Torino Contribuzioni di Geologia Chimica, 40:254–262 (1905)
41. Shternberg, A. A., Controlling the Growth of Crystals in Autoclaves, in: Crystallization Processes under Hydrothermal Conditions (A. N. Lobachev, ed.), p. 225–240, Consultants Bureau, New York (1973)
42. Demianets, L. N., Emelyanova, E. N., and MelniKoV, O. K., Solubility of Sodalite in Aqueous Solutions of NaOH under Hydrothermal Conditions, in: Crystallization Processes under Hydrothermal Conditions (A. N. Lobachev, ed.), p. 125–150, Consultants Bureau, New York (1973)
43. Hosaka, M. and Taki, S., Hydrothermal Growth of Quartz Crystals in NaCl Solution, *J. Crystal Growth*, 100:343–346 (1990)
44. Laudise, R. A. and Ballman, A. A., The Solubility of Quartz under Hydrothermal Conditions, *J. Phys. Chem.*, 65:1396–1400 (1961)
45. Hosaka, M. and Taki, S., Hydrothermal Growth of Quartz Crystals in NaCl Solution, *J Crystal Growth*, 52:837–842 (1981)
46. Lafon, F. and Demazean, G., Pressure Effects on the Solubility and Crystal Growth of α - Quartz, *J. de Physique* IV, 4[C_2]:177–182 (1994)
47. Martin, J. J. and Armington, A. F., Effect of Growth Rate on Quartz Defects, *J. Crystal Growth*, 62:203–206 (1983)
48. Laudise, R. A., What is Materials Chemistry? in: *Materials for Nonlinear Optics (Chemical Perspectives)* (S. R. Marder, J. E. Sohn, and G. D. Stucky, eds.), *American Chemical Soc.*, p. 410–433, Washington D.C. (1991)
49. Yoshimura, J., Miyazaki, T., Wada, T., Kohra, K, Ogawa, T., and Taki, S., *J. Crystal Growth*, 46:691–700 (1979)
50. Iwasaki, F. and Kurashige, M., *J. Appl. Phys.*, 17:817–820 (1978)

51. Johnson, G. R., Irvine, R. A., and Foise, J. W., A Parametric Study of the Variables Involved in Quartz Growth, *IEEE Proc. 44th Annual Symposium on Frequency Control,* p. 216–221 (1990)
52. Demazeau, G. and Lafon, F., Hydrothermal Crystal Growth of α - Quartz: New Specificities Correlated to Applications, *J. de Physique* IV, 4 [C_2]:13–18 (1994)
53. Lipson, H. G., Kahan, A., and O' Connor, J., Aluminum and Hydrogen Defect Centers in Vacuum Swept Quartz, *IEEE Proc. 37th Annual Symposium on Frequency Control*, p. 169–173 (1983)
54. Gualtieri, J. G., The Influence of Temperature and Electric Field on the Etch-Channel Density in Swept Cultured Quartz, *IEEE Proc. 39th Annual Symposium on Frequency Control*, p. 247–254 (1985)
55. Martin, J., Electro-Diffusion or Sweeping of Ions in Quartz, *IEEE Proc. 41st Annual Symposium on Frequency Control*, p. 167–174 (1987)
56. Fraser, B., in: *Physical Acoustics* (W. P. Mason, ed.), 5:54 (1968)
57. Bahadur, H., Sweeping and Irradiation Effects on Hydroxyl Defects in Crystalline Natural Quartz, *IEEE Trans. Ultrasonics, Ferroelectrics, and Frequency Control*, 41:820–833 (1994)
58. Zecchini, P., Yamni, K., and Viard, B., Modifications Induced by Sweeping and Observed in Quartz Crystals According to Their α_{3500}-Value, *J. de Physique* IV, 4 [C_2]:189–194 (1994)
59. Deleuze, M., Cambon, O., Goiffon, A., Ibanez, A., and Philippot, E., Controlled Dissolution of Quartz Material, Part I, Controlled Dissolution of Quartz Plates in Potassium and Sodium Hydroxides: Chemical Thinning Down of SC Cuts, *J. de Physique* IV, 4 [C_2]:79–84 (1994)
60. Brauer, K. and Muller, E., Correlation Between Parameters of Plastic Deformation in Doped NaCl Crystals, *Cryst. Res. Technol*., 19:K101–109 (1984)
61. Cambon, O., Deleuze, M., Michel, J. P., Aubry, J. P., Goiffon, A., and Philippot, E., Controlled Dissolution of Quartz Material, Part II, Quartz Chemical Etching Applied to Blanks Industrial Manufacturing, *J. de Physique* IV, 4 [C_2]:85–91 (1994)
62. Schwarzenbach, D., Verfeinezung der Struktur der Tiefquarz-Modification von $AlPO_4$, *Z. Krist.*, 123:161–185 (1966)
63. Chang, Z. P. and Barsch, G. R., Elastic Constants and Thermal Expansion of Berlinite, *IEEE, Trans. on Sonics and Ultrasonics*, 23:127–130 (1976)
64. O'Connell, R. M. and Corr, P. H. Temperature Compensated Cuts of Berlinite and β-Eucryptite: For Saw Devices, *Proc. 31st Annal. Freq. Control Symp*., p. 182–186 (1977)
65. Kolb, E. D., Glass, A. M., Rosenberg, R. L., Grenier, J. C., and Laudise, R. A., *Proc. 35th Ultrasonic Symp*., New York (1981)

66. US Patent 4,698, 318, Vogel, J., Holand, W., and Vogel, W. (1987)

67. Vogel, W, Vogel, J., Holand, W., and Wange, P., Development of Bioactive Silica-Free Phosphate Glass Ceramics for use in Medicine, wiss. Z. Friedrich Schiller Univ., *Jena, Math. Natur wiss. Reihe*, 36:841–854 (1987)

68. John, V. M. and Kordes, *Chem. of Earth*, 70:75–89 (1953)

69. Stanley, J. M., Hydrothermal Synthesis of Large Aluminum Phosphate Crystals, *Ind. and Eng. Chem.*, 468:1684–1689 (1954)

70. Mason, W. P. *Piezoelectric Crystals and their Application Ultrasonic*, Van Nostrand, New York, pp. 206 (1950)

71. Kolb, E. D. and Laudise, R. A., Hydrothermal Synthesis of Aluminum Orthophosphate, *J. Cryst. Growth*, 43:313–319 (1978)

72. Beck, W. R., Crystalographic Inversions of the Aluminum Orthophesphate Polymorphs and Their Relation to Those of Silica, *J. Amer. Ceram*. Soc., 32:147–153 (1949)

73. Sosman, R. S., *Phases in Silica*, Rutger University Press (1964)

74. Srikantaswamy, S., *Synthesis and Characterization of ABO_4 Crystals*, Ph.D. Thesis, Univ. of Mysore, Mysore, India (1988)

75. Byrappa, K. and Srikantaswamy, S., Recent Progress in the Growth and Characterization of Aluminum Orthophosphate Crystals, *Prog. Crystal Growth and Charact*., 21:199–254 (1990)

76. Byrappa, K., Venkatachalapathy, V., and Puttaraj, B., Crystallization of Orthophosphate, *J. Mater. Sci*., 19:2855–2862 (1984)

77. Byrappa, K., Srikantaswamy, S., Gopalakrishna, G. S., and Venkatachalapthy, V., Infrared Spectra of Aluminum Orthophosphate Crystals, *J. Mater. Sci. Letts*., 5:203–205 (1986)

78. Laudise, R. A., *Crystal Growth of Electronic Materials*, (Kaldis, ed.) Elsevier Science Publ., pp. 159 (1985)

79. Chai, B. H. T., Shand, M. L., Bucher, I., and Gillee, M. A., *Proc. IEEE Ultrasonic Symp.*, pp. 557 (1979)

80. U.S.Patent, 4:234–733, Chai, B. H. T. (1982)

81. Croxall, D. F., Christie, L. R. A., Isherwood, B. J., Todd, A. G., and Brich, J., The Growth and Assessment of Berlinite Single Crystals, *Proc.2nd European Conf. on Crystal Growth*, Lancaster England, C 118 (Sept. 10–15, 1979)

82. Schulz, H. and Kluckou, R., in: *Crystal Growth* (H. S. Peiser, ed.), Pergamon Press, New York (1967)

83. Poignant, H., *Hydrothermal Synthesis of Berlinite*, Ph.D. Thesis Univ. of Rennes (1979)

84. Kolb, E. D., Grenier, J. C., and Laudise, R. A., Solubility and Growth of $AlPO_4$ in a Hydrothermal Solvent: HCl, *J. Crystal Growth*, 51:178–185 (1981)

85. Bryappa, K., Srikantaswamy, S., Gopalakrishna G. S., and Venkatachalapath, V., Influence of Admixtures on the Crystallization and Morphology of $AlPO_4$ Crystals, *J. Mater. Sci.*, 21:2202–2206 (1986)

86. Krauss, V. and Lehann, G., *Z. Naturforsch,* 309:28 (1975)

87. Detaint, J., Phillipport, E., Jumas, J. C., Schwartzel, J., Zarka, A., Capelle, B., and Doukhan, J. C., *39th Annual Frequency Control Symposium,* Phildelphia (1985)

88. Byrappa, K., Shashidhara J., Prasad, and Srikantaswamy, S., Growth and Properties of New Polymorphic Modification of $AlPO_4$, *J. Crystal Growth,* 79:232 (1986)

89. Jumas, J. C., Goiffon, A., Capelle, B., Zaraka, A., Doukhan, J. C., Schwartzel, J., Detaint, J., and Phillipot, F., Crystal Growth of Berlinite, $AlPO_4$: Physical Characterization and Comparison with Quartz, *J. Crystal Growth,* 80:133–148 (1987)

90. Poignant, H., Marechal, L. Le., and Toudic, Y., Etude De La Solubilite du Phosphate d'aluminium ($AlPO_4$) dans des Solutions Hydrothermales d'acide orthophosphoriaue H_3PO_4, *Mater. Res. Bull.*, 14:603–612 (1979)

91. Hasegawa, K., Minegishi, K., and Somiya, S., Effects of Starting Materials and Temperature on the Hydrothermal Synthesis of Aluminum Orthophosphate, *Proc. Ist International Symposium of Hydrothermal Growth,* Tokyo, pp. 509–518 (1982)

92. Yaroslavskii, I. M. and Popolitov, V. I., Growth of Single Crystals of Aluminum Monophosphate (Berlinite), *Izv. Akad. Nauk SSSR,* Neorg. Materialy, 26:1055–1059 (1990)

93. Capulle, B., *Appl. Cryst.*, 18:533–534 (1985)

94. Detaint, H., Poignant, and Toudic, Y., Experimental Thermal Behavior of Berlinite Resonators, *24th Symposium on Frequency Control,* 28–30 (May, 1980)

95. Steinberg, R. F., Roy, M. K., Ester, A. K., Chai, B. H. T., and Morris, R. C., *Ultrasonic Symposium,* Dallas, USA, 14–16 (Nov. 1984)

96. Laudise, R. A., *The Growth of Single Crystals*, p. 109, Prentice Hall, Engelwood Cliffs, N. J. (1970)

97. Laudise, R. A, *Treatise on Solid State Chemistry*, 5:109 (N. B. Hanvy, ed.), Plenam, New York (1970)

98. Detaint, J., Philippot, E., Jumas, J. C., Schwartzel, J., Zarka, A., Capelle, B. and Doukhan, J. C., Crystal growth, Physical Characterization and BAW Devices Applications of Berlinite, 3th Annual Frequency Control Symposium, Philadelphia, USA (May 29–31, 1985)

99. Morris, R. C., Chai, B. H. T., Imperfect Low-Angle Boundaries and Fracture in Hydrothermally Grown Berlinite Crystals, *J. Crystal Growth,* 191:108–112 (1998)

100. Byrappa, K., Srikantaswamy, S., Gopalakrishna, G. S., and Venkatachalapathy, V., Influence of Admixtures on the Alpha-Beta Berlinite Inversion, *J. Mater. Sci. Letts*., 5:347–348 (1986)

101. Troccaz, M., Berger, C., Richard, M., and Byraud, L., Etude de la transformation de phase α–β de la variété «Phosphoquartz» de l'orthophosphate d'aluminium $AlPO_4$, *Bull. Soc. Chim. de France*, 11:4256 (1967)

102. Lang, R., Datars, W. R., and Calvo, C., *Phys. Letts*., 30A:340 (1969)

103. Byrappa, K. and Prahallad, U. D., Thermal Expansion of Berlinite, *J. Mat. Sci. Letts*., 8:1667–1669 (1989)

104. Ballato, A. D. and Iafrate, G. J., The Angular Dependence of Piezoelectric Plate Frequencies and Their Temperature Coefficients, *Proc. 30th Frequency Control Symposium*, pp. 141–156 (1976)

105. Bechman, R., Ballato, A. D., and Lukaszek, T. T., High Order Temperature Coefficients of the Elastic Stiffness and Compliance of α-Quratz, *Proc. IREE*, 30:1812 (1982)

106. Shannon, R. D., Vega, A. J., Chai, B. H. T., and Rossman, G. R., Effect of H_2O on Dielectric Properties of Berlinite: I. Dielectric Constant, *J. Phys. D; Appl. Phys*., 26:93–100 (1993)

107. Fontanella, J. J., Wintersgill, M. C., Shannon, R. D., and Chai, B. H. T., Effect of H_2O on Dielectric Properties of Berlinite: II. Dielectric Loss, *J. Phys. D; Appl. Phys*., 26:101–105 (1993)

108. Thompson, W. K., Infrared spectroscopic studies of aqueous systems, I. *Trans. Faraday Soc*., 61:1635–1640 (1964)

109. Philippot, E., Palmier, D., Pintard, M., and Goiffon, A., A General Survey of Quartz and Quartz-Like Materials: Packing Distortions, Temperature and Pressure Effects, *J. Solid State Chem*., 123:1–13 (1996)

110. Hirano, S., Miwa, K. and Naka, S., Growth of Gallium Orthophosphate Crystals, *J. Crystal Growth* 79:215–218 (1986)

111. Nakae, H., Kihara, K, Okuno, M. and Hirano, S., The Crystal Structure of The Quartz-Type Form of $GaPO_4$ and Its Temperature Dependence, *Zeit. Krist.*, 210:746–753 (1995)

112. Hirano, S. and Kim, P., Physical Properties of Hydrothermally Grown Gallium Orthophosphate Single Crystals, *J. Mat. Sci.*, 25:4772–4775 (1990)

113. Hirano, S., Kim, P., and Orihara, H., Dielectric Properties of Hydrothermally Grown Gallium Orthophosphate Single Orgstals, *J. Mat. Sci.*, 25:2800–2804 (1990)

114. Cochez, M., Ibanez, A., Goiffon, A., and Philippot, E., Crystal Growth and Infrared Characterization of $GaPO_4$ in Phospho-Sulphuric Media, *Eur. J. Solid State Inorg. Chem.*, 30:509–519 (1993)

115. Foulon, J. D., Giuntin, J. C., and Philippot, E., Dielectric Properties of an α-Quartz Type Material: $GaPO_4$, *Eur. J. Solid State Inorg. Chem.*, 31:245–256 (1994)

116. Hirano, S., Kim, P., and Orinara, H., Dielectric Properties of Hydrothermally Grown Gallium Orthophosphate Single Crystals, *J. Mat. Sci.*, 25:2800–2804 (1990)

117. Cochez, M., Foulon, J. D., Ibanez, A., Goiffon, A., Philippot, E., Cappelle, B., Zarka, A., Schwartzed, J., and Detaint, J., Crystal Growth and Characterization of A Quartz-Like Material: $GaPO_4$, *J. de Physique* IV, 4[C_2]:183–188 (1994)

118. Capelle, B., Zarka, A., Schwartzel, J., Detaint, J., Philippot, E., and Denis, J. P., Characterization of Piezoelectric Materials: Old and New Crystals, *J. de Physcique* IV, 4[C_2]:123–134 (1994)

119. Zvereva, O. V. and Mininzon, Yu-M., Growth Elucidation of Gallium Orthophosphate Under Hydrothermal Conditions, *Kristallografia*, 37:1051–1054 (1992)

120. Popolitov, V. I. and Yaroslavskii, I. M., Crystallization of Gallium Monophosphate, *Izv. Akad. Nauk SSSR*, Neorg. Materialy, 26:892–894 (1990)

121. Zvereva, O. V., Mininzon, Yu, M., and Demianets, L. N., Hydrothermal Growth of OH^- free $AlPO_4$ and $GaPO_4$ Crystals the Way of Twin Reducing, *J. de physique* IV, 4[C_2]:19– 24 (1994)

122. Shigarov, A. S., Zvereva, O. V., and Mininzon, Yu. M., Investigation of the Solubility of Gallium Orthophosphate, $GaPO_4$ Under Hydrothermal Conditions, *Kristallografia*, 39:717–719 (1994)

123. Zumsteg, F. C., Bierlein, J. D., and Gier, T. E., K_xRb_{1-x} $TiOPO_4$ A New Nonlinear Optical Material, *J. Appl. Phys.*, 47:4980–4985 (1976)

124. Ashkin, A., Boyd, G. D., Dziedzic, J. M., Smith, R. E., Ballman, A. A., Levinstein, J. J., and Nassau, K., Optically-Induced Refractive Index in Homogeneities in $LiTaO_3$ and $LiNbO_3$, *Appl. Phys. Letts.*, 9:72–77 (1966)

125. Okada, M. and Ieiri, S., Influence of Self-induced Thermal Effects on Phase Matching in Nonlinear Optical Crystals, *IEEE J. Quantum Electron*, QE-7:560–563 (1971)

126. US Patent, 3,949, 323, Bierlein, J. D., Assigned to E. I. Du Pont de Nemours and Company (Apr. 6, 1976)

127. US Patent, 4,231,838, Gier, T. E., Assigned to E. I. Du Pont de Nemours and Company (Nov. 4, 1980)

128. Tordjman, I, Masse, R., and Guitel, J. C., Structure Cristalline du Monophosphate $KTiPO_5$, *Z. Kristallogr.*, 139:103–115 (1974)

129. Ouvard, L., Compt. Rend. (Paris) 121:117 (1890), as reported in The Gmelin Handbook, Vol. 41, T, 8th ed. (1951)

130. Masse, R., and Grenier, J. C., Phase Transformation of $AlPO_4$:Fe^{3+} by Electron Paramagentic Resonance, *Bull. Soc. France. Mineral. Crist*., 94:437 (1971)

131. US Patent 3,949,323, Bierlien, J. D. and Gier, T. E. (Apr. 6, 1976)

132. Liu, Y. S., Drafall, L., Dentz, D., and Belt, R., Nonlinear Optical Phase-Matching Properties of $KTiOPO_4$ (KTP), G.E. Tech. Inf. Series Rep. No. 82 CR DO16, General Electric Company, Schenectady, New York (1982)

133. Liu, Y. S., Dentz, D., and Belt, R., High-Average-Power Intracavity Second-Harmonic Generation Using $KTiOPO_4$ in an Acousto-Optically Q-Switched Nd: YAG Laser Oscillator at 5 KHz, *Opt, Lett*., 9:76 (1984)

134. Laudise, R. A., Cava, R. J., and Caporaso, A. J., Phase Relations, Solubility and Growth of Potassium Titanyl Phosphate, KTP, *J. Cryst. Growth*, 74:275–281 (1986)

135. Laudise, R. A., Hydrothermal Crystal Growth—Some Recent Results, in: *Advanced Crystal Growth* (P. M. Dryburgh, B. Cockayne, and K. G. Barraclough, eds.) p. 267–286, Prentice Hall, New York (1987)

136. US Patent 4654111, Laudise, R. A. (March 31, 1987)

137. Belt, R. F., and Iradi, T., Hydrothermal Growth Produces Large KTP Nonlinear Crystals, *Laser Focus World*, p. 155–162 (Nov. 1993)

138. Laudise, R. A., Sunder, W. A., Belt, R. F., and Gashurov, G., Solubility and *P-V-T* relations and the Growth of KTP, *J. Crystal Growth*, 102:427–433 (1990)

139. Belt, R. F., Low Temperature Hydrothermal Growth of Potassium Titanyl Phosphate (KTP) in 4 liter Autoclaves, Extended Abstract ICCG-9, p. 428, Sendai, Jpn. (Aug. 20–25, 1989)

140. Byrappa, K., Board of Res. in Nuclear Sciences, *Dept. of Atomic Energy, Tech. Report*, p. 4, Bombay (1996)

141. Gettemy, D. J., Harker, W. C., Lindholm, G., and Barnes, N. P., Some Optical Properties of KTP, $LiIO_3$, and $LiNbO_3$, *IEEE. J. Quantum Electronics*, 24:2231–2237 (1988)

142. Bierlein, J. D., Ferretti, A., Brixner, L. H., and Hsu, W. Y., Fabrication and Characterization of Optical Wave Guides in $KTiOPO_4$, *Appl. Phys. Letts*., 50:1216–1219 (1987)

143. Van der Poel, C. J., Bierlein, J. D., Brown, J. B., and Colak, S., *Appl. Phys. Letts*, 57:2974–2977 (1990)

144. Bierlein, J. D., Vanherzeele, H., and Ballman, A., Linear and Nonlinear Optical Properties of Flux Growth KTP, *Appl. Phys. Letts*., 54:783–787 (1989)

145. Brahimi, M. and Durand, J, Structure et propriétés d'optique nonlinéaire de $KTiOAsO_4$, *J. Rev. Chim. Mineral*, 23:146–148 (1986)

146. Belt, R. F. and Ings, J. B., Hydrothermal Growth of Potassium Titanyl Arsenate (KTA) in Large Autoclaves, *J. Cyrstal Growth*, 128:956–962 (1993)

147. Cheng, L. K., Cheng, L. T., Galperin, J., Morris Hotsenpiller, P. A., and Bierlein, J. D., Crystal Growth and Characterization of $KTiOPO_4$ Isomorphs from the Self-fluxes, *J. Crystal Growth*, 137:107–115 (1994)

148. Chani, V. I., Shimamura, K., Endo, S., and Fukuda, T., Substitution of Ti^{4+} with Nb^{5+}- M^{3+} (M = Al, Cr, Ga, Fe, In) in Crystals of $KTiOAsO_4$, *J. Crystal Growth*, 17:117–122 (1997)

149. Deer, W. A., Howie, R. A., and Zussman, J., *An Introduction to the Rock-Forming Minerals*, p. 473, Longman Group Limited, England (1966)

150. Kinloch, D. R., Belt, R. F., and Puttbach, R. C., Hydrothermal Growth of Calcite in Large Autoclaves, *J. Crystal Growth*, 24/25:610–613 (1974)

151. Hirano, S. and Kikuta, K., Solubility and Hydrothermal Growth of Calcite Single Crystals in Hitrate Solutions, *J. Crystal Growth*, 79:223–226 (1986)

152. Lemberg, J., Ueber silicatumwandlungen, Z. *Deut. Geol. Ges*., 35:557–618 (1883)

153. Friedel, C. and Sarasin, E., *Bull. Soc. Min*., 8:304–305 (1885)

154. Gruzensky, P. M.., in: *Crystal Growth* (H. S. Peiser, ed.) p. 365, Pergamon, Oxford (1967)

155. Kaspar, J., in: *Growth of Crystals*, Vol. 2, Consultants Bureau, New York (1959)

156. Morse, H. and Donnay, D. H., *Bull. Soc. Franc. Mineral*, 54:19–25 (1931)

157. Nickl, H. J. and Henisch, H. K., Growth of Calcite Crystals in Gels, *J. Electrochem. Soc*., 116:1258–1264 (1969)

158. Nester, J. F. and Schroeder, J. B., Growth of Synthetic Calcite Single Crystals, *Am. Mineralogist*, 52:276–280 (1967)

159. Belin, C., Brissot, J. J., and Jesse, R. F., The Growth of Calcite Single Crystals by Travelling Solvent Zone Melting, *J. Crystal Growth*, 13/14:597–600 (1972)

160. Balascio, J. F. and White, W. B., Growth of Single Crystal Calcite by Top-Seeded Solution Growth Technique, *J. Crystal Growth*, 23:101–105 (1974)

161. Belin, C., On the Growth of Large Single Crystals of Calcite by Travelling Solvent Zone Melting, *J. Crystal Growth*, 34:341–345 (1976)

162. Yamasaki, N. and Weiping, T., Hydrothermal Hot Pressing of Calcium Carbonate with Sea Water, *J. Mat. Sci. Letts*., 12:516 –519 (1993)

163. Yamasaki, N., Weiping, T., and Yanagisawa, K., Solidification of $CaCO_3$ Containing $SrCO_3$ by Hydrothermal Hot Pressing, *J. Mat. Res*., 8:1972–1976 (1993)

164. Yamasaki, N., Weiping, T., Lei, H., and Hosoi, K., Solidification of Aragonite-type $CaCO_3$ Powder Containing Chitosan with Acetic Acid by Hydrothermal Hot Pressing, *J. Mat. Sci. Letts.*, 14:1751–1753 (1995)

165. Ikornikova, N. Yu., Growth Characteristics of Calcite Crystals in Aqueous Solutions of Carbonic Acid, in: *Crystallization Processes under Hydrothermal Conditions* (A. N. Lobachev, ed.), pp. 93–112, Consultants Bureau, New York (1973)

166. Ikornikova, N. Yu., *Hydrothermal Synthesis of Crystals in Chloride Systems* (in Russian), pp. 1–222, Nauka, Moscow (1975)

167. Higuchi, M., Takeuchi, A., and Kodaira, K., Hydrothermal Growth of Calcite Single Crystals from H_2O-CO_2-$CaCO_3$ System, *J. Crystal Growth*, 92:341–343 (1988)

168. Hirano, S. and Kikuta, K., Hydrothermal Growth of Calcite Single Crystal in $Ca(NO_3)_2$ and NH_4O_3 Solutions, *J. Crystal Growth*, 94:351–356 (1989)

169. Higuchi, M., Miyauchi, D., Takeuchi, A., and Kodaira, K., Hydrothermal Growth of Calcite Single Crystals from H_2O-CO_2-$CaCO_3$ System under Controlled CO_2 Pressure, *J. Crystal Growth*, 110:39–43 (1992)

170. Yanagisawa, K., Feng, Q., Ioku, K., and Yamasaki, N., Hydrothermal Single Crystal Growth of Calcite in Ammonium Acetate Solution, *J. Crystal Growth*, 163:285–294 (1996)

171. Hirano, S., Yogo, T., Kikuta, K. and Yoneta, Y., Hydrothermal Growth of Calcite Crystals in Nitrate Solutions, *J. Ceram. Soc. Jpn.*, 101:113–117 (1993)

172. Malinin, S. D., in: *Geochemical Investigations at High Temperatures and Pressures*, p. 48, Nauka, Moscow (1965)

173. Ellis, A. I., The Solubility of Calcite in NaCl Solutions at High Temperatures, *Amer. J. Sci.*, 261:259–267 (1963)

174. Kikuta, K. and Hirano, S., Hydrothermal Growth and Dissolution Behaviour of Calcite Single Crystal in Nitrate Solutions., *J. Crystal Growth*, 99:895–899 (1990)

175. Lee, Y-K., Chung, S. J., Hydrothermal Growth of Calcite Single Crystals in NH_4Cl Solution, *J. Crystal Growth*, 192:350–353 (1998)

176. Gorai, M. and Syuutou, K., in: *Tikaku Ganseki Koukutsu*, p. 123, Kyuyitsu Publishing House, Jpn. (1981)

177. Ikornikova, N. Yu., Formation and Crystal Growth of Trigonal Carbonates, in: *Hydrothermal Synthesis of Crystals*, pp. 114–140, Nauka, Moscow, (1968)

178. Ikornikova, N. Yu., Crystal Growth Elucidation of the Calcite Crystals in Aqueous Solutions of HCl, in: *Investigations of the Crystallization Processes under Hydrothermal Conditions*, pp. 85–102, Nauka, Moscow (1970)

179. Ikornikova, N. Yu., *Hydrothermal Synthesis of Crystals in Chloride Systems*, p. 220, Nauka, Moscow (1975)

180. Deer, W. A., Howie, R. A., and Zussman, J. (eds.), *Rock-Forming Minerals*, Vol. 5: *(Non-Silicates)* Longmans, Green and Co. Ltd., pp. 323–338 (1962)

181. Simpson, D. R., Problems of the Composition and Structure of the Bone Minerals, *Clin. Ortho. Relat. Res.*, 86:260–286 (1972)

182. Holcomb, D. W. and Young, R. A., Thermal Decomposition of Human Tooth Enamel, *Calcif. Tissue Int.*, 31:189–201 (1980)

183. Waggaman, W. H., *Phosphoric Acid, Phosphates and Phosphatic Fertilizers, 2nd ed.*, p. 3, Reinhold Publishing Corp., New York (1952)

184. Toy, A. D. F., The Chemistry of Phosphorus, in: *Inorganic Chemistry*, Vol. 3., Pergamon Press (1973)

185. Daubree, A. Experiences sur la production artificielle de l'apatite, de latopaze, et de quelques autres métaux fruoriféres, *Compt. Rend. Acad. Sci. Paris*, 32:625 (1851)

186. Ducheyne, P., Kokubo, T., and Van Blitterswijk, C. A., (eds.), *Bone-Bonding Biomaterials*, Rees Healthcare Communications (1992)

187. Aoki, H., *Science and Medical Applications of Hydroxyapatite*, Japanese Association of Apatite Science, JAAS (1991)

188. Hench, L. L., Bioceramics: From concept to clinic, *J. Am. Ceram. Soc.*, 74:1487–1510 (1991)

189. Yanagisawa, K., Toya, H., Feng, Qi, and Yamasaki, N., *In-situ* formation of HApcrystals under hydrothermal conditions, *Phosphorus Res. Bull.*, 5:43–46 (1995)

190. Kanazawa, T. (ed.), *Inorganic Phosphate Materials*, Elsevier Science Publishers, p. 15, Amsterdam (1989)

191. Yoshimura, M. and Suda, H., Hydrothermal Processing of Hydroxyapatite: Part, Present and Future, in: *Hydroxyapatite and Related Materials* (P. W. Brown and B. Constanz, eds.), CRC Press, Inc., pp. 45–72 (1994)

192. Mc Cauley, J. W. and Roy, R., Controlled Nucleation and Crystal Growth of Various Calcium Carbonate Phases by the Silica Gel Technique, *Am. Miner.*, 59:947–963 (1974)

193. Johnson, P. D., Some Optical Properties of Powder and Crystal Holophosphatephosphorous, *J. Electrochem. Soc.*, 108:159–162 (1961)

194. Prener, J. S., The Growth and Crystallographic Properties of Calcium Fluor- and Chlorapatite Crystals, *J. Electrochem. Soc.*, 114:77–83 (1967)

195. Oishi, S., and Kamiya, T., High-Temperature Solution Growth of Chlorspodiosite and Chlorapatite Crystals, *J. Chem. Soc. Jpn.*, 10:1129–1132 (1993)

196. Oishi, S. and Kamiya, T., Flux Growth of Fluorapatite Crystals, *J. Chem. Soc. Jpn*., 9:800–804 (1994)

197. Oishi, S. and Sugiura, I., Growth of Chlorapatite Crystals from a Sodium Chloride Flux, *Bull. Chem. Soc. Jpn.*, 70:2483–2487 (1997)

198. Masuda, Y., Matsubara, K., and Sakka, S., Synthesis of HAp from Metal Alkoxides Through Sol-Gel Technique, *J. Ceram. Soc. Jpn.*, 98:1255–1266 (1990)

199. Brendel, T., Engel, A., and Russel, C., Hydroxyapatite Coating by a Polymeric Route, *J. Mater. Sci., Mater. Med*., 3:175–179 (1992)

200. Náray-Szabo, S., The Structure of Apatite $(CaF)Ca_4(PO_4)_3$, *Zeit. Krist*., 75:387–398 (1930)

201. Mehmel, M., Uber die Struktur des Apatits, *Zeit. Krist*., 75:323–331 (1930)

202. Hendricks, S. B., Jefferson, M. E., and Mosley, V. M., The Crystal Structures of Some Natural and Synthetic Apatite-like Substances, *Zeit. Krist*., 81:352 (1932)

203. Posner, A. S., Perloff, A., and Diorio, A. F., Refinement of the Hydroxyapatite Structure, *Acta Cryst*., 11:308–309 (1958)

204. Kay, M. I., Young, R. A., and Posner, A. S., Crystal Structure of Hydroxyapatite, *Nature*, 204:1050–1052 (1964)

205. Elliott, J. C., The Problems of the Composition and Structure of the Mineral Components of the Hard Tissues, *Clin. Ortho. Relat. Res*., 93:313–345 (1973)

206. Elliott, J. C., Mackie, P. E., and Young, R. A., Monoclinic Hydroxyapatite, *Science*, 180:1055–1057 (1973)

207. Van Rees, H. B., Mengeot, M., and Kostiner, E., Monoclinic-Hexagonal Transition in Hydroxyapatite and Deuterohydroxyapatite Single Crystals, *Mat. Res. Bull*., 8:1307–1310 (1973)

208. Van Wazer, J. R., *Phosphorus and its Compounds*, Vol. 1, *Chemistry*, Wiley-Interscience, New York (1958)

209. Brown, P. W., Phase Relationships in the Ternary System $CaO\text{-}P_2O_5\text{-}H_2O$ at 25°C, *J. Am. Ceram. Soc*., 75(1):17–22 (1992)

210. Brown, P. W., Hocker, N., and Hoyle, S., Variations in Solution Chemistry During the Low-Temperature Formation of Hydroxyapatite, *J. Am. Ceram. Soc*., 74(8):1848–1854 (1991)

211. Biggar, A. M., *Min. Mag*., 35:1110–1115 (1966)

212. Feng, S. S. and Rockett, T. J., The System $CaO\text{-}P_2O_5\text{-}H_2O$ at 200°C, *J. Amer. Ceram. Soc.*, 62:619–620 (1979)

213. Skinner, H. C. W., Studies in the Basic Mineralizing System, $CaO\text{-}P_2O_5\text{-}H_2O$, *Calcif. Tiss. Res*., 14:3–4 (1974)

214. Eysel, W. and Roy, D. M., Hydrothermal Flux Growth of Hydroxyapatites by Temperature Oscillation, *J. Crystal Growth*, 20:245-250 (1973)

215. Andrade, M. C., Ogasawara, T., and Silva, F. T., Hydrothermal Crystallization of HAp, in: *Proc 2nd Int. Symp. Apatite*, 2:41–47 (1997)

216. Morey, G. W. and Ingerson, E., The Pneumatolitic and Hydrothermal Alteration and Synthesis of Silicates, *Econ. Geol*., 32:607–760 (1937)

217. Hayek, E., Lechtleitner, J., and Bohler, W., Hydrothermal Synthesis of Hydroxylapatite, *Angew. Chem*., 67:326 (1955)

218. Perloff, A. and Posner, A. S., Preparation of Pure Hydroxyapatite Crystals, *Science*, 124:583–584 (1956)

219. Jullmann, H. and Mosebach, R., Zur Synthese, Licht-und Doppelbrechung des Hydroxylapatits, *Naturforsch*, 21B:493–494 (1966)

220. Kirn, J. F. and Leidheiser, H., Jr., Progress in Efforts to Grow Large Single Crystals of Hydroxyapatite, *J. Cryst. Growth*, 2:111–112 (1968)

221. Roy, D. M., Crystal Growth of Hydroxyapatite, *Mat. Res. Bull.*, 6:1337–1340 (1971)

222. Mengeot, M., Harvill, M. L., and Gilliam,O. R., Hydrothermal Growth of Calcium Hydroxyapatite Single Crystals, *J. Cryst. Growth*, 19:199–203(1973)

223. Eysel, W. and Roy, D. M., Hydrothermal Flux Growth of Hydroxyapatites by Temperature Oscillation, *J. Cryst. Growth*, 20:245–250 (1973)

224. Aoki, H., Kato, K., and Shiba, M., Synthesis of Hydroxyapatite Under Hydrothermal Conditions, in: Kinetic Analysis of the Reaction Process from Monetite into Hydroxyapatite, *J. Dent. Apparatus and Materials*, 13(27):170–176 (1972)

225. Arends, J., Schuthof, J., van der Linden, W. H., Bennema, P., and van en Berg, P. J., Preparation of Pure Hydroxyapatite Single Crystals by Hydrothermal Recrystallyzation. *J. Crystal Growth*, 46:213–220 (1979)

226. Ito, A., Nakamura, S., Aoki, H., Akao, M., Teraoka, K., Tsutsumi, S., Onuma, K., and Tateishi, T., Hydrothermal Growth of Carbonate-Containing Hydroxyapatite Single Crystals, *J. Crystal Growth*, 163:311–317 (1996)

227. Ito, A., Teraoka, K., Tsutsumi, S., and Tateishi, T., Single Crystal Hydroxyapatite: Preparation, Composition and Mechanical Properties, *Bioceramics*, 9:189–192 (1996)

228. Kikuchi, M., Yamazaki, A., and Otsuka, R., Crystal Structure of Sr-Substituted HAp, Synthesized by Hydrothermal Method, *J. Solid State Chem*., 113:373–378 (1994)

229. Hata, M. and Marumo, F., Synthesis and Superstructure of $(Ca,M)_5(PO_4)_3OH$ (M = Mn, Fe,Co,Ni,Cu,Hg), *Miner. J*., 11:317–330 (1983)

230. Nagata, F., Yokogawa, Y., Toriyama, M., Kawamoto,Y., Suzuki, T., and Nishizawa, K., Hydrothermal Synthesis of HAp Crystals in the Presence of Methanol, *J. Ceram. Soc., Jpn.*, 103:70–73 (1995)

231. Vereecke, G. and Lemaitre, J., Calculation of the Solubility Diagram in the System $Ca(OH)_2$-H_3PO_4-KOH-HNO_3-CO_2-H_2O, *J. Crystal Growth*, 104:820–832 (1990)

232. Onuma, K., Kanzaki, N., Ito, A., and Tateishi, T., Growth Kinetics of the HAp (0001) Face Revealed by Phase Shift In Terferometry and Atomic Force Microscopy, *J. Phys. Chem. B.*, 102:7833–7838 (1998)

233. Kanzaki, N., Onuma, K., Ito, A., Teraoka, K., Tateishi, T., and Tsutumi, S., Direct Growth Rate Measurement of HAp Single Crystal by Moire Phase Shift Interferometry, *J. Phys. Chem. B.*, 102:6471–6476 (1998)